NOTE TO USERS

Physical and Optical Properties of Weakly Charged Polyelectrolyte Multilayer Films

by

Ozzy Mermut

A thesis

submitted to the Faculty of Graduate Studies and Research in

partial fulfillment of the requirements for the degree of

Doctor of Philosophy

Department of Chemistry
McGill University
Montreal, Quebec
H3A 2K6
© Ozzy Mermut   August 2004

Canada

Abstract

Thin multilayer films were prepared through layer-by-layer adsorption of oppositely charged polyelectrolytes in aqueous media using a recently established electrostatic self-assembly approach. The adsorbing polyelectrolytes can be classified as either weak or strong based on their level of dissociation in solution. The density of charge in weakly charged polyelectrolytes, unlike in strongly charged ones, can be controlled by adjusting the solution pH about the value of its dissociation constant. At the onset of this dissertation, there were some fundamental and unresolved questions regarding assembly mechanisms, kinetics, and internal structures of the layers in polyelectrolyte multilayer films (PEMs). The studies here examine how varying the level of dissociation of polyelectrolytes in solution influences the kinetics of assembly, and adsorption behavior, as well as some structural, mechanical, and optical properties of PEMs. Using mainly ellipsometry, fluorescence, UV-vis spectrophotometry, and atomic force microscopy (used as a nanoindentation tool), the following investigations of weakly charged polyelectrolytes in multilayer assemblies were performed:

The affect of assembly pH on the layer thickness of weakly ionized versus strongly charged polycation/polyanion systems, was compared. At adsorption time scales on the order of seconds, weakly charged polyelectrolytes produced layers which were significantly thicker than strongly charged multilayer systems (by as much as 10-fold). Anomalously rapid adsorption of multilayers was found (i.e., within 1 s) when weakly ionized polycation and polyanions were assembled. The strength of counterion binding, and hence the rate of counterion displacement (an integral part of PEM formation), was

also shown to significantly affect the time-dependant growth of multilayers. The effect of polyion chain length on the adsorption of a model polyelectrolyte onto an oppositely charged model polyelectrolyte was examined. At long time scales of adsorption (i.e., 24 hr) preferential deposition of long over short chains was observed. These results were rationalized using thermodynamic arguments involving favorable enthalpy (resulting from a reduction in the electrostatic barrier during adsorption), and entropy gain (from having shorter chains free in solution). Upon adsorption, the relative length of loops (formed between "ionic cross-links" in the layers of weakly charged PEMs assembled at varying pH) exhibited variation by a factor of 50, as implied by mechanical measurement of the film's elastic modulus using an atomic force microscope (AFM). Results from the AFM nanoindentation experiments reported here mark first-time measurements of relative loop lengths in PEMs. With an appreciation of the importance of assembly pH in multilayer build-up, the suitability of weakly charged PEMs, (optically functionalized with azobenzene chromophores) as pH sensors in alkaline media, was assessed. The proposed optical application was based on differences observed in the rate of photo-induced isomerization of azobenzenes in varying pH solutions.

Résumé

L'adsorption consécutive de polyélectrolytes de charges opposées est utilisée dans la préparation de films de multicouches minces. Cette approche établie récemment fait appel au phénomène d'auto-assemblage électrostatique. Les polyélectrolytes adsorbés sont divisés en deux classes: ils sont soit faibles ou forts, dépendamment de leur degré de dissociation en solution. Contrairement aux polyélectrolytes forts, la densité de charge des polyélectrolytes faibles est liée à la constante de dissociation, elle-même contrôlée par l'ajustement du pH de la solution. À l'amorce de cette recherche, des problèmes fondamentaux existaient quant aux mécanismes d'assemblée, à la cinétique, et aux structures internes des films de multicouches de polyélectrolytes (PEMs). La présente étude porte sur l'influence de la variation du degré de dissociation des polyélectrolytes en solution sur la cinétique d'assemblage, l'adsorption et certaines propriétés (structurelle, mécanique et optique) des films de multicouches de polyélectrolytes. Les techniques d'analyse et de caractérisation telles que l'éllipsométrie, la fluorescence, la spectrophotométrie UV-vis et le microscope de force atomique ont permis d'émettre certaines hypothèses sur l'assemblage de multicouche de polyélectrolytes de faibles charges.

L'effet du pH d'assemblage sur l'épaisseur des systèmes de polyanions/polycations faiblement ionisés et fortement chargés est comparé. Lorsque l'échelle du temps d'adsorption est de l'ordre des secondes, les polyélectrolytes faiblement chargés produisent des couches de plus grande épaisseurs que ceux qui sont fortement chargés. Une adsorption anormalement rapide des multicouches (c-a-d en

moins d'une seconde) est observée lors de l'assemblage des espèces ionisées. La force de liaison des contre-ions et leur vitesse de déplacement affectent la croissance (dépendante du temps) des couches par un facteur d'au plus 21%. L'effet de la longueur des chaîne de polyion sur l'adsorption dans le cas du polyelectrolyte et de son homologue de charge opposé est examiné. Pour des temps d'adsorption élevé (c.a.d: 24 heures), la déposition préférentielle des longues chaînes par rapport aux chaînes courtes est observée. Ces résultats sont rationalisés à l'aide d'arguments thermodynamiques qui mettent en jeu une enthalpie favorable (résultant de la réduction de la barrière électrostatique durant l'adsorption) et un gain d'entropie (création de chaînes libres plus courtes en solution). La longueur relative des boucles de chaînes formées entre les couches de polyélectrolytes faibles liés entre elles par des liaisons ioniques, varie selon le pH de la solution utilisée lors de l'assemblage. Les résultats obtenus par mesures mécaniques du module élastique démontrent que ce dernier peut varier d'un facteur de 50, dépendamment du pH. Les résultats rapportés ici des expériences de nanoindentation avec le microscope à force atomique (AFM) marquent la première fois que les longueurs relatives des boucles des PEMs ont été mesurées. Considérant l'importance du pH lors de l'assemblage des multicouches, la possibilité d'utiliser des PEM faiblement chargés (incluant des fonctions optiques par l'addition de chromophore d'azobenzène) comme capteur de pH alcalin est évaluée. Cette application optique est basée sur la différence de la vitesse d'isomérisation photo-induite des groupements azobenzènes à différents pH.

Forward

In compliance with the "Thesis Preparation and Submission Guidelines" for the Faculty of Graduate Studies and Research at McGill University, the work herein is presented in a manuscript- based format. The guidelines are cited as follows.

"As an alternative to the traditional thesis format, the dissertation can consist of a collection of papers of which the student is an author or co-author. These papers must have a cohesive, unitary character making them a report of a single program of research. The structure for the manuscript-based thesis must conform to the following:

1. Candidates have the option of including, as part of the thesis, the text of one or more papers submitted, or to be submitted, for publication, or the clearly-duplicated text (not the reprints) of one or more published papers. These texts must conform to the "Guidelines for Thesis Preparation" with respect to font size, line spacing and margin sizes and must be bound together as an integral part of the thesis. (Reprints of published papers can be included in the appendices at the end of the thesis.)

2. The thesis must be more than a collection of manuscripts. All components must be integrated into a cohesive unit with a logical progression from one chapter to the next. In order to ensure that the thesis has continuity, connecting texts that provide logical bridges preceding and following each manuscript are mandatory.

3. The thesis must conform to all other requirements of the "Guidelines for Thesis Preparation" in addition to the manuscripts.

The thesis must include the following:

1. *a table of contents;*

2. *a brief abstract in both English and French;*

3. *an introduction which clearly states the rational and objectives of the research;*

4. *a comprehensive review of the literature (in addition to that covered in the introduction to each paper);*

5. *a final conclusion and summary;*

6. *a thorough bibliography;*

7. *Appendix containing an ethics certificate in the case of research involving human or animal subjects, microorganisms, living cells, other biohazards and/or radioactive material.*

4. As manuscripts for publication are frequently very concise documents, where appropriate, additional material must be provided (e.g., in appendices) in sufficient detail to allow a clear and precise judgement to be made of the importance and originality of the research reported in the thesis.

5. In general, when co-authored papers are included in a thesis the candidate must have made a substantial contribution to all papers included in the thesis. In addition, the candidate is required to make an explicit statement in the thesis as to who contributed to such work and to what extent. This statement should appear in a single section entitled "Contributions of Authors" as a preface to the thesis. The supervisor must attest to the accuracy of this statement at the doctoral oral defence. Since the task of the examiners is

made more difficult in these cases, it is in the candidate's interest to clearly specify the responsibilities of all the authors of the co-authored papers.

6. When previously published copyright material is presented in a thesis, the candidate must include signed waivers from the publishers and submit these to the Graduate and Postdoctoral Studies Office with the final deposition, if not submitted previously. The candidate must also include signed waivers from any co-authors of unpublished manuscripts."

This dissertation is written in the form of four original published papers and a contribution in a review article. Each paper is presented as one chapter. A comprehensive background of the previous work done in relevant fields as well as an introduction to the work conducted by the author is provided in the first chapter. The studies performed by the author are summarized as general conclusions in the final chapter, and future work is suggested. All four papers have been published in scientific journals, and work from Chapter 5 is being prepared for submission.

Contributions of Authors

All papers presented herein were co-authored by the research director Prof. Christopher J. Barrett of the Department of Chemistry at McGill University. Collaborative experimental work for Chapter 4 was performed under the guidance of Prof. Derek Gray of the Department of Chemistry at McGill University and Julie Lefebvre formerly of McGill University. A review paper was written in co-authorship of Rola H. El Halabieh, and Prof. Christopher J. Barrett. With the supervision, advice and direction of Dr. Christopher Barrett, all work presented in this dissertation was performed

Acknowledgements

Table of Contents

List of Figures

Chapter 3

Chapter 4

Chapter 5

Chapter 6

List of Tables

List of Symbols and Abbreviations

Acronyms and Abbreviations

Abs	Absorbance
AFM	Atomic Force Microscopy
a.u.	Arbitrary units
Azo	Azobenzene
ER	Azo-chromophore, [2-[4-(diethylamino)phenylazo]benzoic acid]
ESA	Electrostatic Self-Assembly
cis	Geometric isomer in which two moieties are on the same side of an imaginary reference line on the molecule
$CI^{\pm}$	Counterion (CI^+ is a positive counterion and CI^- is a negative counterion)
D112	5-dimethylaminonaphthalene-1-(*N*- (2-aminoethyl))sulfonamide (dansyl ethylenediamine)
DLS	Dynamic Light Scattering
LBL	Layer-by-Layer
NMA	1-naphthalmethylamine
OWLS	Optical Waveguide Lightmode Spectroscopy
PAA	Poly(acrylic acid, sodium salt)
PAA-co-PMA	poly(acrylic acid)-copolymer-polymethacrylate
PAH	Poly(allylamine hydrochloride)
P-Azo	Poly-{1-[4-(3-carboxy-4-hydroxyphenylazo)benzene sulfonamido]-1,2-ethanediyl, sodium salt}

PDAC	Poly(diallyldimethylammonium chloride)
PEI	Poly(ethylenimine)
PEM(s)	Polyelectrolyte Multilayer(s)
Piezo	Piezoelectric crystal
pK	Dissociation constant for weak polyelectrolytes
Pol$^{\pm}$	Polyelectrolyte (Pol$^+$ is a polyanion and Pol$^-$ is a polycation)
prepn	Preparation
PSS	Poly(sodium 4-styrenesulfonate)
QCM	Quartz Crystal Microbalance
SAR	Scanning Angle Reflectometry
SEM	Scanning Electron Microscopy
SFA	Surface Force Apparatus
SHG	Second Harmonic Generation
rel	Relative
RMS	Root Mean Square
TEM	Transmission Electron Microscopy
trans	Geometric isomer in which two moieties are on opposite sides of an imaginary reference line on the molecule
UV-vis	Ultraviolet-visible

Mathematical Symbols

A	Absorbance (or Abs)
A_{Ea}	Temperature-independent pre-exponential factor in the Arrhenius Equation

c	Concentration
d	Cantilever deflection in AFM nanoindentation experiments
δ	Indentation depth in AFM nanoindentation experiments
Δ	Heat
Δ_λ	Ellipsometric angle containing the phase shift information upon reflection of light
ε	Extinction coefficient
E	Young's modulus
E_a	Energy of activation
F	Loading force in AFM nanoindentation experiments
G	Modulus of rigidity
h	Average height per layer of film
h	Planck constant, ca. 6.63×10^{-34} J·s
$h\nu_{excitation}$	Excitation energy
$h\nu_{emission}$	Emission energy
k	Rate constant
k_B	Boltzmann constant, ca. 1.38×10^{-23} J·K^{-1}
k_F	Force constant
k_s	Extinction coefficient (used in ellipsometry)
l	Cell path length in absorbance measurements
λ	Wavelength of light
M_x	Mean chain molecular weight
n_L	Number of layers in a polyelectrolye multilayer film

n	Refractive index
p	Polarization of light reflected parallel to the incident plane
r	Radius
R	Gas constant, ca. 8.314 J·K^{-1}
$R_{s/p}$	Fresnel reflection coefficient for s-waves/p-waves
ρ	Density
σ	Poisson ratio
Φ	Quantum yield
s	Polarization of light reflected perpendicular to the incident plane
Ψ	Ellipsometric angle whose tangent is the ratio of magnitudes of the total reflection coefficients
t	Time
T	Temperature
ν	Frequency
z	z-position of a piezo electric crystal in AFM nanoindentation experiments

Chapter 1

Introduction

1.1 Polyelectrolyte Multilayer Thin Films

The study of polymer thin films is of great importance because they are amenable to a large body of technological applications. Most commonly, they are prepared as functional coatings, interfaces, or devices with tailored mechanical, chemical, physical, optical, or electronic properties. One common goal of the various strategies used to assemble polymer films is that of achieving a deeper understanding of the fundamental properties and behavior of polymer surfaces and interfaces. Such an understanding will lead to better control of functional surfaces at the nanoscale by tailoring the structure and molecular organization of macromolecules. To fully exploit various surface properties and optimize the desired functionality of polymer films, scientists in various interdisciplinary fields are interested in studying the mechanism of polymer thin film assembly on surfaces under various assembly conditions. Characterization of the behavior of the film in relevant environments is therefore critical. Various techniques and types of polymer coatings have been investigated in the last 60 years leading to more than 80 review articles written about the fabrication,[1,2] characterization,[3–5] and application[2,6] of these macromolecular films. There exist several established methods for generating well-defined organic films from macromolecules on a nanometer scale. Most commonly, the field of organic multilayer films has been dominated by chemisorption techniques[4,7,8] and the well-recognized Langmuir-Blodgett method (a technique in which monolayers are

formed on a water surface and transferred onto a solid support through mechanically induced compression of organic macromolecules).[9–13] Excluding high-energy routes and photolithographic methods, other common approaches include self-assembly techniques based on mechanical spinning of macromolecule liquids onto surfaces (i.e., spin coating or drop casting, and vapor deposition techniques).[14] Many of these schemes can yield highly ordered arrangements of macromolecules on solid supports.[5,15] However, such techniques have limitations for example, a) with respect to substrate size and topology, b) can be restricted to certain classes or organic molecules and the methods are often synthetically challenging, c) often require specialized equipment and require an ultra clean environment as in the case of the Langmuir-Blodgett technique, and d) need carefully controlled preparation processes to obtain the desired functionality.

One of the main challenges in constructing organic thin films is the task of achieving well-controlled supramolecular architectures through directed assembly of macromolecules, containing a diverse range of functionalities, on the surface. In the last decade, a new and rather technically straightforward method for creating homogeneous organic films has emerged as a promising alternative to previously existing film fabrication approaches that either rely on the formation covalent bonds to a surface (i.e., using a regimented protocol) and/or have strict materials and surface dimension limits. In 1991, it was realized that polyelectrolytes of opposite charge could be assembled in a sequential and alternating layer-by-layer (LBL) fashion onto solid supports to systematically build multilayer organic thin films.[16–18] As evidenced by the publication statistics in the area of polyelectrolyte multilayer films, shown in Figure 1a, interest in this technique of polymer film preparation has grown rapidly since it's introduction and

currently on average of over 100 scientific papers are produced per year which give attention to this technique and its applications.
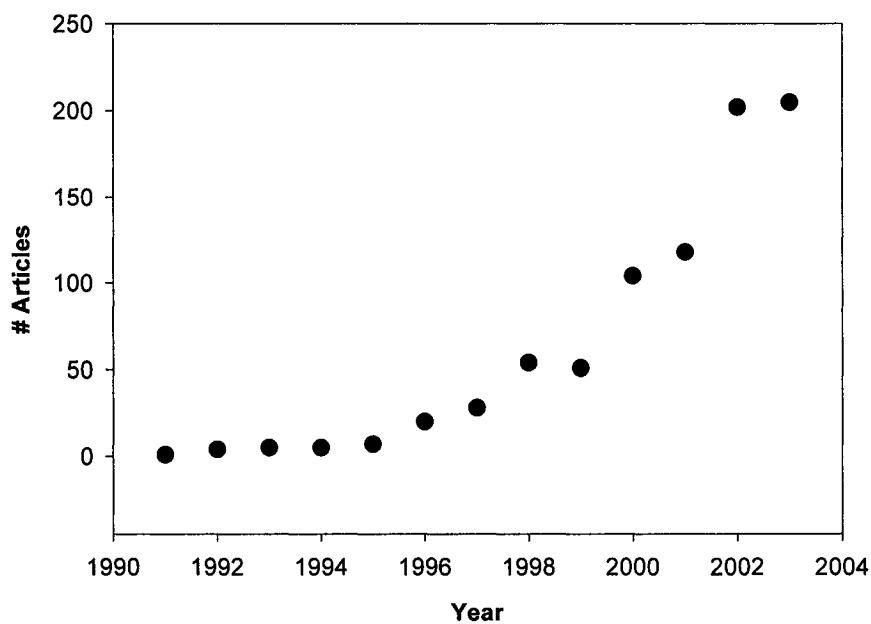
Figure 1.1a Yearly production of scientific papers produced in the area of polyelectrolyte multilayers.
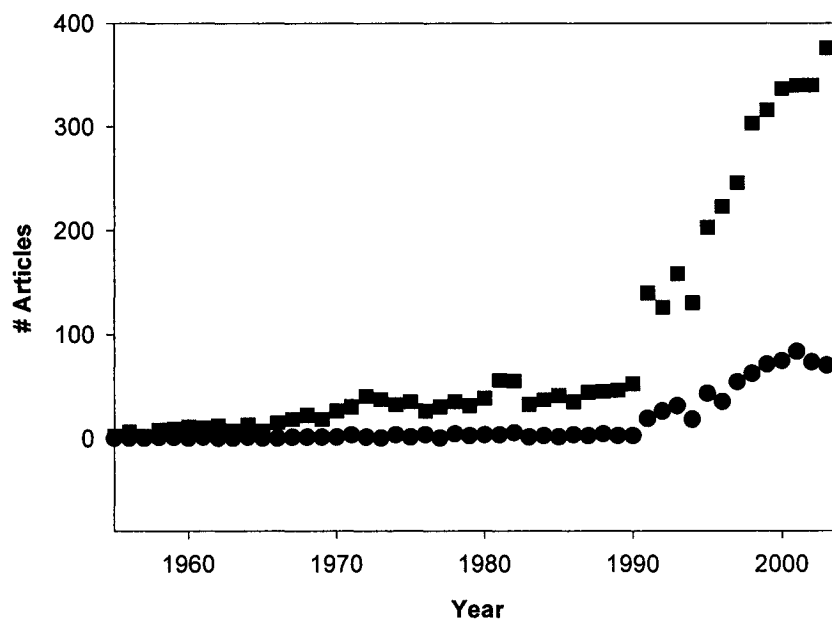
Figure 1.1b Plot of the number of papers investigating azobenzenes (squares), and photoisomerization of azobenzenes (circles).

1.1.1 Method of Layer-by-Layer Assembly

The elegance and distinct advantage of the LBL technique is that it is a direct and simple approach for self-assembling multicomponent polymer thin films entirely from an aqueous environment. Commonly, a practical set-up for multilayer assembly involves exposing a hydrophilic surface such as glass or Si (previously cleaned by 24 h immersion into a 25%H_2SO_4 and 75% H_2CrO_4 mixture) to an aqueous solution containing polycations i.e. by immersion of the substrate into a bath of polymer solution. After adsorption of the polycation, the film is then exposed in a similar manner to a polyanion solution. The stepwise polycation/polyanion assembly process is repeated until the desired number of layers is achieved (Figure 1.2). The adsorption of the polyelectrolytes is relatively rapid, typically requiring an adsorption time on the order of minutes (for planar substrates).[19-23] In most cases, excess concentrations of adsorbate solutions are used (usually 10^{-3} to 10^{-1} M per polyion repeat unit) to ensure surface coverage by the polyelectrolytes.[21,24] Any unadsorbed polymer adhering to the support after an adsorption step is removed with several rinses of the substrate with copious amounts of water. For substrates with dimensions similar to that of a glass microscope slide, washing the polymer-modified surface in 3 separate water baths for a few minutes is usually sufficient for removing unadsorbed polymer and preventing contamination of the succeeding polyelectrolyte solution. The intermittent wash cycles also help to stabilize weakly adsorbed polymer layers.[25] Since the physical properties of the polymer film have been demonstrated to be highly dependant on the ionic strength of the solutions used, our studies of LBL assembled films were conducted using 18 M cm resistivity Millipore Milli-Q water. Unless otherwise stated, all adsorption was performed with pH-controlled solutions (using NaOH and HCl) and in the absence of added electrolyte.

Key to the scheme of electrostatic self-assembled multilayer (ESA) formation is the process of charge reversal such that a greater than stoichiometric number of charges of polymeric material is adsorbed relative to the surface.[26-28] This surface charge reversal prepares each layer for subsequent adsorption of oppositely charged polyelectrolyte.
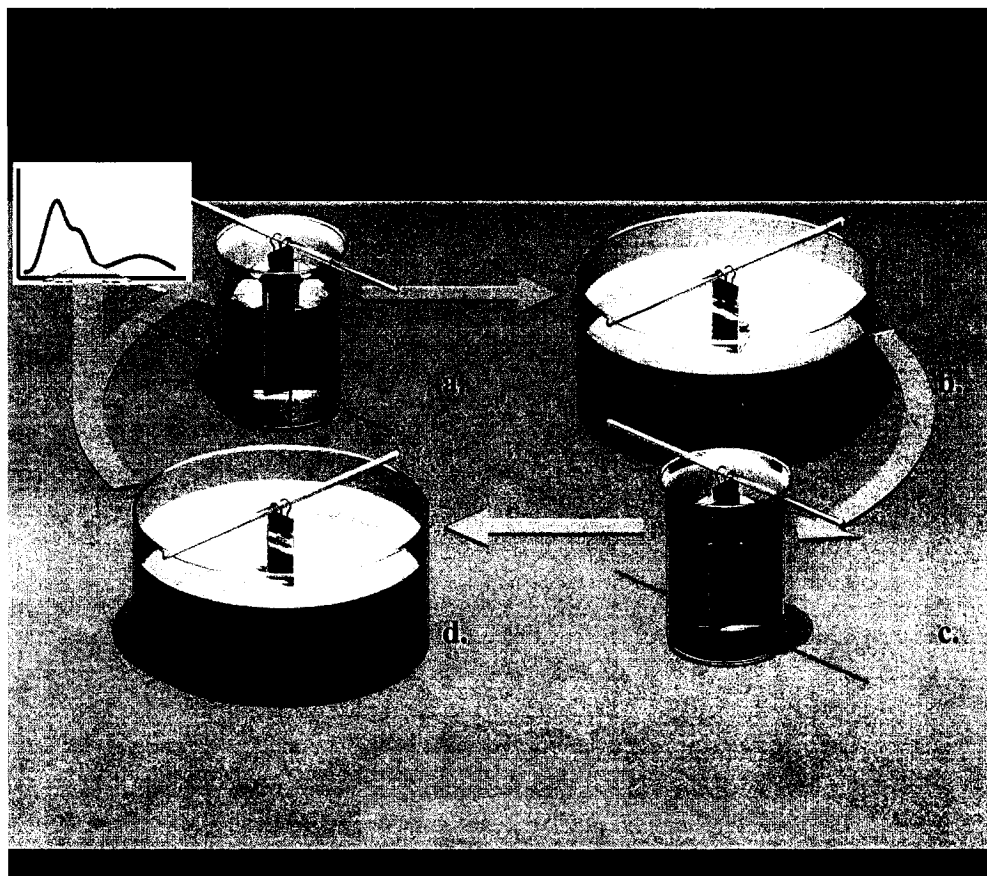
Figure 1.2a A scheme of the stepwise electrostatic layer-by-layer self-assembly of polyelectrolytes onto a solid support. A clean, hydrophilic substrate such as glass, mica, or Si is: **a.** first immersed into a polycation solution, followed by **b.** thorough rinsing of unadsorbed polycation in several water baths, then subsequently **c.** dipped into the polyanion solution and finally, **d.** rinsed in another water bath to remove unadsorbed polyanion. This cycle is repeated until the desired number of layers is obtained.
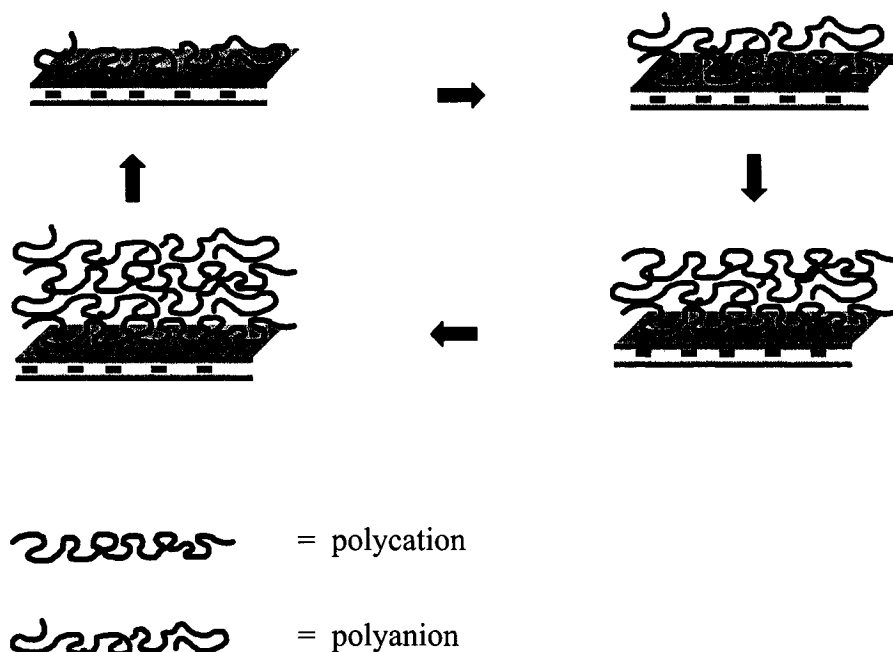
Figure 1.2b   The layer-by-layer build-up of polyelectrolyte multilayers.

There are various ways to introduce polyelectrolyte solutions onto an oppositely charge surface and achieve this multilayering process. The most common technique is direct immersion of the solid support into the polyion solution, as originally described by Decher. For example, substrates may be "hand-dipped" if only a few numbers of layers is desired, while for films of hundreds or thousands of layers, an automated dipping apparatus has now been commercialized. Alternatively, new adsorption methods such as spin-assembly (utilizing a spin coating device),[29-31] and multilayer adsorption onto colloidal particles (of a size scale on the order of tens of nanometers)[32] have recently been demonstrated to be successful, as illustrated in Figure 1.3. In Chapter 6 we explore the versatility of the multilayering scheme by investigating the different adsorption techniques and available geometries of adsorption for polyelectrolytes onto various substrates.
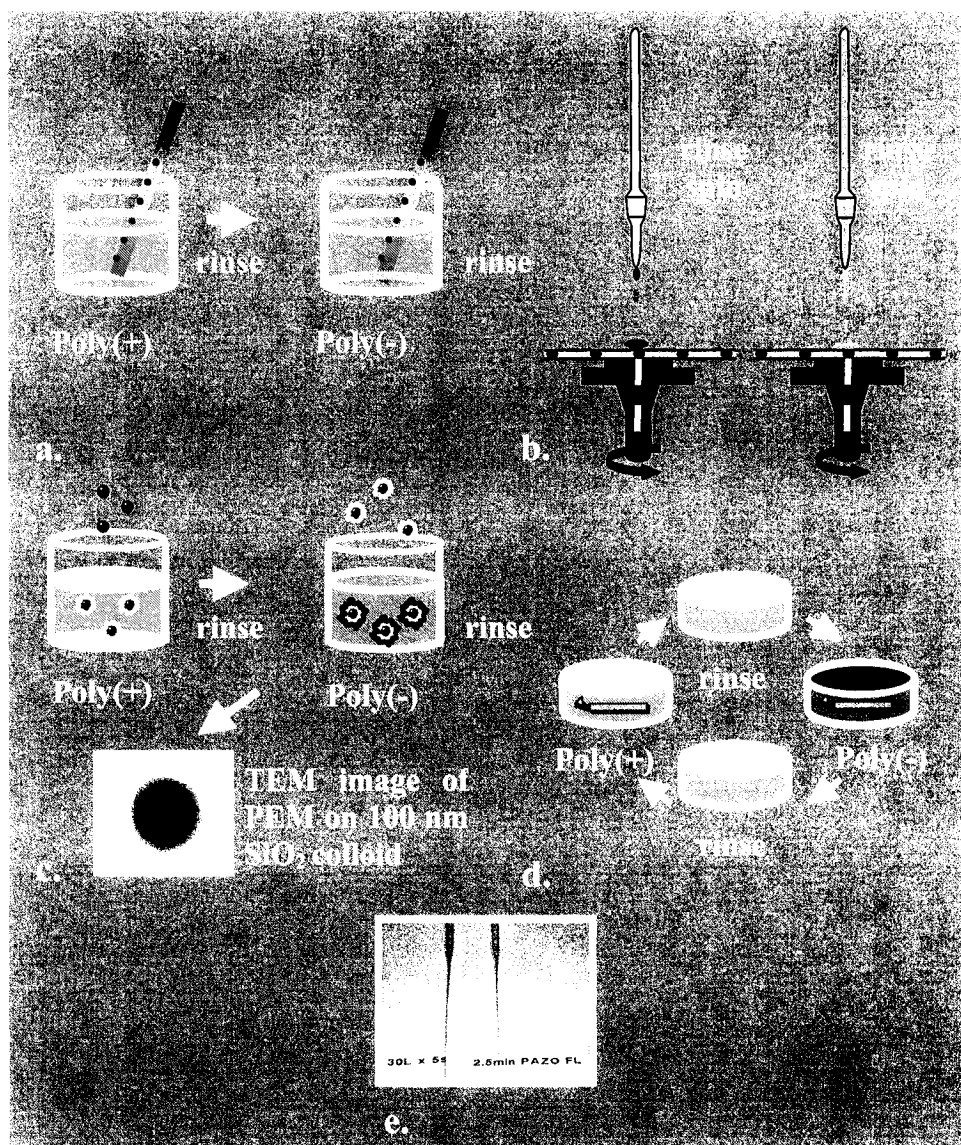
Figure 1.3 Strategies for multilayering on various surfaces are: **a.** the dipping method, **b.** spin deposition, **c.** dispersing of particles in solution, **d.** deposition onto a high curvature surface, and **e.** flowing solution through a cell.

Briefly, the following mechanism of multilayer adsorption has been proposed. The building of polyelectrolyte multilayers are known to result from the formation of weak (i.e., on the order of $k_B T$) but many ionic interactions established between cationic and anionic groups of the polyelectrolytes.[21] Polyelectrolyte from solution ($Pol^{\pm}_{aq}$) is

7

added onto a preexisting multilayer containing counterions ($Pol^{\pm} Cl^{\pm}_{m}$) through the displacement of its counterions in order to allow formation of new electrostatic links with the oppositely charged surface. This corresponds to the addition of a new layer to the multilayer assembly, $Pol^{-}Pol^{+}_{m}$.

$$Pol^{-} Cl^{+}_{m} + Pol^{+} Cl^{-}_{aq} \rightleftharpoons Pol^{-}Pol^{+}_{m} \quad Cl^{+} + Cl^{-} \quad (1.1)$$

Electrostatic condensation of charged repeat units of surface-bound polyelectrolytes with an incoming counter polyion results in the formation of "ionic cross-links". Since charge reversal is a prerequisite for subsequent deposition of polymer layers, charge overcompensation must then occur whereby an excess amount of charges remains on the adsorbed polymer. This overcompensation must be sufficiently large to accommodate layer formation from an oppositely charged polyion to render a charged polymer surface.[33,34] The extent to which overcompensation will occur has been theoretically investigated, showing dependence on the degree ionization of the polyelectrolyte employed.[27]

1.1.2 Suitable Polyelectrolytes and Substrates

Since the ESA technique is based on the attractive interaction of complimentary charges, nearly all polyelectrolytes are suitable for deposition into multilayer films. The requirement is only that the polymers used bear a minimum number of charged groups below which the ESA process cannot occur. In general, the presence of any additional strong interactions that reduce the minimum charge requirement, such as π-π stacking

interactions (i.e., when using certain organic dyes) appear to aid the ESA process.[35-37] In certain cases where large biomolecules are employed in ESA, (such as charged lipids and bolamphiphiles) deposition in the form of aggregates from solution is often observed.[38-40] Although a platform for much recent debate, in some cases hydrophobic fragments can effectively reduce the usable charge fraction in some polyelectrolytes and sterically hinder the ion-ion pair formation that is necessary for ESA. Despite the requirement of a critical minimum charge density, a large number of polymers with a very low charge fraction have been successfully employed in ESA. It is believed that while electrostatic interactions are the dominant force driving the assembly, contributions from other interactions, as mentioned above may help the formation of stable multilayer thin films. With such little materials stringency, nearly any type of polyelectrolyte containing any number of functional groups can be used. In fact, the technique has now been extended to incorporate charged nanoobjects, such as inorganic molecular clusters,[41-43] enzymes,[44,45] and aggregates.[46]

The ESA method is also conveniently amenable to numerous types of charged substrates such as metals, glass inorganics, as well as various geometries, as discussed in Chapter 6. The solid support must only carry a minimal surface charge sufficient to support adsorption of the initial polyion layer. In some cases of unclean or inherently uncharged surfaces, the substrate may be rendered hydrophilic with an oxidizing and acidic surface treatment. In general, the choice of substrates is based on suitability of the surface for various analytical techniques. For example, transparent surfaces such as microscope glass slides, quartz, and mica are appropriate substrates for transmission studies, while Si, Al and Au metals are generally used for reflectivity techniques.

The polyelectrolytes used in the present studies were chosen based on their simple structure. The chemical structures are shown in Figure 1.4. They contain monovalent ammonium, carboxylate or sulfonate species to serve as model polycations/polyanions for fundamental investigations of the influence of charge density on the thickness, kinetic growth and mechanical properties of multilayer thin films.

All polycations and polyanions employed in the PEM studies were commercially purchased and used as received with the exception of fluorescently modified PAA, which was synthesized to investigate chain length dependence on adsorption (Chapter 5). For all films fabricated, no further purification of the polyelectrolyte solutions was performed (i.e., by filtration or dialysis) since initial experiments revealed this to have a negligible effect on the measurements obtained.

1.1.3 Advantages and Applications

Several reasons may explain the continually growing interest and investigations of the LBL approach for organic thin film fabrication. The first is that LBL assembly of the polymeric material is practical and simple, making the fabrication process very inexpensive and undemanding. One can incorporate any number of diverse polycations and polyanions containing a variety of functional groups, limited only by the synthesis of the polyions. In contrast to many other single layer surface modification techniques, such as self-assembled monolayers (SAMs), a dense array of any number of functional species can be incorporated into the film through assembly of many layers of different polyions.

a.

b.

c.

d.

e.

f.
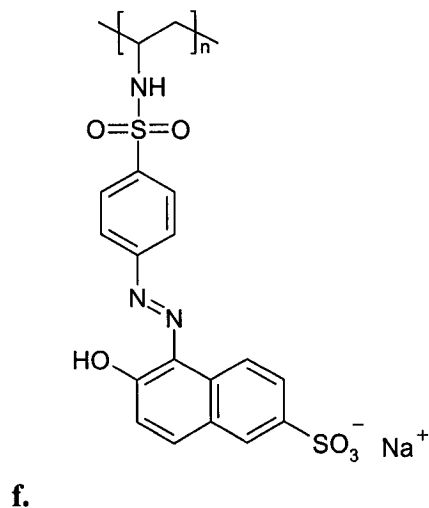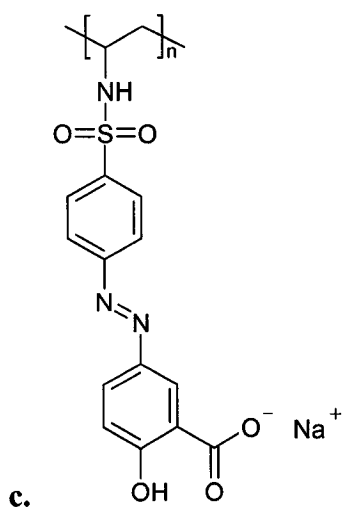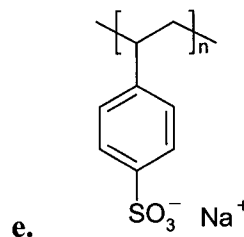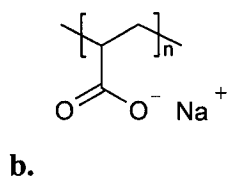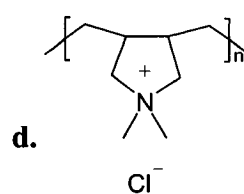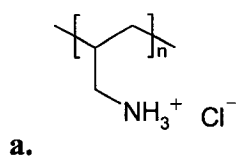
Weak polyelectrolytes   **Strong polyelectrolytes**

Figure 1.4.   Repeat unit structures of all polyelectrolytes used in the investigations of multilayer thin films.   Weakly charged polyions include: **a.** poly(allylamine hydrochloride), **b.** poly(acrylic acid, sodium salt), and azobenzene-containing **c.** poly-{1-[4-(3-carboxy-4-hydroxyphenylazo)benzene sulfonamido]-1,2-ethanediyl, sodium salt}. Strongly charged polyelectrolytes include: **d.** poly(diallyldimethylammonium chloride), **e.** poly(sodium 4-styrenesulfonate), and **f.** azobenzene-containing poly(S119).

11

Various combinations of polyions that are based on electro-active, light-responsive, chemical sensing, and mechanically active polymers have already been demonstrated as good candidates for LBL film fabrication. Whereas the incorporation of functional groups is limited to the surface area coverage, as in the case of SAMs, polyelectrolyte multilayers (PEMs) can include many nanometers of functionality for example, sensor-containing polymer layers, thus greatly increasing the sensitivity of the film. Since the films are highly swellable,[47–51] small molecules such as catalytic nanoparticles,[52] dyes,[53] and drugs[54–58] can be embedded between layers or encapsulated with a permeable multilayer shell with the intention of controlled release in an aqueous environment. Additionally the structural properties of the film can be well dictated during or post self-assembly (i.e., by pH adjustments or exposure to salt solutions).[59–61] Thus PEM films have also found good use as permselective ion[62,63] and gas membranes.[64–66] The versatility of these functional polyelectrolytes that can be used in PEMs allows flexibility in the development of multicomposite and hence multipurpose surfaces.

Since LBL assembly is primarily driven by electrostatic interactions between polycation and polyanion chains, this method is particularly attractive for studying charged biologically important macromolecules (i.e., proteins, and enzymes) in various applications such as surface modification and cell adhesion.[67,68] Also, the films are developed in aqueous media, and therefore do not necessitate the use of stringent protocols for water-sensitive assembly. This also gives the advantage of biocompatibility. In fact, biological applications of PEMs as possible intravascular grafts and thromboresistent stents,[69,70] as well as hydrophilic membranes for coating contact lenses[71] have already been shown.

A major concern in the production and application of functional thin films is their quality and stability. In this regard, PEMs are highly advantageous. For example, thick multilayer films functionalized with dyes have been reported to form optically uniform coatings, as indicated by the interference colors throughout the build-up of films. Examinations with high-resolution techniques (i.e., AFM) typically indicate the formation of coherent films with few defects.[72-77] This attribute is particularly desirable for optical applications of organic multilayer assemblies, such as anti-reflection coatings,[78,79] and organic light emitting diodes.[80,81] Furthermore, by choosing appropriate assembly conditions, smooth layers with the desired optical quality properties can be deposited with a roughness value <1 nm.[19,82] The molecular architecture of the film, which is governed by the interaction between layers, also has important consequences on the stability of film structure over time. For instance, in some multilayer systems comprised of a high density of ionic links between layers, the film structure tends to be highly stable. The stability is in part attributed to the reduced mobility of polyelectrolyte chains once incorporated in a tightly networked film.[83] On the other hand, PEMs can also be designed with controlled structural flexibility by employment of weakly charged polyelectrolytes, as discussed in the following section. In Chapter 6, we will examine the structural implications of varying the charge density of polyelectrolytes during adsorption and perform a thorough investigation of the stability of these PEMs in various solvent environments (Chapter 7).

1.2 Weak Versus Strongly Charged Polyelectrolytes

The simplest form of a polyelectrolyte that can be employed in a multilayer assembly is a chain that is comprised of a charge on each monomeric unit. When all monomeric units maintain a fixed charge fraction in solution, independent of the solution

pH, the polyion is said to be a "strong" polyelectrolyte. Some strong polyelectrolytes that have commonly been employed in previous PEM studies include PSS, PDADMAC, and PEI. Conversely, "weak" polyelectrolytes allow the possibility of variable charge along the chain, i.e. by control of the fraction of charged segments. While polyelectrolytes may be synthesized with a specified charge density, as in the case of PAA-co-PMA (poly(acrylic acid)-copolymer-polymethacrylate), one can simply adjust the pH of a polyelectrolyte assembly solution to vary the degree of ionization in the case of weak polyelectrolytes. To understand how this is achieved, a brief discussion of acid-base equilibria is in order.

The degree of dissociation of a dilute weak polyacid or polybase can be approximated by its dissociation constants K_a or K_b respectively (or pK_a and pK_b expressed in convenient logarithmic units). Through titration of a weak monoprotic polyacid with a base for example, the fraction of protonated ($Pol^-H^+_{aq}$) verses dissociated polyacid ($Pol^- + H^+$) can be determined at a particular solution pH value.

$$Pol^-H^+_{aq} \rightleftharpoons Pol^- + H^+ \qquad (1.2)$$
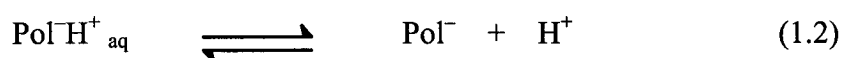
A titration curve may be produced to reveal the fraction of dissociated species (i.e., the percent of Pol^- species) at a particular pH value, as suggested by the Henderson-Hasselbalch equation (Equation 1.3).

$$pH = pK_a + \log\frac{[A^-]}{[HA]} \qquad (1.3)$$

During titration of a weak acid with a base there is continual change of the acid into its conjugate base, and there is a simultaneous change in pH. As the pH approaches the pK_a value a drastic change in the percentage of charge repeat units occurs, and when pH = pK_a approximately 50% of the ionizable species are charged. Thus by manipulating the solution pH value about its normal range (i.e., 1 to 12 units), one can control the degree of protonation of a weak polyelectrolyte in solution and thereby alter its charge density.[84]

Most of the early work on multilayer assemblies has focused on using strong polyelectrolytes, or involved working under pH conditions which render weak polyelectrolytes in their most highly charged form, as in the case with protonated PAH or deprontonated PAA.[19,85] One of the most frequently encountered trends observed in multilayer films prepared from strongly charged polyelectrolytes is that they tend to adsorb as very thin layers.[86] While adding electrolyte, such as NaCl to the assembly solution, has proven to be a plausible route for controlling physical properties of individual layers, such as layer morphology and thickness, it has limitations.[87–90] For instance, decomposition of multilayer films and solubility problems associated with use of salt concentrations beyond a small range has previously been reported.[33] As a result, the use weak polyelectrolytes has recently gained much interest for multilayer thin film fabrication due to their ability to respond to the local electrostatic environment through ionization. Several investigations exploring the effects of assembly pH on multilayer film properties have revealed that employment of weak polyelectrolytes in LBL assembly provides a rich and diverse range of opportunities for structural and organizational control of film layers at the molecular level.[91,92] This is primarily due to the fact that the linear charge density of a weak polyelectrolyte is very sensitive to both the assembly solution pH, as well as the rinse bath pH when operating near the pK_a of the assembled polymer.

To better understand how one can take advantage of this pH-sensitive response to tune various properties, we will now examine a simple multilayer system comprised of a weak polyacid and weak polybase.

1.2.1 Properties of a Simple Weak Polyelectrolyte Multilayer

Multilayer films prepared from both weakly charged PAH and PAA, containing amine and carboxylate species respectively, have served as a simple model system for exploring the various film properties that may be controlled by adjusting the assembly bath pH. Specifically, it has been observed that physical properties such as the mass of polymer adsorbed during an adsorption step, and stability, as well as structural properties of the composite layers, such as layer density, thickness, degree of swelling in solution, and level of interlayer penetration, are highly sensitive to the degree of ionization of both the weakly charged polycation and polyanion.[86,93-96] Such properties have important consequences on the numerous applications proposed for these films. For example, since the acid/base equilibria controls the degree of electrostatic interaction between layers of polycation and polyanion, pH mediated layer properties such as permeability/porosity and stability (i.e., to layer decomposition) offer the possibility of using multilayer films as membranes[92,97] and drug delivery vehicles[98] respectively. In addition, surface properties of the multilayer film, such as roughness,[99,100] friction,[101,102] and surface wettability (as measured through AFM and contact angle of a water droplet) have also demonstrated high pH dependence when the films are prepared from weak polyions. Notably, thin multilayer films composed of PAH and PAA (represented as PAH/PAA) yield the largest root mean square (RMS) surface roughness when the dipping solution pH is near that of

the solution pK_b and pK_a values of the polycation (approximately 9.0 for PAH) and the polyanion (around 4.5 for PAA) respectively.[84]

The effect of pH on the overall film growth behavior, however, is not always intuitive/predictable and is governed by the specific acid/base properties of the unique polyelectrolyte system chosen. For instance, the type of film growth in complex multilayer systems composed of biopolyelectrolytes such as polyL-lysine (PLL) and hyaluronic acid (HA) have been shown to be uniquely dependent on the pH of assembly.[102] For these polyelectrolytes certain pH regimes lead to unusual trends in adsorption such as exponential layer-by-layer growth.[103,104] This anomalous adsorption behavior in the more complex multilayer system, polyL-lysine/hyaluronic acid, is believed to stem from the ability of these biopolyelectrolyte to undergo various secondary structural orderings, as well as chain stiffening, as a function of assembly solution pH.[104] This in turn influences the nature of layer build-up. On the other hand, linear build-up of layers over a large pH range is more commonly observed in more simple systems, as best exemplified for multilayers comprised of PAH and PAA. For simplicity and in order to understand the fundamental effects of the degree ionization on the molecular organization and structure, we shall focus here how the solution pH affects the structural properties of PAH/PAA multilayers.

1.2.2 Structural Properties of PAH/PAA Multilayer Films

1.2.2a Layer Thickness

From early studies, layer thickness has been used as the primary parameter to characterize multilayer build-up. Layer thickness measurements are most commonly obtained using the optical method of ellipsometry (described in Chapter 2). Using this

method much of the initial work has focused on how the ionic strength of the assembly solution can influence the thickness of polyelectrolyte multilayer films. More recent work has shown that layer thickness can be easily controlled with solution pH when working with weak polyelectrolytes. Pioneering studies of PAH/PAA films have shown that the bilayer thickness of these films can be tuned from 10 Å to greater than 100 Å by varying assembly pH. In one of the key studies of this phenomena Rubner et al. showed that with as little change as half a pH unit in the solution of PAH and PAA, dramatic transitions are observed in the average incremental layer thickness, as revealed in Figure 1.5.[86]
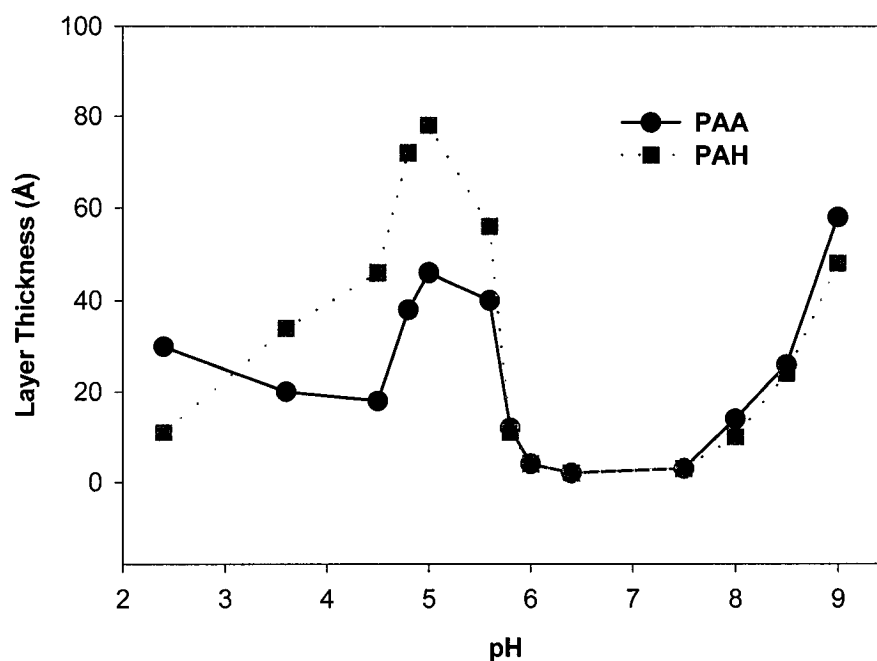
Figure 1.5 Average per layer thickness of the polyanion PAA (black circles), and the polycation PAH (gray squares) adsorbed into multilayer films as a function of the assembly solution pH.[86]

Experiments in which both the pH of the weak polycation and the weak polyanion has been adjusted indicate that an even wider range of tunable layer thickness can be obtained. As indicated in Figure 1.5, the largest values and transitions in average layer thickness are observed when the dipping solution pH approaches near the pK values of 4.5 and 9 respectively for PAH and PAA. Such behavior is believed to arise from the large pH-induced changes in the molecular conformation of the adsorbing polyelectrolyte, as a consequence of altered degree ionization.

1.2.2b Molecular Conformation

It has been suggested that a change in charge density leads to variable polyion adsorption either in the form loops and tails or train-like conformations, particularly when the dipping solution pH is near the polyelectrolyte pK value.[27] Furthermore, closer examinations of the pK values affiliated with the polyelectrolyte as it approaches and adsorbs onto a charged multilayer indicates that the solution value polyelectrolyte acidity (represented by its solution pK value) is often shifted (sometimes by as much as 3 pH units) when it is incorporated as part of a PEM.[84] Major molecular conformation transitions are believed to occur near this "apparent pK" value as polyelectrolytes adsorbs onto multilayers. A schematic representation of the two extremes of adsorbing confirmation is proposed in Figure 1.6. It suggests that for polyions assembled at high versus low charge density, the number of ionized groups, and hence the percent of "ionic cross-linkable" groups is presumed to differ for the two cases. Thus, changing the assembly pH in weakly charged systems allows the flexibility of molecular control over the nature of polyelectrolyte deposition. For instance, strongly ionized polyelectrolytes are speculated to adsorb onto the multilayer in a more train-like configuration since

19

nearly all its repeat units are fully charged, whereas fractionally charged polyelectrolytes are likely to form many loops and tails due to the formation of fewer ionic contacts (represented as **x** in Figure 1.6), with previously adsorbed layers in the PEM.

The commonly observed occurrence of loops and tails, which enable extension of chains into adjacent layers is believed to be in part responsible for the poor stratification of layers.[93] The use of high resolution X-ray and neutron reflectometry techniques, which are based on interferences between waves scattered at interfaces, are capable of revealing detailed information about the internal structure of PEM films and have been particularly useful for studying the interaction of polyelectrolyte chains between neighboring layers.[93,105-107] It is generally agreed that the adsorption of most simple polyelectrolytes (i.e., flexible or polyions with small functional groups) lead to multilayer systems, which exhibit a low level of internal molecular organization, and are nondiscrete adjacent layer interfaces.[108-110] However, little is known about the relative extent of loops and tails versus train-like conformations, since these cannot be trivially determined and thus remain an open question. We explore the use of an AFM nanoindentation technique in Chapter 5, to address this problem.

1.2.3 Kinetics of Adsorption in Polyelectrolyte Multilayers

While many steady-state studies have been devoted to demonstrate that complex adsorption behavior can come from the employment of weakly charged polymers in PEMs, less progress has been made in understanding the kinetics of LBL self-assembly. Kinetic studies of electrostatic multilayer adsorption onto solid supports are crucial for the controlled preparation of these film and optimization of their physical properties.

Weakly charged system

(i.e., pH ~ pK)

Strongly charged system

(i.e., pH << or >> pK
or pH independent)
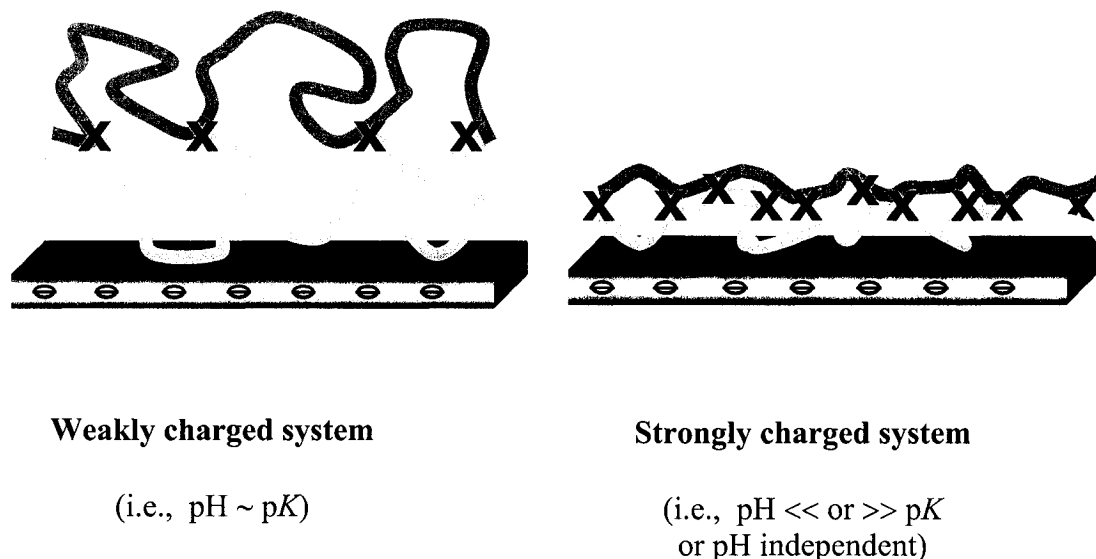
Figure 1.6 Proposed molecular conformation differences giving rise to variable layer thickness values in PEMs from use of weakly charged verses strongly charged polyelectrolytes. Strongly charged polymers are presumed to form a greater percentage of electrostatic interactions with preadsorbed layers, and hence adsorb as thinner layers as compared to weakly charged polyelectrolytes.

Despite much activity, which addresses mechanistic aspects of the LBL process, there still remain many unanswered fundamental questions. For example, equilibrium concepts and models cannot be applied to explain the deposition of PEMs, since no experimental studies have thus far shown the spontaneous formation of PEMs by exposing a hydrophilic surface to a mixed solution of polycations and polyanions.[111,112] Additionally, no theoretical model for single layer polyelectrolyte adsorption has been able to be generalized and extended in order to predict the adsorption behavior of many layers in PEM assemblies, in particular for weak polyelectrolyte systems.

Recent experimental explorations into the mechanism of LBL formation indicate that the mutilayer formation is a multi-step process involving a delicate interplay of both

thermodynamic and kinetic contributions in the build-up of weak polyelectrolyte multilayer systems.[113] A common observation in the formation of multilayers is that the kinetics appear to be influenced by two important steps.[114,115] The first step is believed to involve the diffusion of polyions through solution to the surface, followed by the massive and rapid deposition of polyions (usually on the order of seconds) a process dominated by the rate of polymer diffusion.[91] During the second step, the rate of polyelectrolyte adsorption onto the surface becomes slower, as polymer chains begin to rearrange on the surface, and finally saturation is achieved. It has been shown that during this second step, slow chain rearrangements contribute to the interdiffusion of chain segments into the inner regions of previously deposited layers.[98,116,117] Mixing of positive and negative segments eventually leads to the irreversible charge complexation.[110] The stability of the layer is believed to be attributed to the additive effect of forming many ionic links, each of the order of k_BT.[118] Polycations and polyanions can adsorb on top of each other, by first passing through a strong electrostatic/steric barrier, and then forming an ion-pair linkages from the shorter range attractive forces. The electrostatic barrier limits the amount of polyelectrolyte adsorbed, which in turn is responsible for yielding consecutive layers of equal thickness.[115]

An important consideration, which affects the rate of LBL deposition, is the role of counterions. Many previous studies have shown that increasing salt concentration during assembly causes increased inter- and intra-polyelectrolyte screening of charges.[21,33,119] This leads to enhanced chain coiling and increased adsorbed amount. While the influence of ionic strength on structural parameters, such as deposition thickness, has been extensively investigated,[89,120,121] little is known of the effects of the nature of the counterion on the adsorption. For example, we propose that the degree of

polyelectrolyte adsorption in multilayers should be sensitive to counterions of variable size. One can use simple electrostatic arguments to suggest that different binding energies of different counterions can lead to variances in the displacement of counterions, which is necessary for the addition of polyelectrolyte onto a surface. By this, smaller counterions should exhibit either reduced adsorption or a reduced rate of adsorption due to higher binding energies than larger counterion species, as depicted in Figure 1.7.

Adding to this complex description of adsorption kinetics one has to also consider the nature of the assembling species and the surface, such as variation of the geometry and size of substrate,[122] as well as the chemical structure of the polyelectroyte.[123,124]

Counterions exchange in polyelectrolyte adsorption

F^- I^-

Tight binding: reduced or slower exchange   Loose binding: increased or faster exchange

$F^- = 0.136$ Å
$Cl^- = 0.181$ Å
$Br^- = 0.195$ Å
$I^- = 0.216$ Å

time $= t_o + \Delta t$
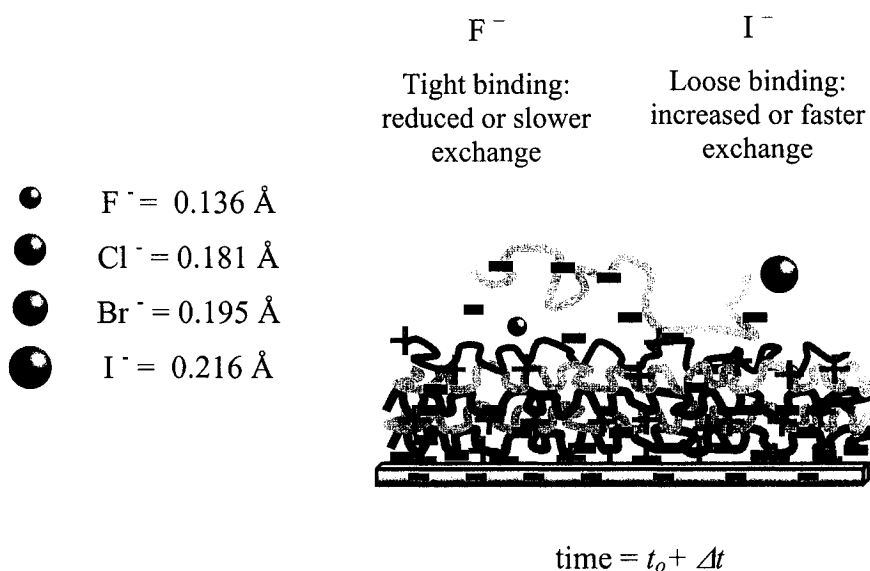
Figure 1.7   Possible model to explain the role of ion displacement on polyion adsorption. Smaller counterions, such as F^- should be more tightly bound to a counterpolymer and thus result in either reduced adsorption or slower exchange with an incoming polyelectrolyte segment as compared to larger I^- species.

However, limited exploratory work has been conducted to determine the effect of polyelectrolyte charge density on the rate of PEM formation. Moreover, no generalized mechanism can fully explain the effect of time and concentration on the adsorption of different polyelectrolytes in multilayer systems. The adsorption rate, and the internal dynamics within multilayers is highly sensitivity to assembly variables such as the effective concentration of the ionic repeat units available for assembly over the deposition time, and the ionic strength or salt concentration of the solutions.[125] The time allowed for adsorption is a particularly interesting parameter which strongly affects the growth behavior of multilayer thin films. This time-dependent adsorption process occurs at polymer concentrations large compared to the saturation concentration of the polymer in the form of PEMs. Initially fabrication of PEMs used long timescales of the order of tens of minutes to achieve saturated adsorption, often cited when purely strongly charged systems were examined (i.e., those containing both strongly charged polycation and polyanion). However, current kinetic investigations of multilayer formation with various systems, including those employing a weakly charged polyion, report much different saturated adsorption times, often in less than 10 min.[124,126] The amount of time necessary to achieve LBL assembly is therefore an interesting question, particularly with regards to understanding the role of kinetics in the mechanism of PEM formation.

1.3 Properties of Azobenzene-Containing Molecules

Azobenzene, with two phenyl rings separated by an azo (N=N) bond, serves as the parent molecule for a broad class of aromatic azo compounds. These chromophores are versatile molecules, and have received much attention in research of optically responsive material incorporated into PEMs, as indicated in Figure 1b. The

strong electronic absorption maximum of azobenzenes can be tailored by ring substitution to fall anywhere from the ultraviolet to red-visible regions, allowing chemical fine-tuning of color. This, combined with the fact that these azo groups are relatively robust and chemically stable, has prompted extensive study of azobenzene-based molecules as dyes and colourants.[127,128]
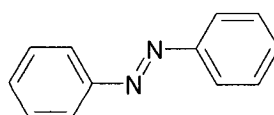
Figure 1.8   The structure of azobenzene.

Azoaromatic chromophores are classified based on the energetic ordering of their (π^*, n) and (π^*, π) electronic states. Azobenzene molecules (shown in Figure 1.8) display a low intensity n→π^* adsorption band in the visible region and a high intensity π→π^* band in the UV. Red or blue shifting of the electronic transition bands may be accomplished by ortho- or para-substitution with electron donor or electron acceptor substituents for example amino and nitro groups respectively.

One of the most interesting properties of these chromophores is the readily-induced and reversible isomerization about the azo bond between the *trans* and the *cis* geometric isomers,[129,130] and the geometric changes that result when azo chromophores are incorporated into polyelectrolyte assemblies. In general, either the polycation or polyanion can bear substituted azobenzene chromophores along the side chain. Variable photoorientation by irradiation of organic mutilayer films prepared from azobenzene-

containting polyelectrolytes has been shown to induce optical effects such as photo-switching,[131,132] in-plane dichroism,[133,134] and holography.[135]

1.3.1 Photoisomerization

Most interesting applications of azobenzene polymers involve exploiting the readily-induced and reversible isomerization about the azo bond between the *trans* and *cis* geometrical isomers, which can be interconverted by light and heat (illustrated in Figure 1.9a). A typical experimental setup for this photoreaction is outlined in Figure 1.9b and is
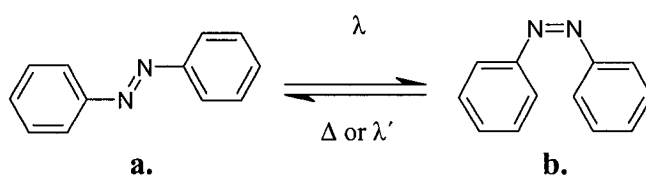
Figure 1.9a   Geometric structures of azobenzene in the form of the: **a.** *trans*, and **b.** *cis* isomer.
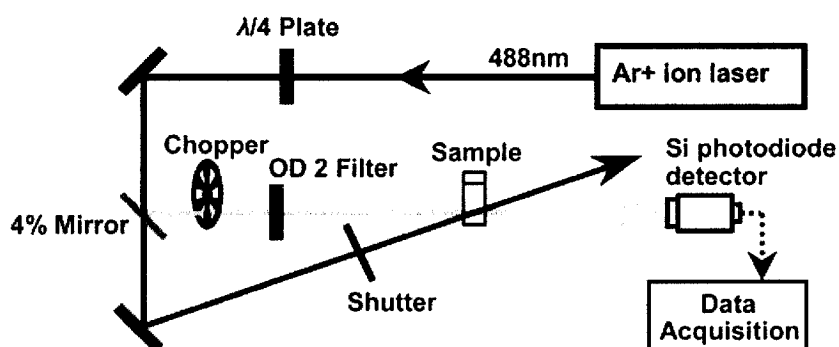
Figure 1.9b   A schematic of a typical setup for an azobenzene isomerization experiment.

based on previously reported methods.[136] Isomerization of an azobenzene-containing amphiphilic co-polymers, for example, can be achieved by irradiation with a circularly polarized beam of an argon laser of $\lambda = 488$ nm, at 425 mWcm^{-2}.[137] As shown in Figure 1.9b the linearly polarized light coming from the argon laser is sent through a $\lambda/4$ wave plate to become circularly polarized. The pump beam (responsible for the isomerization) is sent into the sample at time = 1 s for a duration of 1 s. The probe beam (4% of the laser power) is used to measure the change in the intensity of the signal. The probe beam is sent through the chopper and an OD 2 filter (used to reduce the intensity of the beam by 100-fold) and finally through the sample and into the detector so that the transmission at λ_{max} can be monitored over time.

The isomerization is completely reversible, free from side reactions, and is considered one of the cleanest photoreactions known.[129] The kinetics and extent of isomerization of azobenzenes depend on the irradiation intensity, the quantum yields for the two processes (Φ_{trans} and Φ_{cis}), and the rate constant k, which governs the thermal relaxation from the cis back to the trans form. The net effect of these competing processes can be summarized by the cis concentration in the photostationary state representing the extent of isomeric conversion achieved under irradiation. The composition of the photostationary state, the steady-state of the three conversion processes under irradiation, is unique to each system and can depend on irradiation intensity, temperature, quantum yields, free volume, and substituents. The trans form of azobenzene is the more stable isomer, with a difference in ground state energies of cis and trans of 50 kJ/mol.[138] Unlike the planar trans form, cis azobenzene assumes a geometry with the phenyl rings twisted at right angles to the CNNC plane.[139] In the

photostationary state, the isomeric ratio is predominantly *cis* under usual irradiation levels.[129] In the dark, the concentration of *cis* usually lies below the limit of detection, and the system can be considered to be comprised of 100% *trans* molecules.

In some cases of thin films containing azobenzenes both *trans* and *cis* isomers can be pumped with the same wavelength in the blue or green to induce rapid *trans* → *cis* and *cis* → *trans* photoisomerizations, with a timescale on the order of picoseconds.[140,141] In the absence of light there is a thermal relaxation from the *cis*-containing photostationary state to the *trans*-only state, which has been well studied,[142–145] and is observed to occur on the order of seconds.[136,137,146–149] It is important to realize that for most thin film photo-applications, the molecular orientation of the azobenzene functionalities, as part of a polymer film for example, and the environment of the chromophores significantly influence photoisomerization kinetics.[150,151]

1.3.2 Use as Sensor Probes

The use of photochemical methods for sensing applications in thin films is often desirable from the perspective of minimal contamination and reversibility, as is the case with photoisomerization of azobenzene. Unlike traditional chemisorption or the Langmuir-Blodgett technique, a high number of optically active azobenzene moieties can be electrostatically assembled over many layers. One can also take advantage of the large and well-controlled swelling capability of multilayers to incorporate a dense matrix of sensing material. In the assembly of polyelectrolyte multilayers rearrangements of the uppermost layer and even lower underlying layers (up to 6 layers deep) during film growth has been experimentally observed.[102,152–154] Thus the selective incorporation of

azobenzene chromophores in specified layers of PEMs can provide a simple and direct means for optically tracking (i.e., through spectral shifts measurements) the molecular environment, dynamics and local interactions throughout the film. Recent discovery of a solvato-chromic influence on the photoisomerization kinetics of self-assembling amphiphilic azo-copolymers in aqueous-organic solutions suggests that these photochromes can serve as excellent probes for the local polymer environment in stacked multilayer surfaces.[136] Furthermore, by embedding azo-containing weak polyelectrolytes, which are more sensitive to the local electrostatic environment, it has been suggested that one can optically sense changes in the external environmental conditions that affect the multilayer assembly.[155]

1.4 Scope of Thesis

The following work aims to address the unique kinetic behavior, as well as structural and mechanical aspects, of polyelectrolyte multilayer films prepared from model weakly charged polyelectrolytes. It will be shown that adjusting the charge density of the weak polyelectrolytes assembled serves as an excellent method for achieving control of the physical properties of weak PEMs. The specific properties of weak polyelectrolyte mutilayers that have been investigated herein are: a) total and incremental layer thickness b) optical absorbance and thickness of chromophore-containing PEMs, c) rate of polyelectrolyte adsorption, d) degree and rate of ion displacement, e) elastic modulus f) adhesive force between polycationic and polyanionic layers, g) temperature and solvent stability of PEMs h) stability of LBL adsorption onto various types of surfaces and substrate geometric constraints, and i) rate of photoisomerization of an azo-containing polyelectrolyte. As described in Chapter 2, various optical spectroscopies and

microscopy techniques will be used to study these properties. The chapters in this dissertation will cover the following subjects:

Chapter 3   Effect of Charge Density and Counterions on the Assembly of Polyelectrolyte Multilayers

The kinetics of LBL adsorption of weakly charged PAH, and azo-cromophore-containing P-Azo, is studied using UV-vis spectroscopy and ellipsometry. The growth of multilayers was examined as function of time and concentration. We show that the weak acid-base nature of the polyelectrolytes is a responsible for anomalously rapid adsorption. The role of counterion displacement in multilayer formation is explored by examining the time-dependant P-Azo adsorption in PAH/P-Azo multilayer formation from polymer solutions containing the counterion series F^-, Cl^-, Br^-, and I^-. These results are used to relate the counterion binding energies with the observed extent of displacement by an adsorbing polymer segment.

Chapter 4   Effect of Chain Length on Layer-by-Layer Adsorption of Polyelectrolytes

We examine competitive adsorption of short versus long chains of polyelectrolytes in formation of multilayer assemblies on a long time-scale. Low and high molecular weight PAA are covalently and quantitatively labeled with two different naphthalene molecules to observe preferential adsorption onto PAH coated silica colloids using fluorescence spectroscopy.

Chapter 5   Structural and Mechanical Properties of Polyelectrolyte Multilayer Films Studied by AFM

Force-distance measurements are acquired for the model PAH/P-Azo multilayer system prepared at varying charge densities. We determine the relative elastic modulus of the films prepared with identical thickness, and compare these values as a function of the ionization fraction of the multilayer films. The elastic modulus implies that a relative "loop length" may be obtained for the multilayer assemblies. An estimate of the relative loop length between "ionic cross-links" in the multilayer films is ascertained by analogy to previously studied covalent cross-linked polymer networks. Force-distance measurements obtained by AFM are also used to compare the relative adhesion values between polycation and polyanion layers in films constructed with varying charge densities. This is done by coating an AFM tip with multilayers and indenting into a multilayer surface capped with an oppositely charged surface polyelectrolyte layer.

Chapter 6   Stable Sensor Layers Self-Assembled onto Surfaces Using Azobenzene-Containing Polyelectrolytes

Functionalized polyelectrolytes with photoisomerizable azobenzene chromophores are multilayered onto various inorganic and metal surfaces and investigated for their suitability as sensor host materials. Films are assessed with respect to the criteria of control over physical layer properties such as layer thickness, versatility to different substrates and adsorption geometries, and stability of the formed layers to heat, solvent, and sonication. We examine the variation of adsorption solution pH to evaluate this parameter as a method for achieving good control over individual layer thickness. The limits of the LBL technique are also tested. Stability of the deposited layers is studied by

determining the extent of desorption in a range of organic solvents, aqueous temperatures up to 100 °C, and cleaning protocols such as sonication. Lastly, laser-induced geometric isomerization of the azobenzene chromophores is investigated to demonstrate an application as a hydroxide ion sensor in highly alkaline media.

1.5   References and Notes

(1)   Grainger, D. W. *Prog. Colloid Polym. Sci.* **1997**, *103*, 243.

(2)   Soriaga, M. P.; Stickney, J.; Bottomley, L. A.; Kim, Y. G., Eds.; *Thin Films: Prepartation, Characterization, Applications*; Kluwer Academic/Plenum Publishers: New York, NY, 2002; Chapters 14–17.

(3)   Forster, S.; Rehahn, M.; Rabe, J. P. *Macromol. Chem. Phys.* **2001**, *202*, 2802.

(4)   Somorjai, G. A. *MRS Bull.* **1998**, *23*, 11.

(5)   Tredgold, R. H. *J. Mater. Chem.* **1995**, *5*, 1095.

(6)   Tirrell, M.; Kokkoli, E.; Biesalski, M. *Surf. Sci.* **2002**, *500*, 61.

(7)   Whitesides, G. M.; Ferguson, G. S.; Allara, D.; Scherson, D.; Speaker, L.; Ulman, A. *Crit. Rev. Surf. Chem.* **1993**, *3*, 49.

(8)   Tertykh, V. A.; Yanishpolskii, V. V. *Surf. Sci. Ser.* **2000**, *90*, 523.

(9)   Blodgett, K. B. *J. Am. Chem. Soc.* **1934**, *56*, 495.

(10)   Langmuir, I.; Schaefer, V. J.; Wrinch, D. M. *Science* **1937**, *85*, 76.

(11)   Kuhn, H.; Möbius, D. *Angew. Chem. Int. Ed. Engl.* **1971**, *10*, 620.

(12)   Ulman, A. *An Introduction to Ultrathin Organic Films: From Langmuir-Blodgett to Self-Assembly*; Academic Press: Boston, MA, 1991; pp 101–219.

(13)   Bell, C. M.; Yang, H. C.; Mallouk, T. E. *Adv. Chem. Ser.* **1995**, *245*, 211.

(14)   Petty, M. C. Organic Thin Film Deposition Techniques. In *Encyclopedia of Nanoscience and Nanotechnoloby*; Nalwa, H. S., Ed.; American Scientific Publishers: Stevenson Ranch, CA, 2004; pp 295–304.

(15)   Tsukruk, V. V. *Prog. Polym. Sci.* **1997**, *22*, 247.

(16)   Nicolau, Y. F. *Appl. Surf. Sci.* **1985**, *22/23*, 1061.

(17)   Decher, G.; Hong, J. D. *Ber. Bunsen-Ges. Phys. Chem.* **1991**, *95*, 1430.

(18) Decher, G.; Hong, J. D.; Schmitt, J. *Thin Solid Films* **1992**, *210/211*, 831.

(19) Lvov, Y.; Decher, G.; Möhwald, H. *Langmuir* **1993**, *9*, 481.

(20) Schlenoff, J. B.; Ly, H.; Li, M. *J. Am. Chem. Soc.* **1998**, *120*, 7626.

(21) Dubas, S. T.; Schlenoff, J. B. *Macromolecules* **1999**, *32*, 8153.

(22) Lvov, Y.; Ariga, K.; Onda, M.; Ichinose, I.; Kunitake, T. *Colloids Surf., A* **1999**, *146*, 337.

(23) Kovacevic, D.; van der Burgh, S.; de Keizer, A.; Cohen Stuart, M. A. *Langmuir* **2002**, *18*, 5607.

(24) Schwarz, B.; Schönhoff, M. *Colloid Surf. A* **2002**, *198*, 293.

(25) Hoogeveen, N. G.; Cohen Stuart, M. A.; Fleer, G. J.; Böhmer, M. R. *Langmuir* **1996**, *12*, 3675.

(26) Joanny, J. F. *Eur. Phys. J. B* **1999**, *9*, 117.

(27) Joanny, J. F. *J. Phys.: Condens. Matter* **2000**, *12*, A1.

(28) Riegler, H.; Essler, F. *Langmuir* **2002**, *18*, 6694.

(29) Lee, S. S.; Hong, J. D.; Kim, C. H.; Kim, K.; Koo, J. P.; Lee, K. B. *Macromolecules* **2001**, *34*, 5358.

(30) Chiarelli, P. A.; Johal, M. S.; Holmes, D. J.; Casson, J. L.; Robinson, J. M.; Wang, H. L. *Langmuir* **2002**, *18*, 168.

(31) Lee, S. S.; Lee, K. B.; Hong, J. D. *Langmuir* **2003**, *19*, 7592.

(32) Sukhorukov, G. B.; Donath, E.; Lichtenfeld, H.; Eberhard K.; Knippel, M.; Budde, A.; Möhwald, H. *Colloids Surf., A* **1998**, *137*, 253.

(33) Schlenoff, J. B.; Dubas, S. T. *Macromolecules* **2001**, *34*, 592.

(34) Picart, C.; Lavalle, P.; Hubert, P.; Cuisinier, F. G.; Decher, G.; Schaaf, P.; Voegel, J. C. *Langmuir* **2001**, *17*, 7414.

(35) Ariga, K.; Lvov, Y.; Kunitake, T. *J. Am. Chem. Soc.* **1997**, *119*, 2224.

(36) Advincula, R. C.; Baba, F. K. *Polym. Mat. Sci. Eng.* **1999**, *81*, 95.

(37) Mao, G.; Tsao, M.; Tirrell, H. T.; Davis, V.; Hessel, V.; Ringsdorf, H. *Langmuir* **1993**, *9*, 3461.

(38) Tredgold, R. H.; Winter, C. S.; El Badawy, Z. I. *Electronic Lett.* **1985**, *21*, 554.

(39) Saremi, F.; Tieke, B.; Jordan, G.; Rammensee, W. *Supramol. Sci.* **1997**, *4*, 471.

(40) van Ackern, R.; Krasemann, L.; Tieke, B. *Thin Solid Films* **1998**, *327*, 762.

(41) Caruso F.; Kurth, D. G.; Volkmer, D.; Koop, M. J.; Müller, A. *Langmuir* **1998**, *14*, 3462.

(42) Sun, J.; Gao, M.; Zhu, M.; Feldmann, J.; Möhwald, H. *J. Mater. Chem.* **2002**, *12*, 1775.

(43) Liu, Y.; Wang, R. O. *Appl. Phys. Lett.* **1997**, *71*, 2265.

(44) Forzani, E. S.; Perez, M. A.; Teijelo, M. L.; Calvo, E. J. *Langmuir* **2002**, *18*, 9867.

(45) Rilling, P.; Walter, T.; Pommersheim, R.; Vogt, W. *J. Membr. Sci.* **1997**, *129*, 283.

(46) Kirstein, S.; Bourbon, S.; Gao, M. Y.; Derossi, U. *Isr. J. Chem.* **2000**, *40*, 129.

(47) Sukhorukov, G. B.; Schmitt, J.; Decher, G. *Ber Bunsen-Ges. Phys. Chem.* **1996**, *100*, 948.

(48) Dubas, S. T.; Schlenoff, J. B. *Langmuir* **2001**, *17*, 7725.

(49) Kugler, R.; Schmitt, J.; Knoll, W. *Macrmol. Chem. Phys.* **2003**, *203*, 413.

(50) Gao, C.; Leporatti, S.; Moya, S.; Donath, E.; Möhwald, H. *Chem.—Eur. J.* **2003**, *9*, 915.

(51) Hiller, J.; Rubner, M. F. *Macromolecules* **2003**, *36*, 4078.

(52) Dai, J. H.; Bruening, M. L. *Nanoletters* **2002**, *2*, 497.

(53) Cott, K. E.; Guzy, P. N.; Brands, C.; Heflin, I. R.; Gibson, H. W.; Davis, R. A. *Angew. Chem., Int. Ed. Engl.* **2002**, *41*, 3236.

(54) Moya, S.; Sukhorukov, G. B.; Auch, M.; Donath, E.; Möhwald, H. *J. Colloid Interface Sci.* **1999**, *216*, 297.

(55) Caruso, F.; Yang, W.; Trau, D.; Renneberg, R. *Langmuir* **2000**, *16*, 8932.

(56) Radtchenko, I. L.; Sukhorukov, G. B.; Leporatti, S.; Khomutov, G. B.; Donath, E.; Möhwald, H. *J. Colloid Interface Sci.* **2000**, *230*, 272.

(57) Shi, X.; Caruso, F. *Langmuir* **2001**, *17*, 2036.

(58) Radtchenko, I. L.; Sukhorukov, G. B.; Möhwald, H. *Int. J. Pharm.* **2002**, *242*, 219.

(59) Fery, A.; Schoeler, B.; Cassagneau, T.; Caruso, F. *Langmuir* **2001**, *17*, 3779.

(60) Sui, Z.; Schlenoff, J. B. *Langmuir* **2003**, *19*, 7829.

(61)   Mendelsohn, J. D.; Barrett, C. J.; Chan, V. V.; Pal, A. J.; Mayes, A. M.; Rubner, M. F. *Langmuir* **2000**, *16*, 5017.

(62)   Bruening, M. L.   Controlling the ion-permeability of layered polyelectrolyte films and membranes. In *Multilayer Thin Films: Sequential Assembly of Nanocomposite Materials*; Decher, G., Schlenoff, J. B., Eds.; Wiley-VCH: Germany, Weinheim, 2003; pp 487–510.

(63)   Bruening, M. L.; Stanton, B.; Liu, X.; Harris, J. J. *Polym. Mater. Sci. Eng.* **2003**, *89*, 169.

(64)   Quinn, R.; Laciak, D. V.; Appleby, J. B.; Pez, G. P. Polyelectrolyte Membranes for the Separation of Acid Gases. U.S. Patent 5336298 A, April 9, 1994.

(65)   Levaesalmi, J. M.; McCarthy, T. J. *Macromolecules* **1997**, *30*, 1752.

(66)   Tieke, B.; van Ackern, F.; Krasemann, L.; Toutianoush, A. *Eur. Phys. J. E* **2001**, *5*, 29.

(67)   Hammond, P. *Curr. Opin. Colloid Interface Sci.* **2000**, *4*, 430.

(68)   Graul, T. W.; Schlenoff, J. B. *Anal. Chem.* **1999**, *71*, 4007.

(69)   Thierry, B.; Winnik, F. M.; Merhi, Y.; Silver, J.; Tabrizian, M. *Biomacromolecules* **2003**, *4*, 1564.

(70)   Thierry, B.; Winnik, F. M.; Merhi, Y.; Tabrizian, M. *J. Am. Chem. Soc.* **2003**, *125*, 7494.

(71)   Rubner, M. F.; Mendelsohn, J. D.; Yang, S. Y. Method of Depositing Polyelectrolyte Multilayers and Articles Coated Thereby. PCT Int. Appl. WO 2003035278 A1, May 1, 2003.

(72)   Wang, L.; Fu, Y.; Wang, Y.; Sun, C.; Fang, Y.; C.; Zang, X. *Macromol. Chem. Phys.* **1999**, *200*, 1523.

(73)   Lvov, Y. M.; Rusling, J. F.; Thomsen, D. C.; Papadimitrakopoulos, T.; Kunitake, K. T. *J. Chem. Soc., Chem. Commun.* **1998**, 1229.

(74)   Fendler, J. J. *Stud. Surf. Sci. Catal.* **1997**, *103*, 261.

(75)   Kotov, A.; Dekany, I.; Fendler, J. H. *J. Phys. Chem.* **1995**, *99*, 13065.

(76)   He, J. A.; Samuelson, L.; Li, J.; Kumar, J.; Tripathy, S. K. *Langmuir* **1998**, *14*, 1674.

(77)	Menchaca, J. L.; Flores, H.; Cuisinier, F.; Pérez, E. *J. Phys. Condens. Matter* **2004**, *16*, S2109.

(78)	Hattori, H. *Adv. Mater.* **2001**, *13*, 51.

(79)	Hiller J.; Mendelsohn, J. D.; Rubner, M. F. *Nature Materials* **2002**, *1*, 59.

(80)	Baur, J. W.; Kim, S.; Balanda, P. B.; Reynolds, J. R.; Rubner, M. F. *Adv. Mater.* **1998**, *10*, 1452.

(81)	Yoo, D.; Wu, A.; Lee, J.; Rubner, M. F. *Synth. Met.* **1997**, *85*, 1425.

(82)	Lvov, Y.; Decher, G. *Crystal. Rep.* **1994**, *39*, 628.

(83)	Smith, R.; Reven, L.; Barrett, C. J. *Macromolecules* **2003**, *36*, 1876.

(84)	Burke, S. E.; Barrett, C. J. *Langmuir* **2003**, *19*, 3297.

(85)	Decher, G.; Schmitt, J. *Prog. Colloid Polym. Sci.* **1992**, *89*, 160.

(86)	Shiratori, S. S.; Rubner, M. F. *Macromolecules* **2000**, *33*, 4213.

(87)	Lvov, U.; Decher, G.; Haas, H.; Möhwald, H.; Kalachev, A. *Physica B* **1994**, *198*, 89.

(88)	Clark, S. L.; Montague, M. F.; Hammond, P. T. *Macromolecules* **1997**, *30*, 7237.

(89)	Lösche, M.; Schmitt, J.; Decher, G.; Bouwman, W. G.; Kjaer, K. *Macromolecules* **1998**, *31*, 8893.

(90)	Arys, X.; Jonas, A. M.; Laguitton, B.; Legras, R.; Leschewsky, A.; Wischerhoff, E. *Prog. Org. Coat.* **1998**, *34*, 108.

(91)	Schönhoff, M. *J. Phys.: Condens. Matter* **2003**, *15*, R1781.

(92)	von Klitzing, R.; Tieke, B. *Adv. Poly. Sci.* **2004**, *165*, 177.

(93)	Decher, G. *Science* **1997**, *277*, 1232.

(94)	Lukkari, J.; Salomaeki, M.; Viinikanoja, A.; Aeaeritalo, T.; Paukkunen, J.;

(95)	Kim, B.S.; Vinogradova, O. I. *J. Phys. Chem. B* **2004**, *108*, 8161.

(96)	Liu, X.; Bruening, M. L. *Chem. Mater.* **2004**, *16*, 351.

(97)	Jiang, C.; Markutsya, S.; Tsukruk, V. V. *Adv. Mater.* **2004**, *16*, 157.

(98)	Wang, L.; Schönhoff, M.; Möhwald, H. *J. Phys. Chem. B* **2004**, *108*, 4767.

(99)	Koetse, M.; Laschewsky, A.; Jonas, A. M.; Verbiest, T. *Colloids Surf., A* **2002**, *198*, 275.

(100)	Voigt, U.; Jaeger, W.; Findenegg, G. H.; von Klitzing, R. *J. Phys. Chem. B* **2003**, *107*, 5273.

(101) Pavoor, P. V.; Gearing, B. P.; Bellare, A.; Cohen, R. E. *Wear* **2004**, *256*, 1196.

(102) Burke, S. E.; Barrett, C. J. *Biomacromolecules*, **2003**, *4*, 1773.

(103) Lavalle, P.; Gergely, C.; Cuisinier, F. J.; Decher, G.; Schaaf, P.; Voegel, J. C.; Picart, C. *Macromolecules* **2002**, *35*, 4458.

(104) Lavalle, P.; Picart, C.; Mutterer, J.; Gergely, C.; Reiss, H.; Voegel, J. C.; Senger, B.; Schaaf, P. *J. Phys. Chem. B* **2004**, *108*, 635.

(105) Schmitt, J.; Grünewald, T.; Kjaer, K.; Pershan, P.; Decher, G.; Lösche, M. *Macromolecules* **1993**, *26*, 7058.

(106) Kellog, G. J.; Mayes, A. M.; Stockton, W. B.; Ferreira, M.; Rubner, M. F.; Satija, S. K. *Langmuir* **1996**, *12*, 5109.

(107) Laschewsky, A.; Mayer, B.; Wischerhoff, E.; Arys, X.; Jonas, A. *Ber. Bunsen-Ges. Phys. Chem.* **1996**, *100*, 1033.

(108) Cochin, D.; Pabmann, M.; Wilbert, G.; Zental, R. *Macromolecules* **1997**, *30*, 4775.

(109) Hong, H.; Steitz, R.; Kirstein, S.; Davidov, D. *Adv. Mater.* **1998**, *10*, 1104.

(110) Arys, X.; Lashewsky, A.; Jonas, A. M. *Macromolecules* **2001**, *34*, 3318.

(111) Panchagnula, V.; Jeon, J.; Dobrynin, A.V. *Phys. Rev. Lett.* **2004**, *93*, 037801.

(112) Schlenoff, J. B.; Li, M. *Ber. Bunsen-Ges. Phys. Chem.* **1996**, *100*, 943.

(113) Kovacevic, D.; van der Burgh, S.; de Keizer, A.; Cohen Stuart, M. A. *Langmuir* **2002**, *18*, 5607.

(114) Fleer, G.; Hoogeveen, N. G.; Cohen Stuart, M. A. *Langmuir* **1996**, *12*, 3675.

(115) Lowack, K.; Helm, C. A. *Macromolecules* **1998**, *31*, 823.

(116) Plech, A.; Salditt, T.; Munster, C.; Peisl, J. *J. Colloid Interface Sci.* **2000**, *223*, 74.

(117) Leporatti, S.; Gao, C.; Voigt, A.; Donath, E.; Möhwald, H. *Eur. Phys. J. E* **2001**, *5*, 13.

(118) Netz, R. R.; Joanny, J.F. *Macromolecules* **1999**, *32*, 9013.

(119) Ladam, G.; Schaad, P.; Voegel, J. C.; Schaaf, P.; Decher, G.; Cuisinier, F. *Langmuir* **2000**, *16*, 1249.

(120) Steitz, R.; Leiner, V.; Siebrecht, R.; von Klitzing, R. *Colloids Surf., A* **2000**, *163*, 63.

(121) Steitz, R.; Jaeger, W.; von Klitzing, R. *Langmuir* **2001**, *17*, 4471.

(122) von Goeler, F.; Muthukumar, M. *J. Chem. Phys.* **1994**, *100*, 7796.

(123) Ladam, G.; Schaaf, P.; Cuisinier, F. J.; Decher, G.; Voegel, J. C. *Langmuir* **2001**, *17*, 878.

(124) Sukhishvili, S. A.; Granick, S. *J. Chem. Phys.* **1998**, *109*, 6869.

(125) Ulrike, V.; Jaeger, W.; Findenegg, F.; von Klitzing, R. *J. Phys. Chem. B* **2003**, *107*, 5273.

(126) von Klitzing, R.; Steitz, R. Internal Structure of Polyelectrolyte Multilayers. In *Handbook of Polyelectrolytes and Their Applications*; Tripathy, S. K.; Kumar, J.; Nalwa, H.S., Eds.; American Scientific Publishers: Stevenson Ranch, CA, 2002; Vol. 1; pp 313–334.

(127) Zollinger, H. *Azo and Diazo Chemistry*; Interscience: New York, **1961**.

(128) Zollinger, H. *Colour Chemistry. Synthesis, Properties, and Applications of Organic Dyes*; VCH: Weinheim, **1987**.

(129) Rau, H. *Photochemistry and Photophysics*; Rabek, J. F. Ed.; CRC Press: Boca Ratan, **1990**; Vol. 9, Chapter 4.

(130) Rau, H. *Photochromism: Molecules and Systems*; Dürr, H. Ed.; Elsevier: New York, **1990**; Chapter 4.

(131) Toutianoush, A.; Tieke, B. *Macromol. Rapid Commun.* **1998**, *19*, 591.

(132) Saremi, F.; Tieke, B. *Adv. Mater.* **1998**, *10*, 388.

(133) Wang, H.; He, Y.; Tuo, X.; Wang, X. *Macromolecules* **2004**, *37*, 135.

(134) Hong, J. D.; Park, E. S.; Park, A. L. *Langmuir* **1999**, *15*, 6515.

(135) Viswanathan, N. K.; Balasubramanian, S.; Li, L.; Kumar, J.; Tripathy, S. K. *J. Phys. Chem. B* **1998**, *102*, 6064.

(136) Norman, L. L.; Barrett, C. J. *J. Phys. Chem. B* **2002**, *106*, 8499.

(137) Barrett, C.; Natansohn, A.; Rochon, P. *Macromolecules* **1994**, *27*, 4781.

(138) Mita, I.; Horie, K.; Hirao, K. *Macromolecules* **1989**, *22*, 558.

(139) Naito, T.; Horie, K.; Mita, I. *Polym. J.* **1991**, *23*, 809.

(140) Kobayashi, T.; Degenkolb, E. O.; Rentzepis, P. M. *J. Phys. Chem.* **1979**, *83*, 2431.

(141) Lednev, I.; Ye, T.; Hester, R.; Moore, J. *J. Phys. Chem.* **1996**, *100*, 13338.

(142) Tabek, D.; Morawetz, H.; *Macromolecules* **1970**, *3*, 403.

(143) Ueda, M.; Kim, H.; Ikeda, T.; Ichimura, K. *Chem. Mater.* **1992**, *4*, 1229.

(144) Morishima, Y.; Tsuji, M.; Seki, M.; Kamachi, M. *Macromolecules* **1993**, *26*, 3299.

(145) Angiolini, L.; Caretti, D.; Carlini, C. *J. Polym. Sci. A* **1994**, *32*, 1159.

(146) Haitjema, H.; Tan, Y.; Challa, G. *Macromolecules* **1995**, *28*, 2783.

(147) Sanchez, A. M.; de Rossi, R. H. *J. Org. Chem.* **1995**, *60*, 2974.

(148) Böhm, N.; Materny, A.; Kiefer, W.; Müller, M.; Schottner, G. *Macromolecules* **1996**, *29*, 2599.

(149) Barrett, C.; Natansohn, A.; Rochon, P. *Chem. Mater.* **1995**, *7*, 899.

(150) Sekkat, Z.; Knoll, W. Photoisomerization and Photo-orientation of Azo Dye in Films of Polymer: Molecualr Interaction, Free Volume, and Polymer Structural Effects . In *Photoreactive Organic Thin Films*; Academic Press: San Diego, CA, 2002; Vol. 133. pp 107–143.

(151) Yitzchaik, S.; Kakkar, A. K.; Roscoe, S. B.; Orihashi, Y.; Marks, T. J.; Lin, W.; Wong, G. K. *Mol. Cryst. Liq. Cryst. Sci. Tech. Sect. A* **1994**, *240*, 9.

(152) Diederich, A.; Losche, M. *Adv. Biophys.* **1997**, *34*, 205.

(153) Laschewsky, A.; Wischerhoff, E.; Kauranen, M.; Persoons, A. *Macromolecules* **1997**, *30*, 8304.

(154) Yamada, T.; Shiratori, S. *Mol. Crys. Liq. Crys. Sci.Technol. Sect. A* **2001**, *370*, 289.

(155) Luo, S.; Lo, K. P.; Groger, H. P.; Churchill, R. J. Optical chemical sensor based on multilayer self-assembled thin film sensors for aquaculture process control. US Patent 6051437, May 4, 1998.

Chapter 2

Experimental Techniques

2.1 Preface

This chapter describes the main methods that were used to examine various properties of the polyelectrolyte multilayer films. These techniques include spectroscopic methods (such as UV-vis spectroscopy, and fluorescence spectrophotometry), an optical reflectivity method (using an ellipsometer), and a microscopy-based technique (using an atomic force microscope).

2.2 UV-vis Spectroscopy

UV-visible spectroscopy is an optical technique involving the measurement of the wavelength and absorption intensity of near-ultraviolet and visible light (approximately 190–750 nm) through a sample, thereby probing the electronic transitions of molecules. In this electromagnetic spectral region, the energy is sufficient to promote valence electrons of low excitation energy to higher energy levels (i.e., transitions of n or π electrons to the π^* excited state in organic molecules containing chromophores). UV-vis spectroscopy can be used for quantitative measurements and characterization of the optical or electronic properties of materials.[1]

Generally, the absorbance spectrum of a material is obtained, which shows absorption bands corresponding to structural groups within the molecule. An important

aspect of UV-vis spectroscopy is the relation of absorbance (A) to the concentration of analyte, c, in the sample as given by the Beer–Lambert law,

$$A = \varepsilon c\, l \tag{2.1}$$

where ε is the extinction coefficient, and l is the path length (or thickness of the sample). It allows us to calculate the concentration from the absorbance if ε and l are known. In polyelectrolyte multilayer characterization, UV-vis spectra were obtained for PEM films prepared from P-Azo polyanions to quantify its adsorption through the layers. The absorbance maximum was optically tracked at $\lambda = 365$ nm as a function of the number of layers deposited.

Standard instrumentation includes a hydrogen or deuterium lamp, which is used for UV measurements, while a tungsten lamp is generally the light source for visible measurements.[1] Selection of the wavelengths from these continuous light sources is achieved using a wavelength separator such as a prism or grating monochromator. Spectra are acquired by scanning the wavelength separator and quantitative measurements can be made from a spectrum or at a single wavelength.

UV-vis lamp   lens   monochromator   sample   detector   amplifier
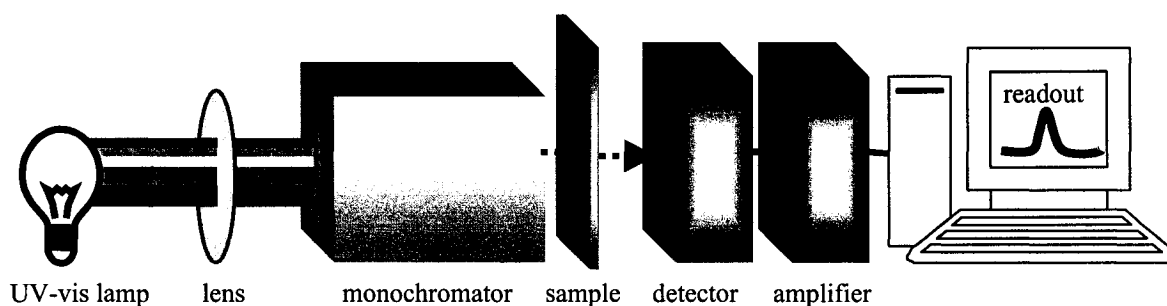
Figure 2.1   Instrumentation of a UV-vis spectrophotometer.

2.3 Ellipsometry

Ellipsometry is a common reflectance-based thin film technique that uses polarized light to characterize the dielectric properties of a flat sample.[2,3] An ellipsometer monitors the change in the state of polarization and intensity of a reflected beam of light (from the various interfaces of a film sample) upon shining incident light onto a sample surface at an oblique angle.[2-4] As depicted in Figure 2.2, an incident linearly polarized light is reflected off a film surface as elliptically polarized. The instrumentation thus requires a light source, a polarizer, a rotating analyzer (relative to the polarizer) and a detector. For a film containing various interfaces, the resultant reflected beam is comprised of the initial reflected beam and the series of beams which are transmitted through all the interfaces. According to Equation 2.2, reflection from the surface induces a phase shift of light reflected parallel (p) and perpendicular (s) to the incident plane, and amplitude reduction of these two waves.

$$\tan{(\Psi)}\,e^{(i\Delta_\lambda)} = \frac{R_p}{R_s} \qquad (2.2)$$

At various incidence angles, the p- and s-polarized components are reflected differently. In practice, data values for the ellipsometric angles delta (Δ_λ) and psi (Ψ), are acquired for a given wavelength and incident angle (respectively related to the relative phase shift, and reflection amplitude relationships between the p- and s-wave). For a given multi-interface surface, the Fresnel reflection coefficients in the two planes, R_s and R_p, define the ratio of the magnitude of the resulting outgoing wave (reflected electric field amplitude) to the magnitude of the incoming wave (initial electric field).[5]

By analyzing the state of polarization in light reflected from the sample, one can

determine properties such as thickness and refractive index for film layers that are thinner

than the wavelength of light (i.e., on the order of angstroms). An optical model describing

the sample structure and accounting for all layers is required to obtain parameters such as

thickness and other optical constants by determining the best fit to experimental values.[5]

Incident | **Reflection**
linear polarized light | **elliptical polarized light**
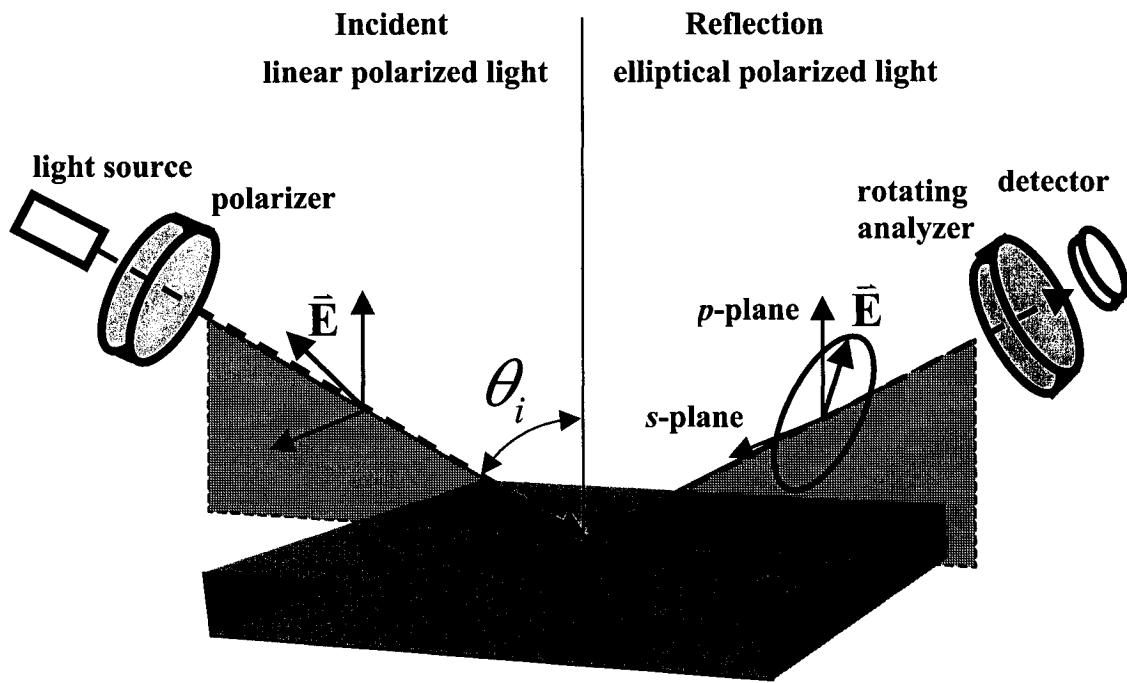
Figure 2.2   Schematic representation of the ellipsometry technique, where a linear polarized input beam of electric field $\bar{E}$ is reflected from a surface, converted and detected as elliptically polarized light.

For analysis of multilayer films a 3-layer model is used. The substrate layer Si is given a

fixed refractive index (n_s = 3.875) and extinction coefficient (k_s = -0.018). The SiO_2 layer

is also given a fixed refractive (n_o = 1.458) and the thickness of this oxide layer is experimentally determined (~27 Å). The multilayer film is treated as a single polymer layer and the thickness and refractive index are independently determined. In order to determine the thickness and refractive index of the multilayer film, an estimated refractive index (in the range of n_p = 1.5–1.6) and thickness must be supplied since there are multiple solutions to delta (Δ_λ) and psi (Ψ). The multilayer film and SiO_2 is assumed to have a negligible absorption coefficient at the laser wavelength (λ = 632 nm). In all ellipsometry measurements, the thickness values of the polyelectrolyte multilayer films were obtained in air and the measured refractive index of the film was found to be in the expected range for common organic polymers.

Applications of ellipsometry to surface characterization include analysis of surface film formation[6] (i.e., thickness measurements of adsorbed polymers[9] and proteins[10]), and determination of surface optical properties (such as the index of refraction),[7,8] The advantage of ellipsometry in thin film characterization is that it measures a ratio of two values (the Fresnel reflection coefficients). Thus even using low intensity of light, highly accurate and reproducible measurements can be obtained without requiring a reference sample.

2.4   Atomic Force Microscopy- Nanoindentation Measurements

Atomic force microscopy (AFM) is an optical lever technique in which a sharp probe (such as a tip on the end of a cantilever) is raster scanned over-the-top of a surface and receives topographical information about the surface in response to the force between a tip (usually Si_3N_4) and a sample.[11] The technique is based on detection of laser light

reflection from the cantilever into a split photodiode as a result of the bending of the cantilever. For small deflection, d, we can assume that the cantilever behaves according to Hooke's law,

$$F = k\,d \tag{2.3}$$

where F is the loading force and k is cantilever spring constant. In practice, a piezoelectric crystal is used to make small and precise movements of the tip or sample towards one another. The deflection is the difference between the z-movement of the piezoelectric crystal and the consequent indentation, δ, of the surface.[12-14] In imaging, an electronic feedback is used to allow the piezoelectric to respond to changes in force as the tip–sample separation changes and alter the separation to restore the force to a fixed value. This mode of operation has been coined "constant force". In the simplest method of obtaining an image, the tip and sample are maintained in close contact as the surface is scanned. While this is the most common method of imaging, lateral forces from dragging the tip over the sample can contribute to poor imaging.

While traditionally the AFM method has primarily been used for high-resolution imaging of surfaces (i.e., on the nanometer scale), recently this technique has been successfully extended to perform nanomechanical measurements on soft polymer-coated films.[12-15] The AFM can provide information about the amount of force felt by the cantilever as the probe tip is brought close to, and indented into a sample surface and then pulled away, as suggested in Figure 2.3. Through the measurement of force over the vertical indentation depth, one can determine for example, the elasticity of a polymer

film.[12,14] This is achieved by indenting a tip (usually with a radius r, on the order of tens of nanometers) onto a planar surface. Through this process, a force curve is obtained, which is related to the interaction between the tip and the sample at a given separation/indentation value.

Attractive and repulsive forces are measured

for a series of distances

$r \sim 35$ nm
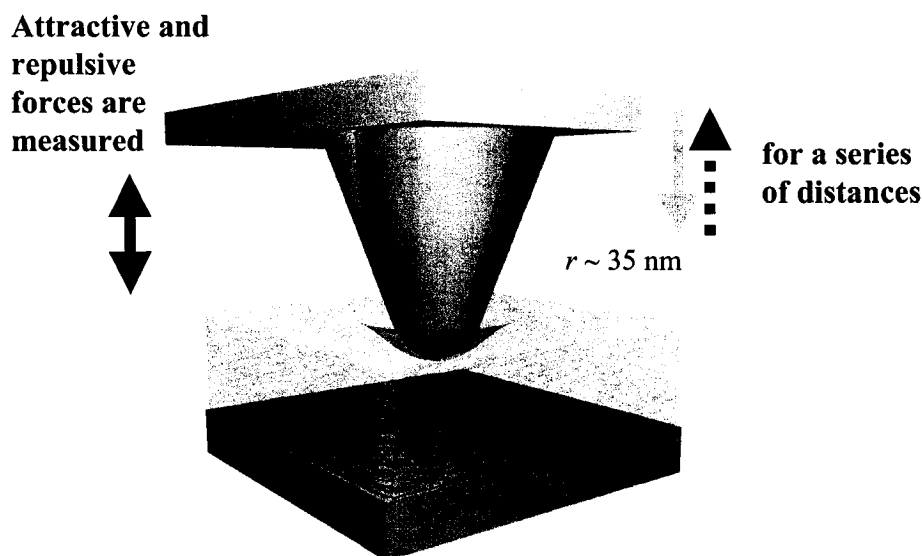
Figure 2.3 A schematic illustration showing the indentation of an AFM tip into a soft film.

To obtain a force curve, the vertical position of the tip is varied systematically with respect to the sample. As the tip indents the sample, the acting force leads to bending in the cantilever. In the approach segment of the curve, the tip begins to feel an attractive potential towards the surface at a given inter-molecular distance. This attractive force causes the bending of the cantilever towards the surface until the tip "jumps-to-contact" the surface. The net attractive force then vanishes when both the attractive and repulsive interaction forces exactly balance each other. Eventually, as indentation progresses, deformation of the sample occurs, which leads to the observation of repulsive

forces between the tip and sample. The retraction of the tip is then invoked after a given maximum force is achieved and force, as a function of separation, is recorded in the reverse direction. Notably, the force curve is not traced exactly in the retraction portion of the cycle. This is especially evident in the "snap-off" portion of the curve, which is primarily attributed to the combination of various tip–surface inter-molecular adhesion forces. The main regimes of this force-distance method are depicted in Figures 2.4a–2.4f.

Nanomechanical information about our multilayer systems was extracted from force-distance measurements obtained in aqueous solution. Analysis of the region of indentation into the film (i.e., specifically the change in the slope of the linear regime of the indentation) allowed determination of the film elasticity in a manner similar to previous described methods.[12] This procedure is discussed in detail in Chapter 5.
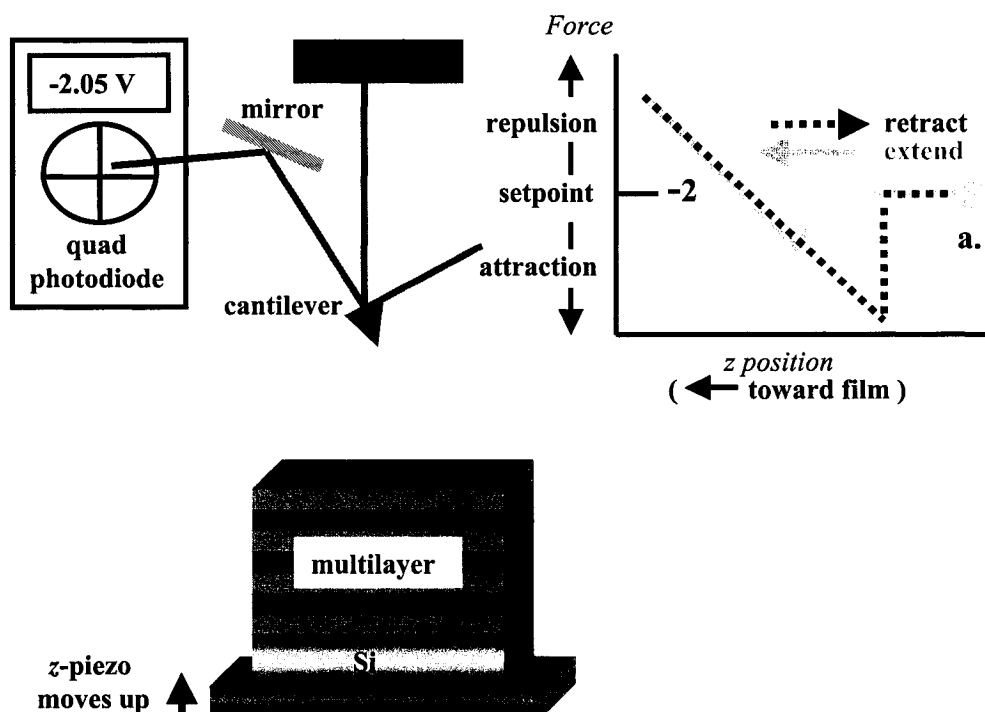
Figure 2.4a Initially, the tip–sample separation is large and there is no interaction force. The piezoelectric (piezo) is moved upward to bring the sample towards the tip.
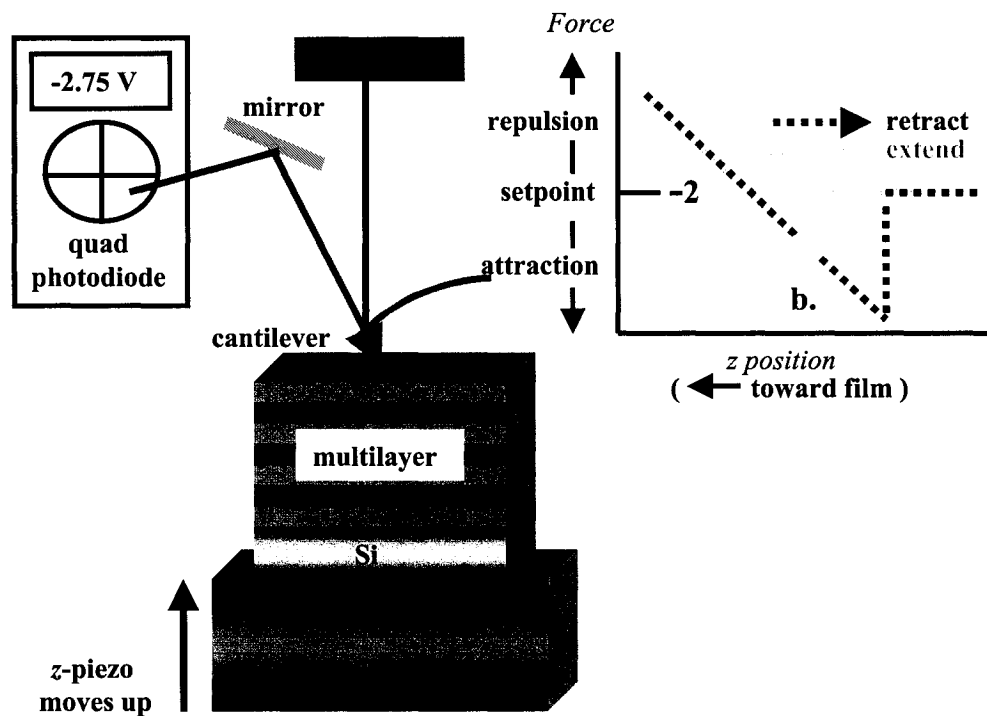
Figure 2.4b An attractive potential at small tip–surface separation causes the tip to "jump-to-contact" and the cantilever bends, which moves the deflected light position.
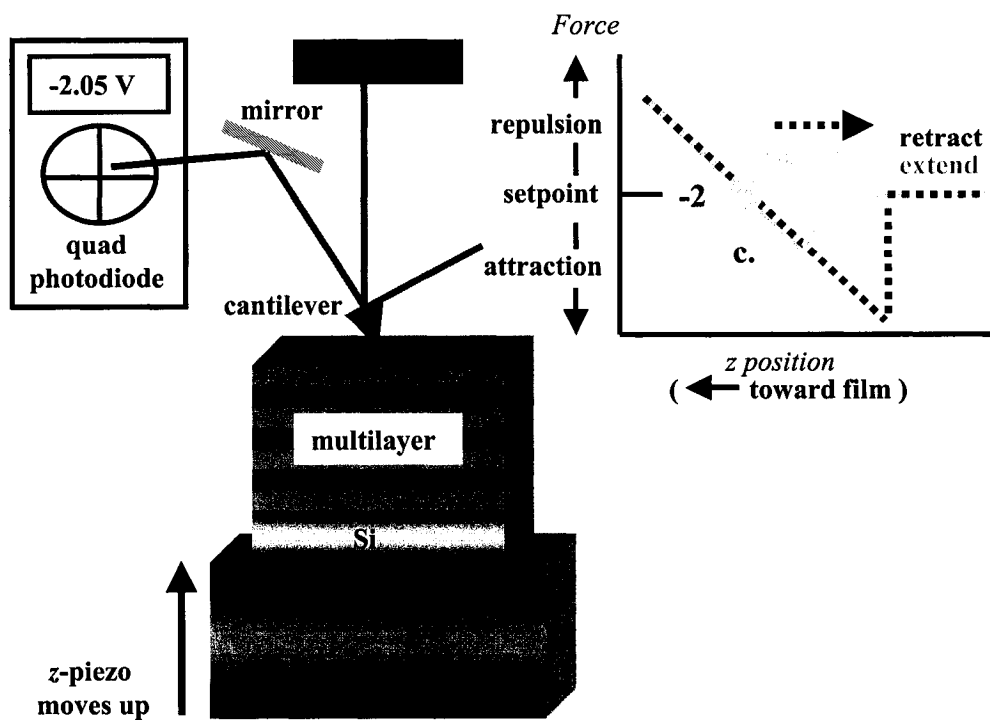
Figure 2.4c The sample and tip are in contact with no net force being exhibited and thus the cantilever does not bend.
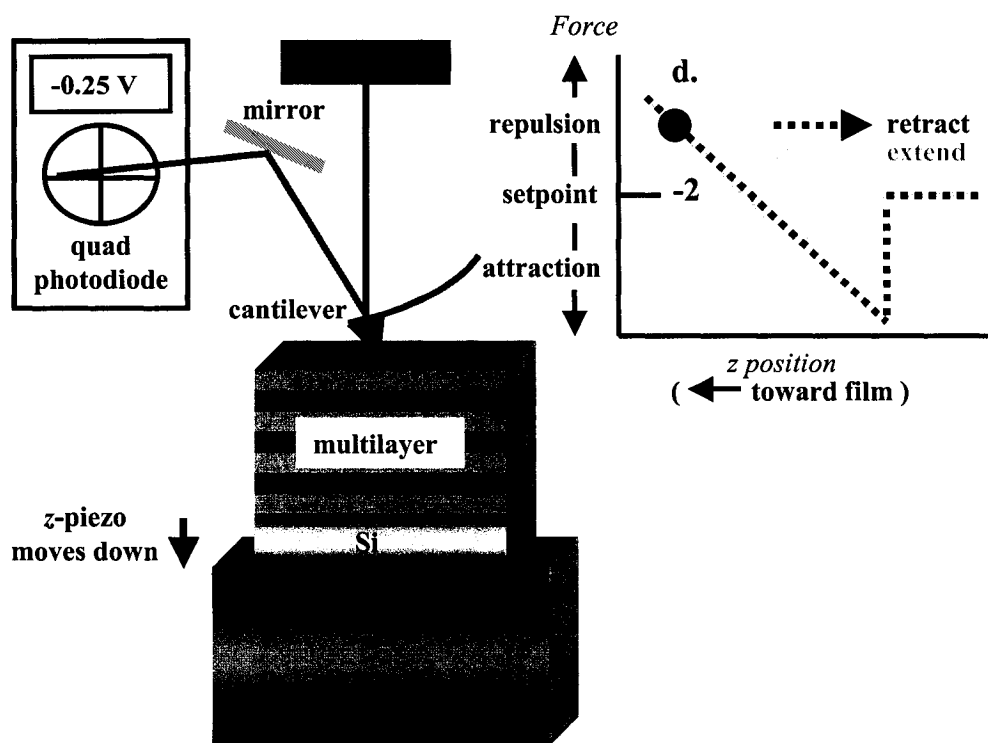
Figure 2.4d Light deflection related to surface indentation occurs due to repulsive interaction. After full extension, the piezo reverses direction for the retraction segment.
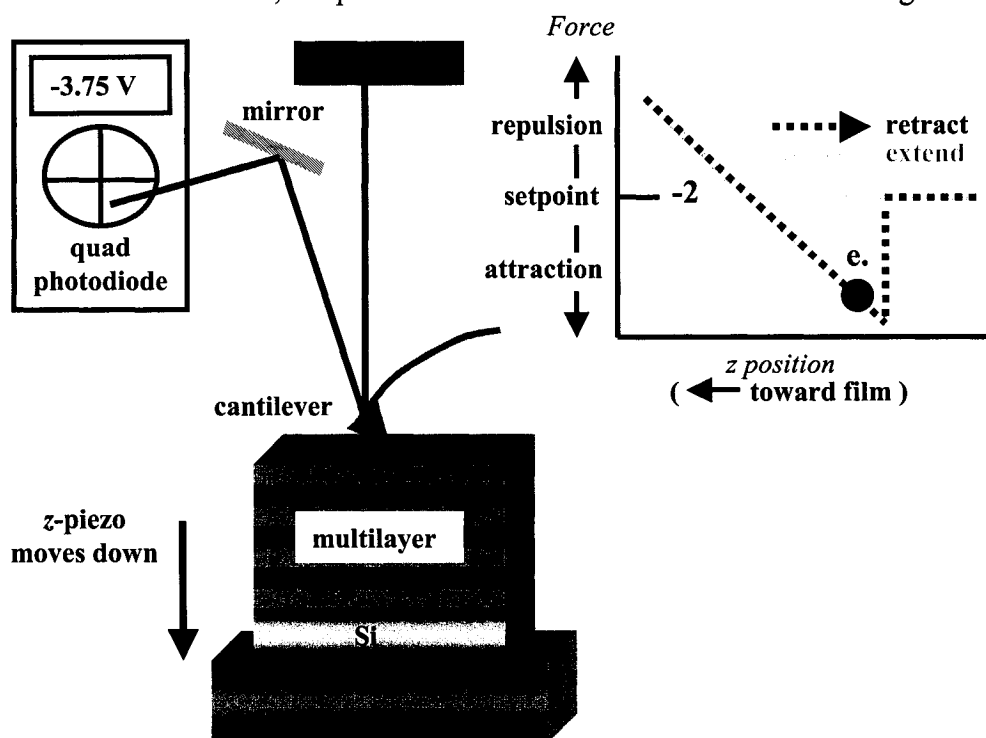
Figure 2.4e Tip continues to retract from the surface with attractive forces bending the cantilever.

49
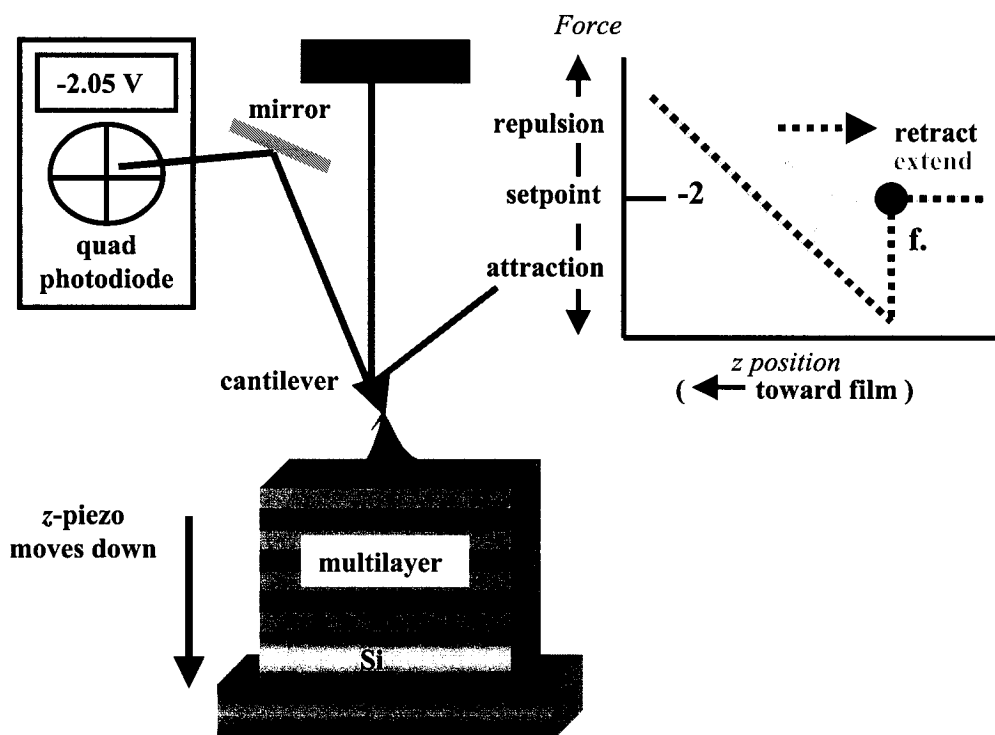
Figure 2.4f The tip "snaps-off" the surface after a sufficient degree of retraction, bringing the cantilever to neutral position.

2.5 Fluorescence Spectrophotometry

Fluorescence is a three-stage photophysical process that occurs when certain molecules, called fluorophores, emit photons (of a longer wavelength) after absorption of shorter wavelength photons. This occurs as result of excitation of the molecule to a higher electronic energy state. As illustrated in a Jablonski energy diagram (shown in Figure 2.5) a fluorophore, which is originally in its ground electronic state at room temperature (S_o) first absorbs energy ($h\,\nu_{excitation}$) in a transition that brings its energy to a higher electronic singlet state, S_1'.[16,17] The absorption process is very rapid, occurring on the order of 10^{-15} s.[18] After this time, the fluorophore may undergo conformational changes and various possible interactions with its molecular environment. As a result,

relaxation of the molecule to the lowest vibrational level of this excited state, S_1, follows

in a process known as internal conversion (approximately 10^{-12} s).[18]
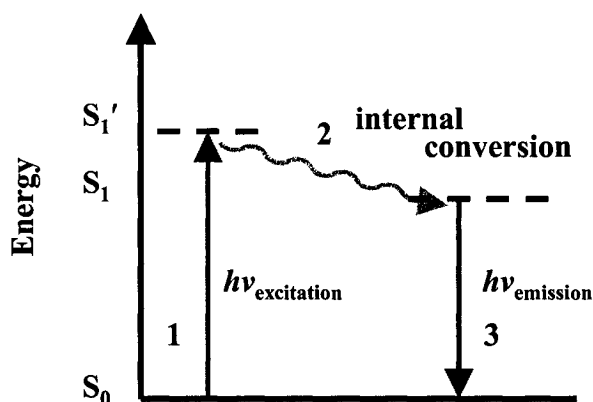
Figure 2.5 A simplified Jablonski diagram showing the fluorescence process by: **1.** excitation of a ground state fluorophore, S_o, to an electronic energy level, S_1', followed by **2.** relaxation to a lower vibrational level, S_1, and lastly **3.** radiative emission at a longer wavelength. Note that competing processes such as collisional quenching have been omitted for simplicity.

After the excited molecule has dissipated its energy in this manner radiative fluorescence

emission ($h\,v_{emission}$), originating from the lower energy S_1 state, then occurs on the order

of 10^{-9} s to bring the molecule back down to the ground state energy (at a higher

wavelength than the excitation).[18] Both fluorescence and non-radiative processes, such as

collision quenching, can compete to depopulate the S_1 state.

The difference in excitation and emission energy is known as the Stokes shift and

is fundamental to this highly sensitive analytical technique. It allows emission photons to

be detected against a low background, isolated from excitation photons. Therefore,

fluorescence, unlike absorbance spectrophotometry, is highly specific due to the fact that

few materials both absorb and emit light at the same wavelength. Also, by labelling with

fluorophores, which have a known and unique excitation and emission energy, it is unlikely that potentially absorbing non-target compounds will emit light at a wavelength similar to the target being detected.

An important aspect of fluorescence detection is that the same fluorophore can be repeatedly excited and detected. The entire fluorescence process is thus cyclical. A single fluorophore can generate many thousands of detectable photons, which contributes to making this optical detection technique a highly sensitive one (usually concentrations on the order of 1 ppm are sufficient for detection). However, a limiting factor in fluorescence detection is the competing photochemical process known as photobleaching. This occurs when excited state fluorophores are irreversibly destroyed as a result of high intensity illumination.

In the work described in Chapter 4, we use fluorescence spectrophotometry to track the preferential adsorption of short versus long chains of PAA onto a PAH covered colloidal surface. Poly(acrylic acid) chains of two extreme molecular weights are selectively and quantitatively labeled with two different naphthalene-based fluorophores, 5-dimethylaminonaphthalene-1-(N-(2-aminoethyl))sulfonamide (dansyl ethylenediamine, or D112), and 1-naphthalmethylamine (NMA) by covalently attaching the fluorophore amine units to the carboxylic acid of the polyanion.[19] The structures of the aromatic fluorophores used are shown in Figure 2.6 (as **a.** and **b.** respectively). A typical example of excitation/fluorescence emission spectrum is also displayed in Figure 2.6 (**c.**) for the D112 fluorophore. Our adsorption studies require detection of polymer concentrations that are on the order of 10^{-4} mol of polymer, of which less than 5% is modified with optical labels. Thus, the fluorescence method is a suitable technique for this analysis because it offers a high level of sensitivity.

N(CH$_3$)$_2$

N(CH$_3$)$_2$

a.

b.

SO$_2$NHCH$_2$CH$_2$NH$_2$

Absorption   **Emission**

Intensity (a.u.)

λ λ'

300 350 400 450 500 550 600

Wavelength (nm)
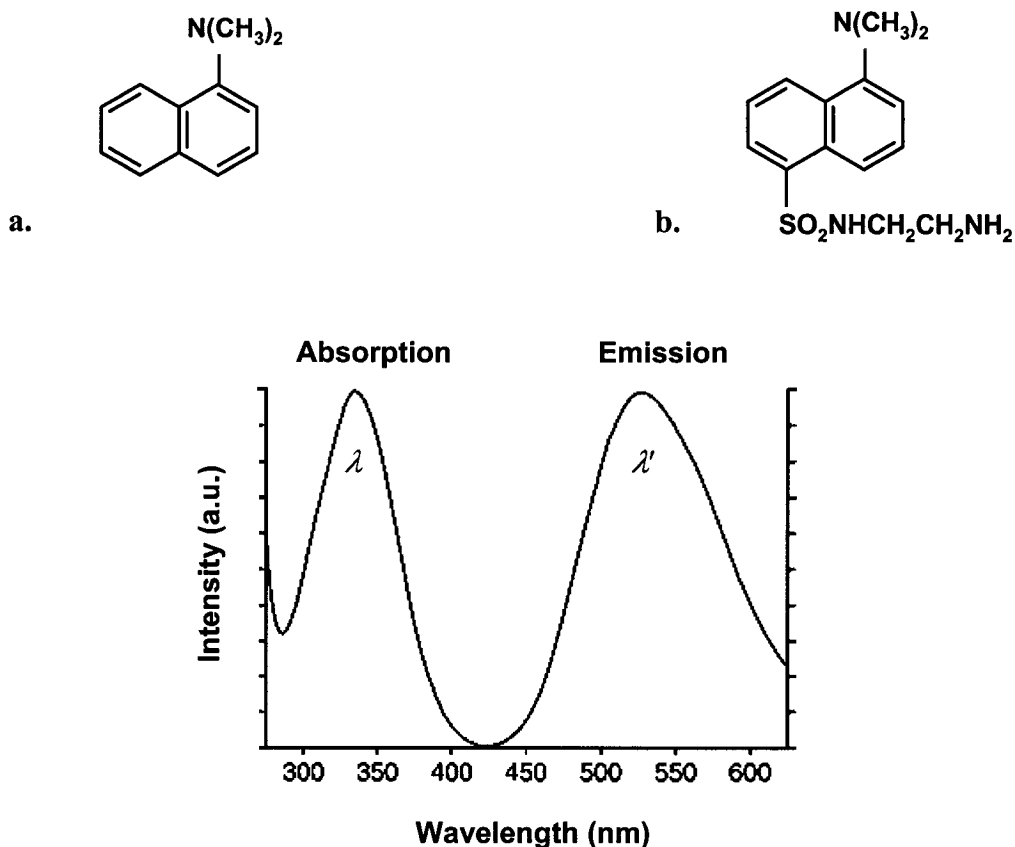
Figure 2.6   Structures of fluorophores, which are attached to PAA through amide linkages, are: **a.** 1-naphthylmethylamine, and **b.** dansyl ethylenediamine (D112). The absorption (at λ), and fluorescence emission (at λ') of D112 in methanol is shown in **c.**[20]

2.6   References and Notes

(1)   Pavia, D. L.; Lampman, G. M.; Kriz, G. *Introduction to Spectroscopy*, 2nd ed.; Harcout Brace College Publisher: New York, NY, 1996; pp 267–271.

(2)   Pliskin, W. A. Nondestructive Optical Techniques for Thin-Film Thickness Measurements. In *Physical Measurements and Analysis of Thin Films*; Murt, E. M., Guldner, W. G., Eds.; Plenum Press: New York, 1969; pp 1–34.

(3)   Zaininger, K. H.; Revesz, A. G. *RCA Rev.* **1964**, *25*, 85.

(4)   Miller, D. R.; Peppas, N. A. *Biomaterials* **1985**, *6*, 33.

(5)   Thompkins, H. G. *A User's Guide to Ellipsometry*; Academic Press: San Diego, CA, 1993; pp 7–34.

(6)   Vasicek, A. *J. Opt. Soc. Amer.* **1947**, *37*, 145.

(7)   Rothen, A.; Hansen, M. *Rev. Sci. Instr.* **1948**, *19*, 839.

(8)   McGahon, W. A.; He, P.; Woollam, J. A.; Sequeda, F. O. *App. Phys. Comm.* **1992**, *11*, 375.

(9)   Lipatov, Y. S.; Sergeeva, L. M. *Adsorption of Polymers*; Wiley: New York, NY, 1974.

(10)   Morrissey, B. W.; Smith, L. E.; Stromber, R. R.; Fenstemaker, C. A. *J. Colloid Interface Sci.* **1976**, *56*, 557.

(11)   Donald, C. A.; Magonov, S. Advanced Surface Microscopy. In *Comprehensive Desk Reference of Polymer Characterization and Analysis*; Brady, R. F. Ed.; Oxford University Press: New York, NY, 2003; pp 490–531.

(12)   Domke, J; Radmacher, M. *Langmuir* **1998**, *14*, 3320.

(13)   Nie, H. Y.; Motomatsu, M.; Mizutani, W.; Tokumoto, H. *Thin Solid Films* **1996**, *273*, 143.

(14)   Akhremitchev, B. B.; Walker, G. C. *Langmuir* **1999**, *15*, 5630.

(15)   Costa, K. D.; Yin, F. C. *J. Biomech. Eng.* **1999**, *121*, 462.

(16)   Itagaki, H. Fluorescence Spectroscopy. In *Experimental Methods in Polymer Science*; Tanaka, T. Ed.; Academic Press: San Diego, CA, 2000; pp 155–260.

(17)   Redmond, R. W. Introduction to fluorescence and photophysics. In *Handbook of Biomedical Fluorescence*; Mycek, M. A., Pogue, B. W., Eds.; Marcel Dekker, Inc.: New York, NY, 2003; pp 1–27.

(18)   Lakowicz, J. R. *Principles of Fluorescence Spectroscopy*, 2nd ed.; Plenum Press: New York, NY, 1999; Chapters 1–3.

(19)   Anghel, D. F.; Alderson, V.; Winnik, F. M.; Mizusaki, M.; Morishima, Y. *Polymer* **1998**, *39*, 3035.

(20)   Moraczewska, J.; Wawro, B.; Seguro, K.; Strzelecka-Golaszewska, H. *Biophys. J.* **1999**, *77*, 373.

Chapter 3

Effects of Charge Density and Counterions on the Assembly of Polyelectrolyte Multilayers

3.1 Preface

In Chapter 1, the layer-by-layer method was introduced as a method for assembling polyelectrolytes into multilayer films. A list of tools and techniques that were used in the studies of such films was presented in Chapter 2. In this chapter, we use some of these techniques, namely UV-vis spectroscopy and ellipsometry, to examine how the rate of the layer-by-layer assembly is affected by the charge density of polyelectrolytes and the role of counterions in the adsorption mechanism.

3.2 Introduction

The sequential adsorption of charged polymers onto oppositely charged surfaces is a straightforward and versatile technique for the preparation of polymer thin films.[1] The layer-by-layer approach is suitable for designing functionalized polymer films over broad length scales, ranging from angstroms to microns. Polyelectrolyte multilayer films have thus become useful for many applications, including capsules for drug delivery,[2] chemical sensors,[3] ultra-thin ion selective membranes,[4] electrochromic devices,[5] and all-optically patterned surfaces.[6,7] Such applications have fueled much experimental study of various thermodynamic aspects of multilayer formation with the aim gaining better chemical

control of film properties such as layer morphology,[8,9] interpenetration,[10–12] and thickness.[13,14]

Recent steady-state studies have shown that multilayers constructed from weakly charged polymers can exhibit a rich and complex behavior, owing to their variable charge density. In particular, the thickness of the multilayer films has been shown to be highly dependant on the pH of the polymer solutions during assembly by over two orders of magnitude, as demonstrated in the now well-studied poly(allylamine hydrochloride) (PAH) and poly(acrylic acid) (PAA) system.[15] Thus, by manipulating the charge fraction in adsorption baths of weakly charged polymers, one has good molecular control over the adsorption of polyelectrolyte chains, which can lead to variable layer structures and thickness transitions in the film.[16–18] An understanding of the kinetics of electrostatic layer-by-layer assembly of polyelectrolytes onto solid supports is also necessary for the controlled preparation of functional polymer films, and optimization of their physical properties. However, many fundamental questions concerning multilayer formation remain unclear. While several theoretical studies have provided some insight into the effects of adsorption variables for a single polyelectrolyte layer (i.e., concentration of counterions, pH, and surface charge density),[19–22] the predictions for adsorption behavior from the models are still poor in many systems, especially for weak polyelectrolytes. Furthermore, although the kinetics of polyelectrolyte adsorption onto an uncharged surface have been theoretically examined,[20,23] there remains a limited amount of detailed experimental data on adsorption kinetics of oppositely charged polymers into multilayer assemblies, particularly for films made from weak polyelectrolytes. Recent results of the interplay between kinetic and thermodynamic contributions in multilayer adsorption of

weak polyelectrolytes have broadened our understanding of the process, but also prompt further studies into these systems.[24]

In an effort to examine some of the variables that govern the rate of polymer adsorption, we have conducted studies to determine the time-dependant thickness of a model weakly charged system. Specifically, we optically measured and mapped the growth profiles of weakly charged polycation PAH, and a polyanion containing azobenzene dye moieties, P-Azo (poly{1-[4-(3-carboxy-4-hydroxyphenylazo) benzenesulfonamido]-1,2-ethanediyl, sodium salt} as a function of various polymer concentrations. We then compared the thicknesses after just 1 s adsorption of nine different multilayer systems in order to identify the origins of the substantial increase in film thickness observed over time in our model weak PAH/P-Azo system. Lastly, we examined the influence of counterion exchange on the adsorption of weak polyelectrolytes. This study involved comparing the time-dependant adsorption of P-Azo onto a weakly charge PAH surface in the presence of halogen salts F^-, Cl^-, Br^-, and I^-.

3.3   Experimental Section

3.3.1   Materials

The principal polycation/polyanion combination investigated was PAH (Polysciences, M_w 60K), and P-Azo (Aldrich, M_w 90K) respectively. Other polyions employed were poly(diallyldimethylammonium chloride) (PDAC; Aldrich, M_w 200–350K), poly(acrylic acid, sodium salt) (PAA; Aldrich, M_w 90K), poly(sodium 4-styrenesulfonate) (PSS; Aldrich, M_w 70K) and an azobenzene containing poly(S119), (Aldrich). Figure 3.1 depicts the chemical structures of the various polyelectrolytes used. Unless otherwise indicated, aqueous solutions containing 10^{-2} M per repeat unit of

polyion were prepared with 18 MΩ·cm resistivity Millipore Milli-Q water. Where indicated, the pH of the solutions was adjusted using NaOH and HCl. For the counterion study, polymer solutions of concentrations 10^{-3} M were adjusted to pH = 9, and salt of concentration 5×10^{-2} M was added (NaF, NaCl, NaBr, or NaI; Fisher, used as received at minimum 99% purity). To prevent replacement of the target ions, the quantity of NaOH used for pH adjustments was ensured to be at least one order of magnitude lower than the concentration of the examined salt.
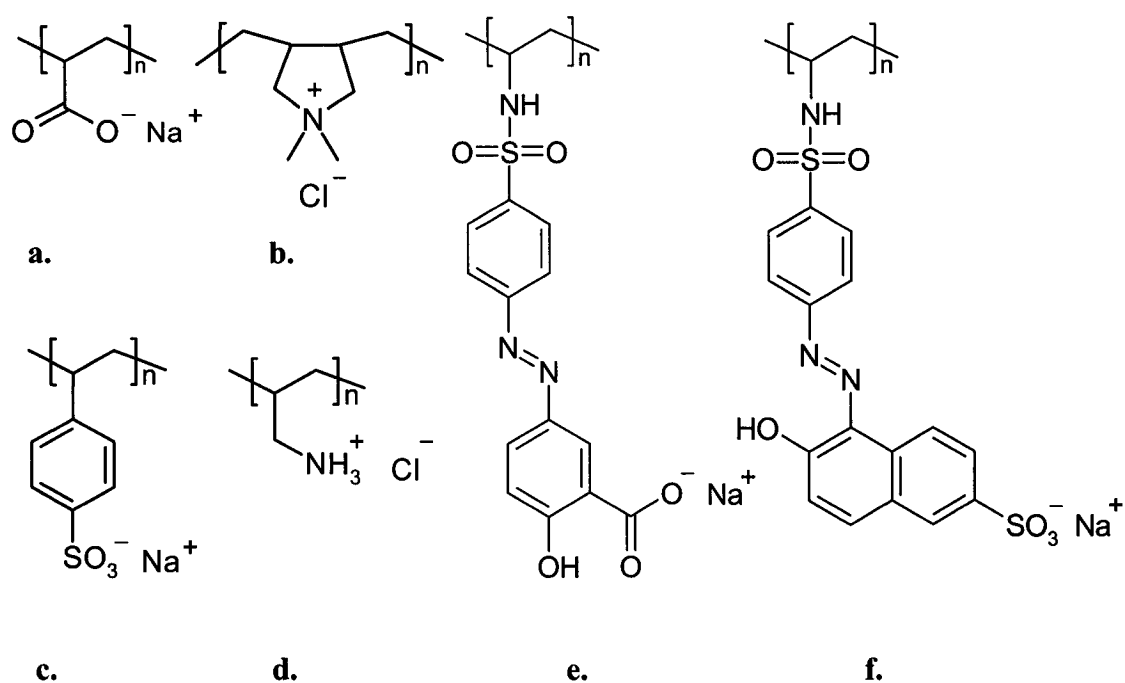
Figure 3.1 Repeat units of the polyelectrolytes used for multilayering: **a.** PAA (weak polyanion), **b.** PDAC (strong polycation), **c.** PSS (strong polyanion), **d.** PAH (weak polycation), **e.** P-Azo (weak polyanion), and **f.** P-S119 (strong polyanion).

3.3.2 Multilayer Film Preparation

Glass microscope slides (Fisherbrand), and silicon wafer substrates (Wafernet) were cleaned by immersion in a bath of 25% H_2SO_4 and 75% H_2CrO_4 for a minimum of 24 h. Substrates were subsequently washed with neutral Milli-Q water (pH ~7.5) in preparation for electrostatic deposition of the initial polycationic layer. Except where specified, multilayer films were constructed with the aid of an automatic slide stainer (Shandon) using matched dipping times for both polycation, and polyanion as indicated. The dipping protocol was a repeated and alternating immersion of substrates in polycation solution, followed by the polyanion solution. Between each adsorption cycle of polymer layers, the films were rinsed thoroughly with neutral Milli-Q water.

3.3.3 Film Characterization

Optical absorbance measurements of P-Azo containing multilayer films on glass microscope slides were performed with a UV-vis spectrophotometer (Varian Cary 300-Bio; scan rate 100 nm·min^{-1}). The optical thickness of P-Azo containing multilayers was quantified (an average of 3 measurements) by observation of the $\pi \rightarrow \pi^*$ absorbance maximum of P-Azo at λ_{max} = 365 nm for the *trans* azobenzene isomer. Transmission results are represented as the calculated average of three replicate measurements and blank corrected. Reflective data for multilayers deposited on Si substrates were obtained using a Gaertner Ellipsometer at λ = 633 nm, solved for both refractive index and layer thickness. All total layer thickness values are reported as the statistical mean of 13 acquired measurements followed by a surface oxide subtraction of 27 ± 3 Å, determined independently. The average error associated with the UV-vis absorbance and

ellipsometry measurements was determined as approximately ± 5%, and ± 3% respectively.

3.4 Results and Discussion

3.4.1 Layer Thickness

Several recent studies have reported the pH-dependant thickness of weakly charged polyelectrolytes assembled into multilayer films.[21,22,25] In a similar manner, we characterized the growth of the PAH/P-Azo system prepared under conditions of varying charge density by assembling multilayers at matched solution pH values ranging from 3 to 11, and using a dipping time of 12.5 min. The optical absorbance resulting from variable P-Azo adsorption was measured as a function of the assembly bath pH, at intervals of every 4 layers up to 62 layers, as displayed in Figure 3.2. A trend of increasing P-Azo adsorption with increasing assembly solution pH toward the pK_a was observed, in agreement with the previous studies. This effect was most prominent in the multilayer series assembled at pH values 9 to 11, where a nearly 20-fold increase in optical absorbance was obtained by increasing the pH of the assembly bath from a value of 3 to 10. Recent acid-base equilibria studies of layered colloids prepared from PAH and PAA indicate that the apparent local pK_a of the adsorbed polycation, as determined through ξ potential measurements, is approximately in the range of 9.9 and 10.8.[26] For PAH/P-Azo films made near the half neutralization point of PAH, i.e. at pH = 9 and 10, the measured average optical thickness of ~19 Å/layer corresponds to an intermediate value between the weakly charged (~35 Å/layer at pH = 11) and strongly charged systems (~3 Å/layer at pH = 4). In order to characterize the time-dependant thickness of the

multilayers constructed from weakly charged PAH, we examined the effect of assembly bath pH on the kinetics of PAH/P-Azo adsorption.
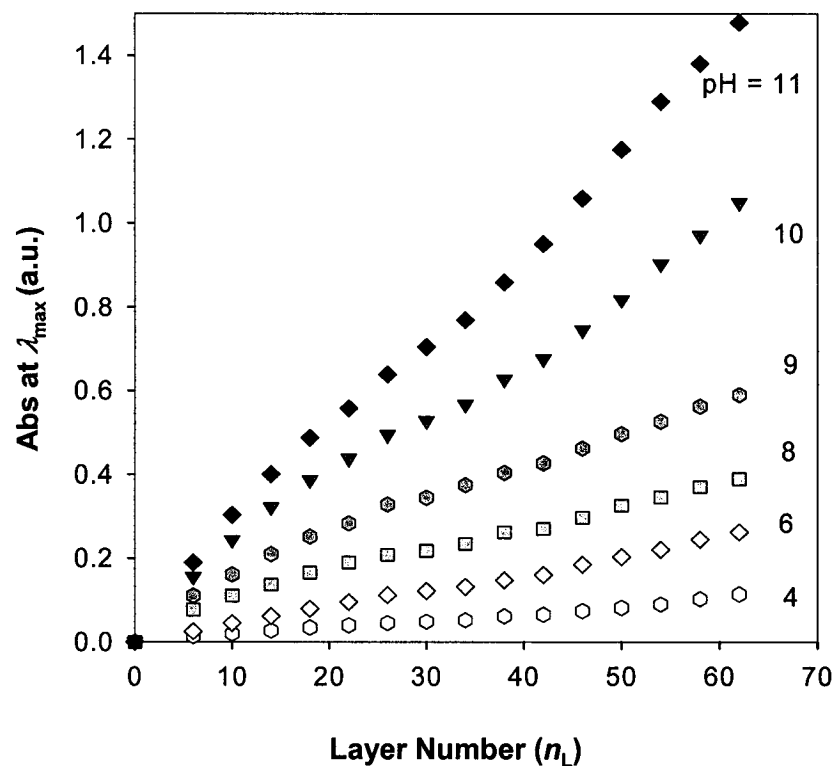
Figure 3.2   UV-vis absorbance at λ_{max} = 365 nm from 0 to 62 layers of PAH/P-Azo self-assembled under varying pH matched polycation/polyanion solutions.

3.4.2 Time-Concentration Profile

While there have been some kinetic studies on the formation of multilayer assemblies from strongly charged polyelectrolytes,[27] there is little information on the kinetics of layer-by-layer adsorption of weakly charged polyelectrolytes. We performed static experiments to measure the multilayer growth for PAH/P-Azo prepared at pH = 9 as a function of immersion time and concentration. Polyelectrolyte solutions of PAH and P-

Azo were prepared at various concentrations ranging from $10^{-2.0}$ to $10^{-5.0}$ M per repeat unit, and films of 30 layers were fabricated on Si substrates using various immersion times, ranging from 1 to 120 s, matched for both the polycation and polyanion. The average layer thickness of films prepared using various dipping times was measured using ellipsometry. In this fashion, a layer growth profile was constructed and compared for seven sets of polycation/polyanion pairs at matched concentrations. Figure 3.3 illustrates the indirectly observed time-dependant growth of several PAH/P-Azo films prepared at concentrations ranging from $10^{-2.0}$ to $10^{-4.5}$ M (3.16×10^{-5} M). No significant growth was detected when the concentration of the assembly solutions was $10^{-5.0}$ M. The data indicate that when polymer solutions of at least $10^{-4.0}$ M are used, multilayers adsorb and reach saturation (>80%) in approximately 60 s. Thus, saturated adsorption is rapidly achieved in the case of PAH/P-Azo assembled under conditions employing weakly charged polycations. At the saturation point, we also obtained the widest range in layer thickness for PAH/P-Azo films of 1 to 12 Å. Note that this static experiment suggests that a measurably thick layer of polymer is adsorbed within the first few seconds of substrate immersion into a polymer bath. However, the true thickness (which can be obtained from dynamic experiments) would not include experimental contributions to layer thickness, seen at short immersion times of Figure 3.3. For example, the adsorption of polyelectrolyte resulting from the presence of a concentration gradient, which exists on the surface of the film, during the rinse cycles.

Furthermore, experiments conducted using longer immersion times of 4 and 12.5 min revealed no significant increase in average layer thickness beyond the 1 min saturation point (i.e., a maximum of 12.5 Å/layer). The highest layer thickness, determined as 8 to 12 Å, is obtained with more concentrated solution baths of the order

10^{-3} and 10^{-2} M respectively, while in more dilute systems a significant reduction to 1/2, 1/3, and 1/12 the maximum layer thickness occurs at concentrations of $10^{-3.5}$ (3.16 x 10^{-4} M), $10^{-4.0}$, and $10^{-5.0}$ M respectively.
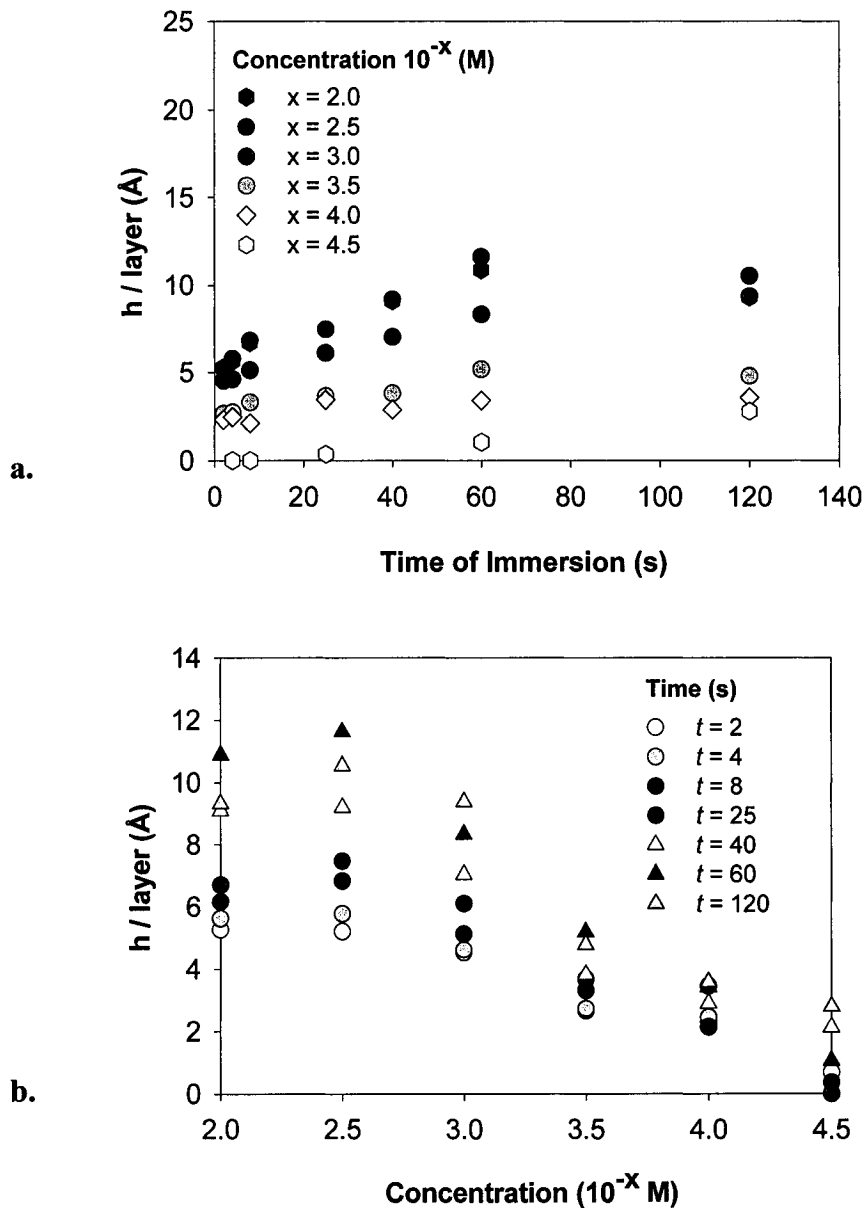
Figure 3.3 Layer thickness growth profiles for 30 layers of PAH/P-Azo adsorbed at pH = 9 for both polyion solutions. Ellipsometric average height (h), per layer measured: **a.** as a function of time, using various matched concentrations of polycation/polyanion solutions, and **b.** as a function of concentration, for various deposition times (t).

In a separate study, we deposited 30 layers for various adsorption times and examined the layer thickness as a function of solution concentration. Figure 3.3b illustrates the resulting concentration-dependant decay curves in layer thickness for a series of six different adsorption times. As previously determined from the variable time experiments, Figure 3.3b confirms that the largest variation in layer thickness is between 1 and 12 Å, which is observed when multilayer films are prepared near the saturation point, t = 60 s. These results are presented in Figure 3.4 as sets of superimposed time and
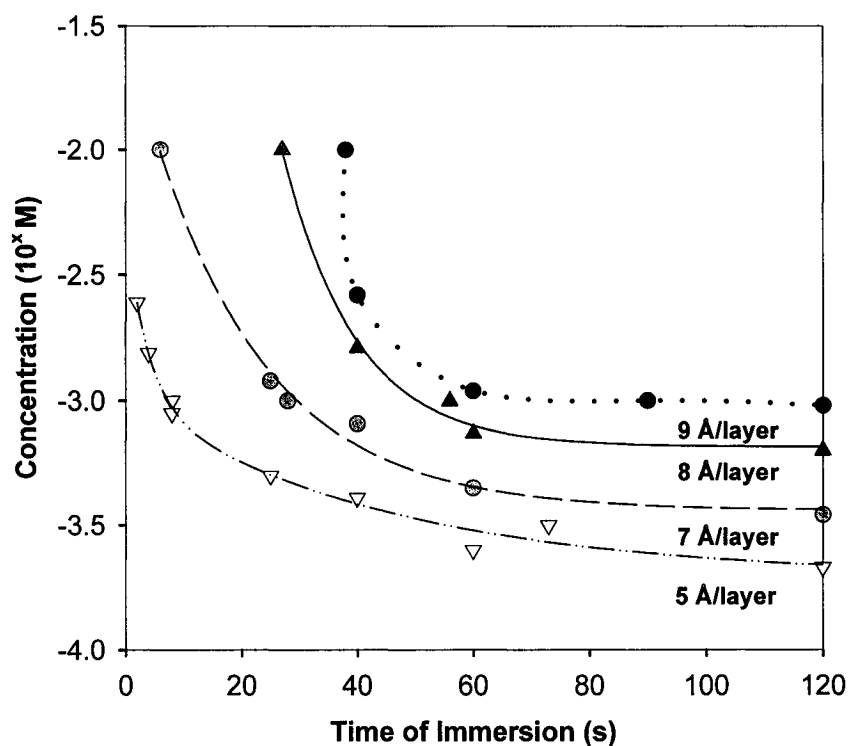
Figure 3.4   Concentration-time plot of the growth of PAH/P-Azo multilayers with both polyion adsorption baths set to pH = 9.

concentration variables, which provide a constant layer thickness in the early growth regime, in this case between 5 and 9 Å. The lines provided are intended to be visual

guides only. Most notably, we observed rapid increase in film thickness of thin polymer layers after 1 s of substrate contact with the polymer solution. Whereas many previously studied multilayer combinations typically report adsorption times on the order of minutes or even tens of minutes,[28] our data for the PAH/P-Azo system indicate unusually rapid adsorption within the first few seconds of substrate immersion into a polymer bath adjusted to pH = 9.

3.4.3 Dependence of Adsorption Kinetics on Charge Density

In an effort to understand the source of the anomalously rapid growth observed in PAH/P-Azo films constructed at pH = 9, we examined various other polyelectrolyte multilayers on Si prepared from 1-s immersions, and measured the resulting thicknesses by ellipsometry every 5 layers. We first obtained the 1-s layer growth of a model PAH/PAA system over 25 layers, in which the charge density of either the polycation or the polyanion was selectively altered by suitable pH adjustments of the polymer solutions. The resulting 1-s thickness of the PAH/PAA films made from polyelectrolyte solutions at matched pH values of 7, and 9 is displayed in Figure 3.5. At assembly pH = 9, we observed a large 1-s thickness of ~20 Å/layer. Conversely, we did not detect a significant increase in the 1-s layer thickness when PAH/PAA films were prepared from solutions set to pH = 7. The anomalously fast 1-s growth observed for the PAH/PAA system assembled at pH = 9 is in agreement with the rapid adsorption kinetics observed in the case of PAH/P-Azo films, which were also prepared using weakly charged polycations (Figure 3.3a).

In a more broad study, we similarly obtained the 1-s thickness profile of various other polyelectrolyte pairs, each assembled with their unique pH dependant charge

densities. The results, shown in Figure 3.5, suggest that all films made from both a strongly charged polycation and polyanion exhibit considerably less or negligible 1-s thicknesses in comparison to multilayers prepared using at least one weakly charged component. For example, no significant 1-s thickness was detected for PDAC/PSS films (i.e., ~1 Å/layer) prepared from polycation/polyanion solutions at matched pH values of either 5 or 9. Notably, both PDAC and PSS are strongly charged polyelectrolytes in the pH range of 3 to 11. Similarly, a reduced 1-s thickness of ~2 Å/layer was detected in both cases of PAH/PSS and PAH/P-Azo multilayered at pH = 5. The estimated pK_a of P-Azo is ~3.3 based on observations of precipitation near this pH value, and in agreement with a recent report of the dissociation constant of P-Azo in multilayer thin films.[29] Since both PAH and P-Azo remain strongly charged at pH = 5 we did not observe the usual weakness effect, which appears to give rise to the adsorption of thick polymer layers at a short immersion time.

In contrast, multilayer films prepared using one weakly and one strongly charged polyelectrolyte exhibit much greater 1-s thickness of 8 Å/layer and 10 Å/layer respectively for both the PAH/PSS, and the PAH/P-S119 systems assembled at a pH value of 9. Although both PSS and P-S119 (an alternate azobenzene containing polyanion) are fully charged polyanions, the polycation here remains weakly charged, which leads to thicker layers after only 1-s immersion times. Our result is also in agreement with the rapid adsorption recently noted in the assembly of PAH/P-S119 multilayers.[30] Notably, when we changed the assembly solution pH to a value of 5 in the PAH/PSS system, the 1-s thickness value was reduced by 5-fold. All 1-s thickness results reported here are consistent with the hypothesis that reduced charge density in adsorbing

polyelectrolytes is mainly responsible for larger film thicknesses observed at short immersion times. Although previous in situ studies, through second harmonic generation, indicate fast adsorption of PDAC/PSS multilayers (<10 s),[31] our 1-s thickness studies suggest that considerably thicker layers are a consequence of reduced charge fraction in
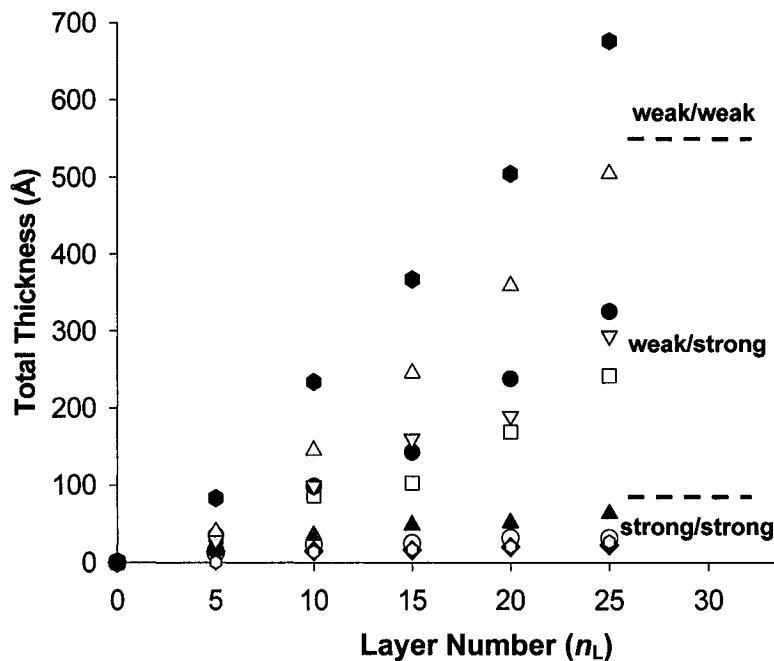
Figure 3.5   Multilayer film growth using 1-s adsorption times for variously charged polycation/polyanion combinations. A weak/weak system demonstrating unusually large 1-s thickness is: (●) $PAH_{pH\ 9}/PAA_{pH\ 5}$. Intermediate 1-s thicknesses are observed in weak/strong systems including: (◓) $PAH_{pH\ 9}/P\text{-}S119_{pH\ 9}$, and ($\triangledown$) $PAH_{pH\ 9}/P\text{-}Azo_{pH\ 9}$, which contain azobenzene chromophores, as well as ($\triangle$) $PAH_{pH\ 9}/PAA_{pH\ 9}$, and ($\square$) $PAH_{pH\ 9}/PSS_{pH\ 9}$. Strong/strong systems displaying minimal 1-s thickness include: (▲) $PAH_{pH\ 5}/P\text{-}Azo_{pH\ 5}$, (O) $PAH_{pH\ 5}/PSS_{pH\ 5}$, (◑) $PAH_{pH\ 7}/PAA_{pH\ 7}$, and (◆) $PDAC_{pH\ 9}/PSS_{pH\ 9}$.

the assembling polymers. This is supported by the fact that all strongly charged polycation/polyanion multilayer combinations examined here demonstrate little or negligible adsorption on the time scale of 1 s. Furthermore, the largest 1-s growth is expressed in a system assembled with both a weakly charged polycation (PAH at pH = 9) and a weakly charged polyanion (PAA at pH = 5), resulting in films of ~28 Å/layer. Since the weakness effect is most pronounced in a system prepared using both a weakly charged polycation and polyanion, we suggest that the degree to which the 1-s thickness is increased is therefore related to the extent to which charge fraction may be reduced in the assembly of both the polyelectrolytes. We speculate that this effect may arise from a variable "effective" charge density of weak polyelectrolytes upon approaching the surface for adsorption. This charge readjustment of the polymer near the surface can consequently result in a net larger degree of charge overcompensation, and therefore yield greater layer thicknesses at low immersion times. The ability of weak polyelectrolytes to alter their charge due to an "effective" local pH in the interface, which is different from that in the bulk solution, has previously been shown both experimentally[26,32] and theoretically.[33] In addition, it has been demonstrated that the local pH during adsorption is influenced by the ionization fraction of the underlying polymer layers, which oscillates with the number of layers deposited. Thus, the extent to which the 1-s layer thickness increases (observed in our studies as large differences between a purely weak polyelectrolyte system and a purely strong one) is not only influenced by the alteration of local charge density at the surface during adsorption, but also by the changing ionization fraction of the of the relevant underlying polymer layers.[34]

3.4.4   Ion Displacement and Adsorption Kinetics

The finding of anomalously fast adsorption kinetics in multilayer assemblies prepared from weakly charged polyelectrolytes leads to questions regarding the mechanism of adsorption, such as the role of ion displacement in the formation of polymer layers. It is known that when a polyion segment approaches a surface containing an oppositely charged polyelectrolyte layer, a displacement of the salt ion must occur to allow for segment adsorption.[35] This exchange of salt ions for the repeat units of strongly charged polyelectrolytes has been confirmed by direct observation with radio-labeled ion probes.[36] Results from X-ray photoelectron spectroscopy studies have shown that the residual ion content trapped within formed multilayers made from strongly charged polymers is negligible.[37] However, there is a lack of experimental data on the effect of counterion displacement on the kinetics of polyelectrolyte adsorption into layer-by-layer assemblies. In addition, these effects cannot be generalized to the adsorption behavior of weakly charged polyelectrolytes.

The role of ion exchange in the adsorption kinetics of multilayers was investigated here by comparing the relative rate of P-Azo adsorption on partially charged PAH (pH = 9) for a series of polyelectrolyte solutions containing one of NaF, NaCl, NaBr or NaI of concentration $5 \times 10^{-2.0}$ M. Multilayer films containing 30 layers were assembled onto glass slides using various adsorption times ranging from 1 s to 15 min for the P-Azo component while the saturated adsorption of polycation was ensured by maintaining a constant immersion time of 15 min. Reported optical measurements on multilayer films were time-corrected for prolonged polyelectrolyte adsorption resulting from significant polymer concentration at the surface of the film during rinse cycles initially, which was quantified using UV-vis. As shown in Figure 3.6 of the UV-vis absorbance of the various

PAH/P-Azo films prepared, immediate adsorption of P-Azo results for all ion solutions

within 5 s of immersion.
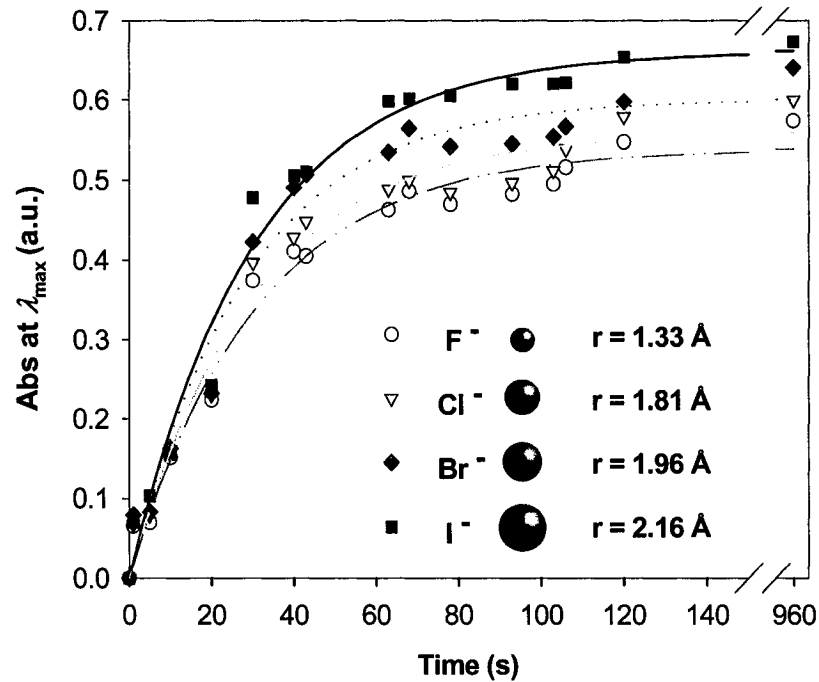
Figure 3.6   Effect of ion exchange on the time-dependant adsorption of PAH/P-Azo multilayers (at a constant pH value of 9 for both polyelectrolyte solutions).

The optical thickness measurements show that saturation is nearly achieved in approximately 60 s of adsorption time. The results from this time-dependant study of film thickness for PAH/P-Azo on glass slides is in agreement with the thickness values obtained from reflective ellipsometry measurements obtained for thickness of PAH/P-Azo (Figure 3.4), which suggests that maximum polyelectrolyte adsorption is obtained upon approaching 1 min of immersion time. No distinguishable difference in the kinetics of P-Azo adsorption for the films prepared with varying halogen ion salt films was observed up to 20 s. After 20 s, significant differences in the optical thickness revealed a

reduced adsorption of the P-Azo when the multilayers were prepared in the presence of small F^- counterions. Conversely, an increase of 21% in the UV-vis absorbance of multilayer films prepared from I^- containing solutions suggests that polymer solutions containing larger counterions exhibit faster adsorption of P-Azo than those containing an equivalent amount of F^- counterions. The analogy to weak polymer systems is that lower charge density similarly facilitates rapid adsorption by effectively reducing the number of ionic interaction sites required for adsorption and hence lowering the energy barrier.

The observed variances in the rate of polyanion adsorption based on the presence of either F^-, Cl^-, Br^- or I^-, can be rationalized using a simple electrostatic argument considering the binding energies of the tested anions with various cations (Table 3.1). The Arrhenius equation (Equation 3.1) is used to qualitatively compare the adsorption rates at constant temperature. The rate constant k here is proportional exponentially to the chemical bond strength of ionic dissociation.

$$k = A e^{-E_a/RT} \tag{3.1}$$

As a first approximation, we assume first-order kinetics. The rate of dissociation for the anions thus scales with k, suggesting slower displacement of the smaller F^- counterion, with a relative rate ~53% of the larger I^-, as shown in Table 3.1.

Since P-Azo must exchange with the bound counterions existing on the PAH surface for adsorption to occur, systems with larger I^- ions (i.e., more loosely bound) would be expected to exchange more rapidly than that of the more tightly bound F^- ions, as observed. In comparing the relative (rel) rates of adsorption, it is also important to

71

consider the effect of the hydrated radii of the counterions when they are displaced from their counter-charge on the polyelectrolyte. For example fluoride ions, while having the smallest ionic radius, have the largest hydrated radius and are therefore much slower to

target counterion	ionic radius (Å)	av $E*$ ^{a} (kcal·mol^{-1})	$E*$ rel to I$^-$	rel k	k rel to I$^-$	exptl rel k
F$^-$	1.33	137.5	1.63	0.20	53	81
Cl$^-$	1.81	111.9	1.32	0.27	73	84
Br$^-$	1.96	100.2	1.19	0.30	83	91
I$^-$	2.16	84.6	1	0.37	100	100

^{a} E* determined from the average ionic binding energies of target counterion with Li$^+$, Na$^+$, K$^+$, and Rb$^+$.[38]

Table 3.1   Calculated and Experimental Relative k for Multilayer Formation with Target Counterions

diffuse away into water than chloride, bromide, and iodide ions, which have smaller hydrated radii respectively. As indicated in Table 1, a trend of faster counterion dissociation (and thus thicker polymer layers at equivalent time) with increasing counterion radius (decreasing hydrated radius) is indeed observed qualitatively. The expected variance in the counterion diffusion rates due to the different sizes of the hydrated radii, combined with the effect of the binding energies (proportional to the ionic, not hydrated radius) both further support our experimental finding of more rapid adsorption with larger halide counterions. However, the scaling argument based on

counterion binding energies alone does not adequately describe the full increase in rate of layer-by-layer adsorption observed for weakly charged polyelectrolytes. Thus, while our kinetic study of counterion displacement suggests that this process may not necessarily be the rate-limiting step in multilayer formation, it has a significant and measurable effect on the rate at which weakly charged polyelectrolytes adsorb.

3.5   Conclusions

We observed anomalously rapid adsorption for the formation of PAH/P-Azo multilayers, on the order of seconds. This was attributed to the reduced charged density on the polyelectrolytes since significantly large 1-s thicknesses could only be obtained with weak polyelectrolytes. The resulting 1-s film thickness of polyelectrolyte multilayers prepared using weakly charged polycations or polyanions can be approximately 10-fold greater than that obtained from similar polyelectrolytes, which are strongly ionized. Furthermore, when both the polycation and the polyanion are assembled at low charge fraction, this weakness effect gives rise to much thicker 1-s films, by a factor of up to 30, as compared to both strongly charged polyelectrolytes. Our studies have also shown that the process of counterion displacement has a significant and easily measurable contribution to the time-dependant growth of multilayers up to the point of saturation. The time-dependant thickness of weakly charged polymers appears sensitive to the variables of concentration, charge fraction and counterion species, and demonstrates that the layer-by-layer technique can be highly advantageous from the point of view of achieving a precise control of thickness in multilayer assemblies.

3.6   References and Notes

(1)   Decher, G.; Schmitt, J. *Prog. Colloid Polym. Sci.* **1992**, *89*, 160.

(2)   Qui, X.; Leporatti, S.; Donath, E.; Möhwald, H. *Langmuir* **2001**, *17*, 5375.

(3)   Yang, X.; Johnson, S.; Shi, J.; Hoesinger, T.; Swanson, B. *Sens. Actuators, B.* **1997**, *B45*, 87.

(4)   Krasemann, L.; Tieke, B. *Langmuir* **2000**, *16*, 287.

(5)   Hammond, P. T.; DeLongchamp, D. *Adv. Mater.* **2001**, *13*, 1455.

(6)   Wang, X.; Balasubramanian, S.; Kumar, J. T.; Tripathy, S.; Li, L. *Chem. Mater.* **1998**, *10*, 1546.

(7)   He, J.; Bian, S.; Lian, L.; Kumar, J.; Tripathy, S. *J. Phys. Chem. B.* **2000**, *104*, 10513.

(8)   Kerimo, J.; Adams, D. M.; Barbara, P, F.; Kaschak, D. M.; Mallouk, T. E. *J. Phys. Chem. B.* **1998**, *102*, 9451.

(9)   Arys, X.; Laschewsky, A.; Jonas, A. M. *Macromolecules* **2001**, *34*, 3318.

(10)   Decher, G. *Science* **1997**, *277*, 1232.

(11)   Loesche, M.; Schmitt, J.; Decher, G.; Bouwma, W. G.; Kjaer, K. *Macromolecules* **1998**, *31*, 8893.

(12)   Baur, J.; Rubner, M. F.; Reynold, J. R.; Kim, S. *Langmuir* **1999**, *15*, 6460.

(13)   Lvov, Y.; Decher, G.; Sukhorukov, G. *Macromolecules* **1993**, *26*, 5396.

(14)   Caruso, F.; Niikura, K.; Furlong, D. N.; Okahata, Y. *Lamgmuir* **1997**, *13*, 3422.

(15)   Shiratori, S. S.; Rubner, M. F. *Macromolecules* **2000**, *33*, 4213.

(16)   Wang, T.; Rubner, M. F.; Cohen, R. E. *Langmuir* **2002**, *18*, 3370.

(17)   Chung, A. J.; Rubner, M. F. *Langmuir* **2002**, *18*, 1176.

(18)   Mendelsohn, J. D.; Barrett, C. J.; Chan, V. V.; Pal, A. J.; Mayes, A. M.; Rubner, M. F. *Langmuir* **2000**, *16*, 5017.

(19)   van de Steeg, H. G.; Cohen Stuart, M. A.; de Keizer, A.; Bijsterbosch, B. H. *Langmuir* **1992**, *8*, 2538.

(20)   Filippov, L. K.; Filippova, N. L. *J. Colloid Interface Sci.* **1997**, *189*, 1.

(21)   Bohmer, M. R.; Ever, O. A.; Scheutjens, J. M. H. *Macromolecules* **1990**, *23*, 2288.

(22)   Dobrynin, A. B.; Deshkovski, A.; Rubenstein, M. *Phys. Rev. Lett.* **2000**, *84*, 3101.

(23) Cohen Stuart, M. A.; Hoogendam, D. W.; de Keizer, A. *J. Phys.: Condens. Matter* **1997**, *9*, 7767.

(24) Kovacevic, D.; van der Burgh, S.; de Keizer, A.; Cohen Stuart, M. A. *Langmuir* **2002**, *18*, 5607.

(25) Antipov, A.; Sukhorukov, G. B.; Leporatti, S.; Radtchenko, I. L.; Donath, E.; Mohwald, H. *Colloids and Surf., A.* **2002**, *198-200*, 535.

(26) Burke, S. E.; Barrett, C. J. *Langmuir* **2003**, *19*, 3297.

(27) Lvov, Y.; Ariga, K.; Onda, M.; Ichinose, I.; Kunitake, T. *Colloids Surf., A.* **1999**, *146*, 337.

(28) Losche, M.; Schmitt, J.; Decher, G.; Bouwman, W. G.; Kjaer, K. *Macromolecules* **1998**, *31*, 8893.

(29) Rmaile, H. H.; Schlenoff, J. B. *Langmuir* **2002**, *18*, 8263.

(30) Heflin, J. R.; Figura, C.; Marciu, D. *Appl. Phys. Lett.* **1999**, *74*, 495.

(31) McAloney, R.; Goh, C. M. *J. Phys. Chem. B.* **1999**, *103*, 10729.

(32) Shin, Y.; Roberts, J. E.; Santore, M. M. *J. Colloid Interface Sci.* **2002**, *247*, 220.

(33) Bohmer, M. R.; Evers, O. A.; Scheutjens, H. M. *Macromolecules* **1990**, *23*, 2288.

(34) Xie, A. F.; Granick, S. *Macromolecules* **2002**, *35*, 1805.

(35) Farhat, T. R.; Schlenoff, J. B. *Langmuir* **2001**, *17*, 1184.

(36) Schlenoff, J. B.; Ly, H.; Li, M. *J. Am. Chem. Soc.* **1998**, *120*, 7626.

(37) Laurent, D.; Schlenoff, J. B. *Langmuir* **1997**, *13*, 1552.

(38) *CRC Handbook of Chemistry and Physics*; Weast, R. C., Ed.; Chem. Rubber Co.: Cleveland, Ohio, 1970; p F–158

Chapter 4

Effect of Chain Length on the Layer-by-Layer Adsorption of

Polyelectrolytes

4.1   Preface

In the previous chapter, it was established that variation of the charge density in polyelectrolytes has measurable effects on the adsorption kinetics of layer-by-layer self-assembly.   Particularly when weakly charged polyelectrolytes are employed, the adjustment of kinetic assembly parameters, namely the adsorption time and adsorbant concentration, allows for wide-range control over the individual layer thickness of polyelectrolyte multilayers.   In this chapter, we investigate how thermodynamics influence the adsorption behavior of polyelectrolyte chains onto oppositely charged polyelectrolytes.   Specifically, the effect of entropy and enthalpy on the competitive adsorption of long versus short chains of weakly charged polyelectrolytes is examined using fluorescence spectrophotometry.

4.2   Introduction

In the interest of developing new molecular architectures that cover a wide range of length scales, various methods to self-assemble and organize polymers on surfaces continue to be explored, from covalent attachment techniques[1-3] to physisorption approaches.[4,5]   Recently, a new technique for preparing polymer thin films which uses electrostatic interactions between oppositely charged polyelectrolytes to assemble a

multilayer organic film, has attracted attention from broad areas of materials science.[6] Polyelectrolyte multilayer films (PEMs) are built-up layer-by-layer (LBL) by alternating adsorption of polycations and polyanions from aqueous solution onto a surface.[7] Growing interest in these self-assembled films can in part be attributed to the fact that their fabrication is experimentally simple, and versatile with respect to the surfaces and materials that can be utilized. Furthermore, industrial applications of functional polyelectrolyte multilayer films (PEMs), for example as biomedical materials, have given impetus to explore in detail the driving forces in LBL formation, interactions between adsorbed polyelectrolyte layers, and the limitations for LBL self-assembly of polyelectrolytes.

Key to controlling the LBL process and the multilayer film properties is understanding factors which govern the adsorption of polyions from solution onto surfaces containing oppositely charged polymers. Extensive theoretical work regarding the adsorption criteria for neutral polymers onto surfaces has previously been done, which have given both quantitative predictions[8,9] and scaling relations.[10,11] For example, theoretical calculations for neutral polymers have shown that its adsorption is dependant on the chain length,[12] and these results have been confirmed by experiment.[12,13] Theoretical attempts to predict polyelectrolyte adsorption are more recent, and have proven difficult to generalize to the formation of PEMs, since these assemblies are nonequilibrium. In addition to accounting for complex electrostatic forces (i.e., by incorporating Debye-Hückel length-scales for polyions whose charge density can be highly sensitive to the local ionic strength at assembly),[14] one must also consider thermodynamic and kinetic factors, which are both integral to the build-up of PEMs.[15]

In this study, we examine the role of polyelectrolyte chain length in the adsorption of a simple model polyanion, poly(acrylic acid) onto silica particles capped with a model polycation, poly(allylamine hydrochloride). Such studies of the adsorption behavior of charged macromolecules are important in order to understand various relevant biological surface and biointerface phenomena. For instance, the adhesion of bacterial cells to solid surfaces (governed by electrostatic, van der Waals, and Lewis acid-base interactions) is often largely affected by cell-surface polymers, such as lipopolysaccharides.[16] The affinity and reversibility of this adsorption process have been found to depend significantly on the molar mass of the cell surface polysaccharides involved in the adhesion.[16]

4.3 Experimental Section

4.3.1 Materials

We used poly(allylamine hydrochloride) (PAH) as received from Polysciences, Inc. Poly(acrylic acid sodium salt) (PAA) of two different molecular weights (M_w 2K and 450K) was purchased from Sigma-Aldrich and modified as described in section 5.3.2. The two different molecular weights of PAA were chosen based on the large difference in the average chain length (i.e., by greater than 2 orders of magnitude). Furthermore, dynamic light scattering characterization (Brookhaven BI9000; Thorn EMI Electron B2FBK RFI photomultiplier tube; Coherent Technologies Compass 315M-150 laser) of the low and high molecular weight PAA, showed very little overlap in the histograms of the hydrodynamic radius of the polymers under the solution conditions used for the adsorption experiments. Chemical structures for the polycation, unmodified polyanion,
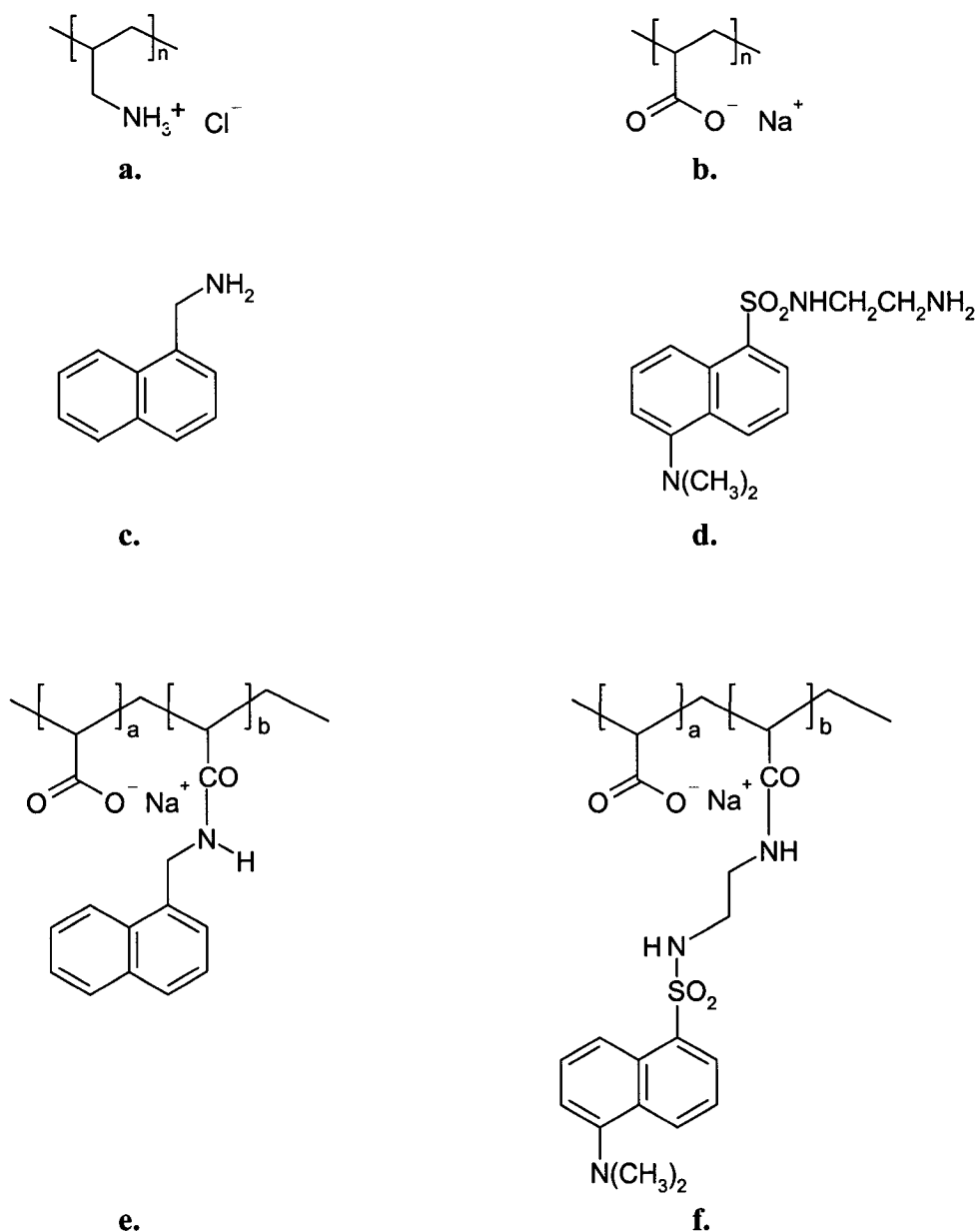
Figure 4.1 Structures of the polyelectrolytes used are: **a.** poly(allylamine hydrochloride), and **b.** poly(acrylic acid sodium salt). Fluorophores used to label the polyanion are: **c.** 1-naphthalmethylamine, and **d.** dansyl ethylenediamine (D112). Structures of labeled poly(acrylic acid) are: **e.** NMA-PAA$_{450K}$, and **f.** Dan-PAA$_{2K}$

and the two labeled poly(acrylic acids) are presented in Figure 4.1. We prepared aqueous polyelectrolyte solutions of concentration 10^{-2} M (based on the molecular weight of repeat units) using 18.2 MΩcm resistivity Millipore Milli-Q water and the adsorption experiments were done in the presence of 1 M NaCl.

Two naphthalene-based fluorophores with amine functional groups, 5-dimethylaminonaphthalene-1-(N-(2-aminoethyl))sulfonamide (also known as dansyl ethylenediamine), and 1-naphthalmethylamine were purchased from Molecular Probes, and Sigma-Aldrich respectively. Our adsorbing surface was colloidal silica of 70–100 nm in diameter, received from Nissan Chemical Industries. The pH of the solutions was adjusted to a value of 9.0 using NaOH. At pH = 9.0, we can observe the adsorption of strongly charged PAA onto a mostly weakly charged PAH surface (since PAH was first adsorbed onto the colloidal particles).

4.3.2 Derivatization of PAA with Fluorophores

Through a method previously described,[17,18] partial conversion of the carboxylic acid units of the 2K and 450K PAA to amide derivatives (amidization) was achieved in two separate reactions as follows: Inside a dry three-neck flask attached to a condenser, vacuum dried PAA (2.0 g) was mixed with an anhydrous solvent, 1-methylpyrolidone (approximately 100 ml), in the presence of flowing nitrogen. The mixture was stirred to allow for dissolution (in the case of 2K PAA) or additionally heated to 60 $^{\circ}$C for 2 hr (in the case of 450 K) to promote dissolution. In a dry and nitrogen-rinsed flask, the fluorophore (7.0 × 10^{-4} mol) was dissolved in some 1-methylpyrolidone (approximately 5 ml) and injected into the PAA reaction pot. Subsequently, dicyclohexylcarbodiimide (DCC, 8.0 × 10^{-4} mol), a coupling agent commonly used to promote amide formation

was also injected into the reaction mixture upon dissolving in dry 1-methylphyrolidone (approximately 5 ml). The use of an aprotic solvent, 1-methylphyrolidone, and DCC promotes the random covalent attachment of the hydrophobic fluorophores onto PAA.[18] The final mixture was stirred in the dark at 60 $^\circ$C for 96 hr. The reaction flask was then cooled in an ice bath, and concentrated NaOH was added dropwise to neutralize the solution, which resulted in precipitation of the sodium salt of the modified PAA. The solid product was obtained by vacuum filtration and subsequently purified by twice precipitating an aqueous solution in methanol. All solvents were removed to yield the final product by drying in a vacuum oven.

Both the unmodified and labeled PAA were characterized by ^{1}H NMR (300 MHz Varian Mercury) performed in D_2O. In the case of 1-naphthalmethylamine-labeled PAA (NMA-PAA$_{450K}$) NMR spectrum analysis shows the expected ratio of naphthalene (7) and amide (1) protons at chemical shifts of 7–8 ppm while the alpha aromatic proton (1) appears at 4.7 ppm. In unmodified PAA, only methylene protons from the backbone (1–2.3 ppm) appear in the NMR spectrum. The NMR spectrum of dansyl ethylenediamine-labeled PAA (Dan-PAA$_{2K}$) also reveals the expected chemical shifts at 7.2–8.3 ppm from the aromatic protons of the fluorophore, and the β, γ methylene protons (4) from the amide link at around 3.4 ppm. Both UV-vis absorption (Varian Cary 300-Bio Spectrophotometer), and ^{1}H NMR spectral analysis of the final product suggested little contamination of labeled PAA and the degree of modification was calculated by integration of the ^{1}H NMR spectral peaks. It was determined that PAA of 450 K was 3.8 mol% modified while 4 mol% of the 2 K PAA was labeled. The degree of derivatization of PAA was kept at a low value to prevent interference from the hydrophobic fluorescent

tags on the electrostatic adsorption of the polyelectrolyte. Fluorescence intensity calibration plots at variable concentration of NMAPAA$_{450K}$ and Dan-PAA$_{2K}$ were prepared using a FluoroMax-2 (Jobin Yvon-SPEX; slit width set to 2.5 cm).

4.3.3a Preliminary Adsorption of PAH onto Colloids

An excess amount of the polycation layer, poly(allylamine hydrochloride), was first provided for adsorption onto colloidal SiO$_2$ according to the following standard protocol previously outlined for the preparation of PAH/PAA multilayers onto SiO$_2$.[19] In this protocol the polyelectrolyte adsorption conditions are set to a pH value of 9.0 and 1.0 M of NaCl was used to ensure highest coverage of the colloid with the polycation. Colloids were dispersed in a polyelectrolyte solution for 30 min, followed by 1 h of centrifugation at 4500 rpm. The supernatant is then removed and the colloids are washed three times with copious amounts of Milli-Q H$_2$O (adjusted to pH = 9) to remove unadsorbed polymer. Each wash step consists of 30 min of sonication (to expose colloids to wash solution while preventing aggregation), 1 h centrifugation, and finally extraction of the liquid.

4.3.3b Competitive Adsorption of PAA onto a PAH-Coated Surface

The competitive adsorption of long (450 K) versus short (2 K) chains of PAA was examined by supplying in solution a stoichiometric surface coverage amount of each of Dan-PAA$_{2K}$ and NMA-PAA$_{450K}$ to 2.0 g/L of PAH-coated particles. This required surface coverage amount of polyelectrolyte (3–5 $\times$ 10^{-4} M repeat units of each type of PAA) for 2.0 g/L of PAH-coated particles was determined from quantitative titrations of PAH/PAA-coated particles with poly(diallyldimethyl-ammonium chloride) (PDAC).[19]

The molar concentration of labeled PAA necessary to cover the PAH surface ($3-5 \times 10^{-4}$ M for 2.0 g/L of particles) was obtained by converting the bare mass of titrant (PDAC) required to achieve charge overcompensation, and thus multilayer formation, to a molar surface coverage value (as determined by ζ potential measurements).[19] Specifically, this point refers to the mass of titrant at the initial plateau point after the half neutralization point in the titration curve (i.e., 0.05g/L of PDAC for 2.0 g/L of coated particles). Although this estimation of the surface coverage value is based on a titration experiment involving a different polyelectrolyte than that used in our experiment, it provides a reasonable approximation of the required coverage amount. Furthermore, the titration experiment was performed under comparable solution conditions to our PAA adsorption study (1mM NaCl and solution pH = 9) and in both cases the adsorbing polyelectrolyte is strongly charged. Thus, assuming that the adsorption isotherms are comparable, the error in determining the surface coverage value is estimated to be in the range of the experimental uncertainty reported in the titration study, $\pm$ 9.6 %. We allowed 24 h to ensure coverage adsorption of the labeled PAA onto PAH since previous PAH/PAA multilayer studies have shown significant time-dependent adsorption at low polyelectrolyte concentrations (i.e., $<10^{-3}$ M).[20]

4.4 Results and Discussion

4.4.1 Fluorescence Calibration Plots of Labeled PAA in Solution

As shown in Figure 4.2, we initially characterized the fluorescence emission intensity of the labels on the short- and long-chain PAA in solution. Fluorescence spectra
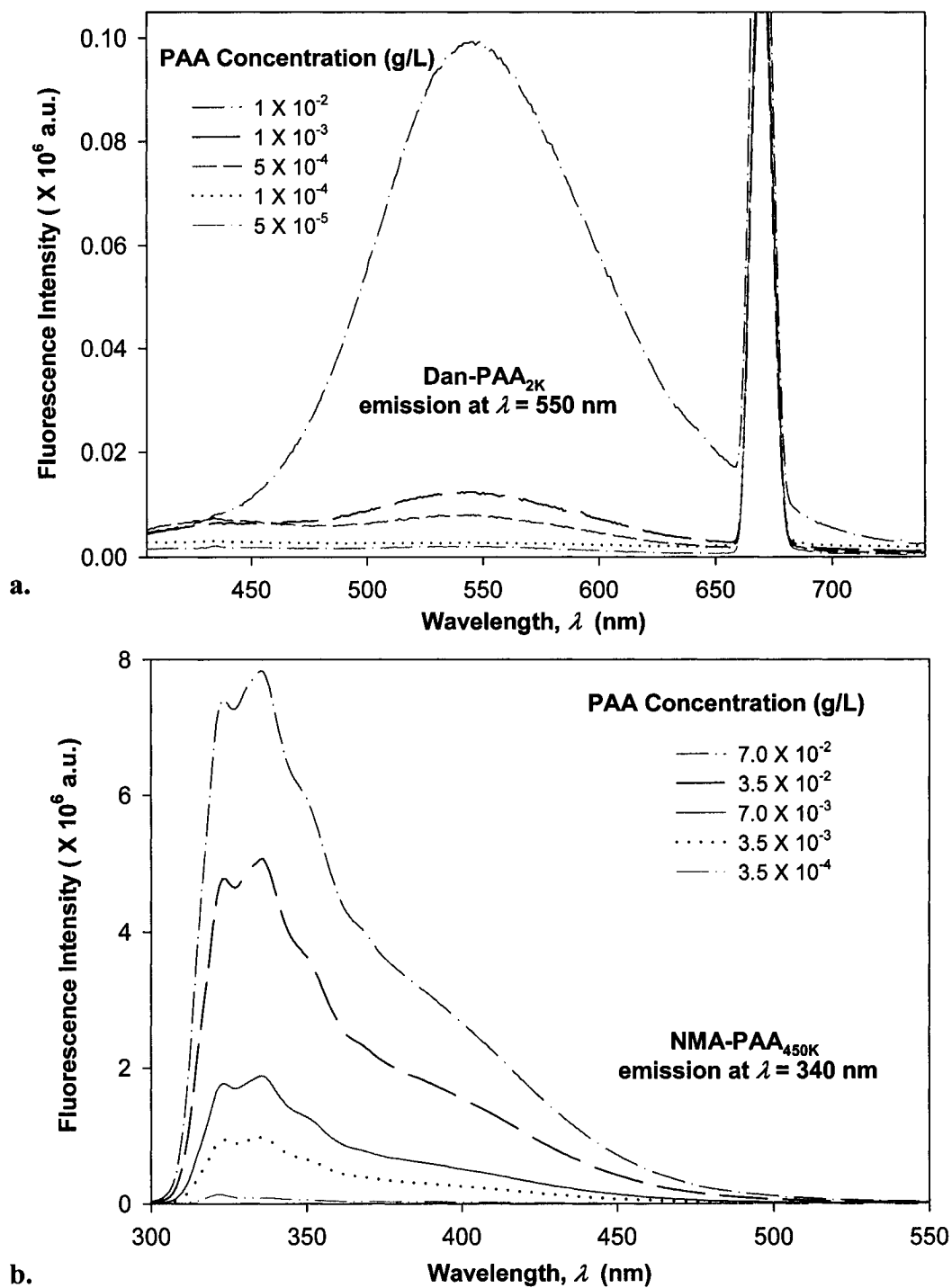
Figure 4.2 Fluorescence emission spectra obtained for variable concentration of: **a.** short-chain labeled PAA (Dan-PAA$_{2K}$), and **b.** long-chain labeled PAA (NMA-PAA$_{450K}$) in water.

were acquired for NMA-PAA$_{450K}$ (by excitation at λ_{Ex} = 290 nm; emission at λ_{Em} = 340),[18] and Dan-PAA$_{2K}$ (by excitation at λ_{Ex} = 335 nm; emission at λ_{Em} = 550 nm)[21] in the concentration range of 10^{-1} to 10^{-5} g/L of PAA. Note that the sharp peaks centered at twice the excitation wavelength, 580 nm (in the NMA-PAA$_{450K}$ sample) and 670 nm (in the Dan-PAA$_{2K}$ sample), are instrumental artefacts. Specifically, they are scattered light transmitted as the second order diffraction of the emission monochromator.

We compared the fluorescence intensity of the two fluorophore-labeled PAA samples, at the peak maximum. Although both of the PAA samples were modified by approximately 4% fluorophores, the fluorescence intensity exhibited by NMA-PAA$_{450K}$ was found to be greater by an order of magnitude than that of Dan-PAA$_{2K}$ prepared at an identical solution concentration. The smaller fluorescence signal from the Dan-PAA$_{2K}$ is attributed to the dansyl fluorophore, which is known to fluoresce much less intensely in water as compared to nonpolar organic solutions.[17,21,22] A fluorescence signal for both samples, however, was detectable at concentrations above the critical coverage adsorption concentration used for the study (10^{-4} M). As indicated in Figure 4.3, we also determined that there was no significant quenching of one fluorophore by the other, by obtaining the fluorescence spectrum of a mixed sample of both NMA-PAA$_{450K}$ and Dan-PAA$_{2K}$ in solution at identical concentrations of 5.0×10^{-3} g/L (above the coverage concentration). From Figure 4.3, the relative ratio of the NMA-PAA$_{450K}$ to Dan-PAA$_{2K}$ emission peak in the mixed solution was determined as 13:1. The relative fluorescence intensity of NMA-PAA$_{450K}$ to Dan-PAA$_{2K}$ obtained from isolated solutions was similar to that of the mixed PAA solution indicating that the emission of one fluorophore did not perturb the emission of the other by any measurable amount. (Figure 4.3).
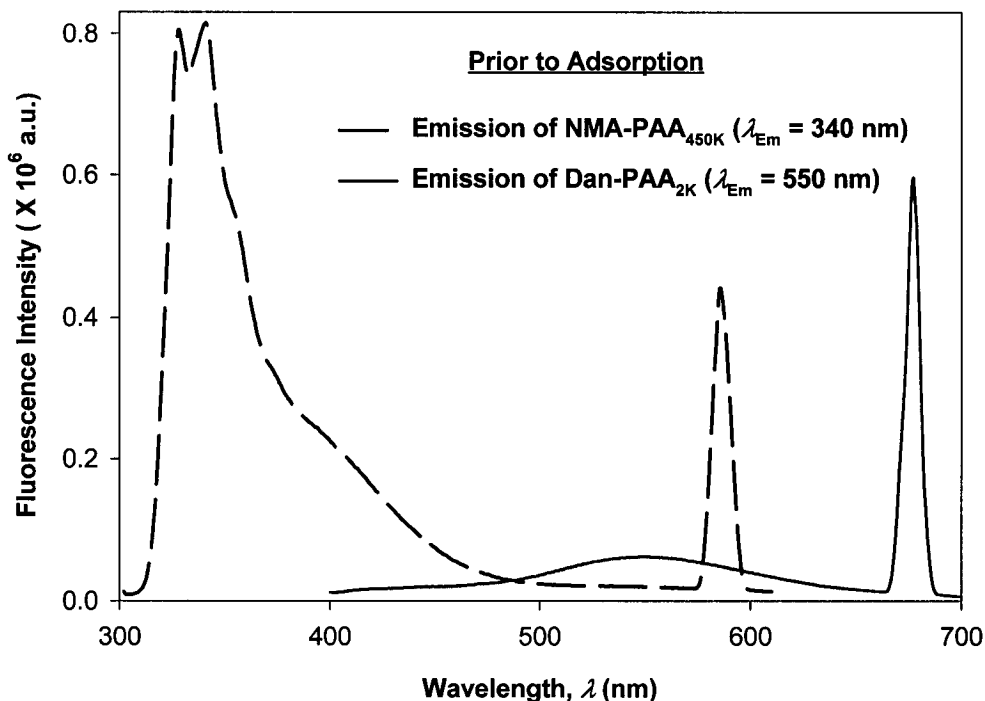
Figure 4.3   Pre-adsorbed fluorescence spectrum of a mixed solution containing 5.0 ×
10^{-3} g/L of each of NMA-PAA$_{450K}$ (λ_{Ex} = 290 nm), and Dan-PAA$_{2K}$ (λ_{Ex} = 335 nm).
Emission intensity ratio of NMA-PAA$_{450K}$ to Dan-PAA$_{2K}$ is 13:1.

4.4.2   Competitive Adsorption of Labeled PAA onto a PAH Surface

Successful adsorption of PAA onto a PAH coated surface is known from previous

ζ potential measurements and solid-state NMR spectroscopy of similar multilayer

systems.[19,23]   We provided an equal surface coverage concentration of both the 2K and

the 450K PAA repeat units to a quantitative amount of PAH layered SiO$_2$.   At

concentrations lower than that required for complete coverage, both 2K and 450K PAA

would adsorb to meet until surface coverage achieved, and such an experiment would fail

to test for preferential adsorption.   If experiments are conducted at concentrations higher

than that required for surface coverage, we might not observe a significant change in the
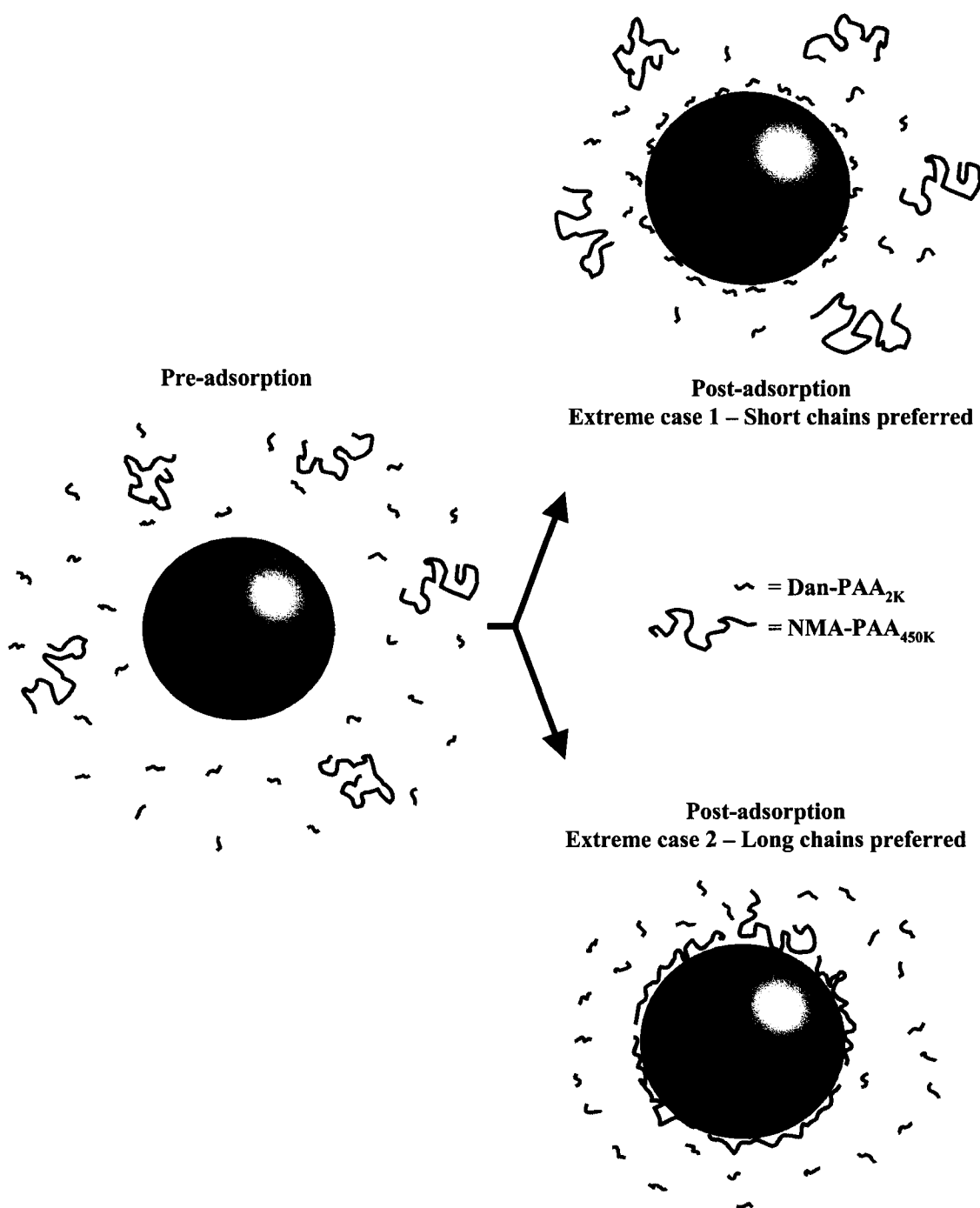
Figure 4.4 Possible extreme results for the competitive adsorption experiment of PAA onto PAH-coated particles. The two extreme cases show preference of the surface for only the short chains (emission only at λ_{Em} = 550 from adsorbed Dan-PAA$_{2K}$), or solely the long chains (emission only at λ_{Em} = 550 from adsorbed NMA-PAA$_{450K}$). The third intermediate case (not shown) is that of indifferent adsorption.

fluorescence signal to identify preferential adsorption. Figure 4.4 illustrates the two extreme outcomes for this competitive adsorption study. Given an identical concentration of repeat units, the two extreme cases involve either sole preference for shorter chains of PAA (i.e., Case 1, where fluorescence is only detected from Dan-PAA$_{2K}$) or the longer ones (i.e., Case 2, where only NMA-PAA$_{450}$ fluorescence is observed). A third possible scenario is that of an unbiased adsorption of both short and long chains, in which no change in the relative fluorescence signals would be expected before and after the adsorption.

Although previous studies examining the preparation of PAH/PAA multilayers suggest adsorption times on the order of tens of minutes, (supplying excess concentration of the adsorbing polyelectrolyte), we allowed 24 h for the competitive adsorption study of PAA since here, we supply only a minimum coverage concentration of short and of long chains of PAA. After 24 h, we examined the fluorescence of both the PAA/PAH-coated particles (thoroughly rinsed free of excess polymer), and the remaining unadsorbed PAA in the supernatant. Figure 4.5 shows the relative fluorescence intensity obtained for the labeled PAA adsorbed on the particles while Figure 4.6 shows that of the unadsorbed PAA remaining in the supernatant. After exciting both fluorophores on the particles, no detectable fluorescence emission from Dan-PAA$_{2K}$ at λ_{Em} = 550 nm was observed. However, the particles did exhibit a strong emission signal from at λ_{Em} = 340 nm. Similar inspection of the supernatant indicated an opposite trend, where we observed significant fluorescence from Dan-PAA$_{2K}$. Furthermore the intensity ratio of NMA-PAA$_{450}$: Dan-PAA$_{2K}$ in the supernatant was 3.4:1, which was significantly less than the original pre-adsorption ratio of 13:1. Fluorescence analysis of both the PAA adsorbed
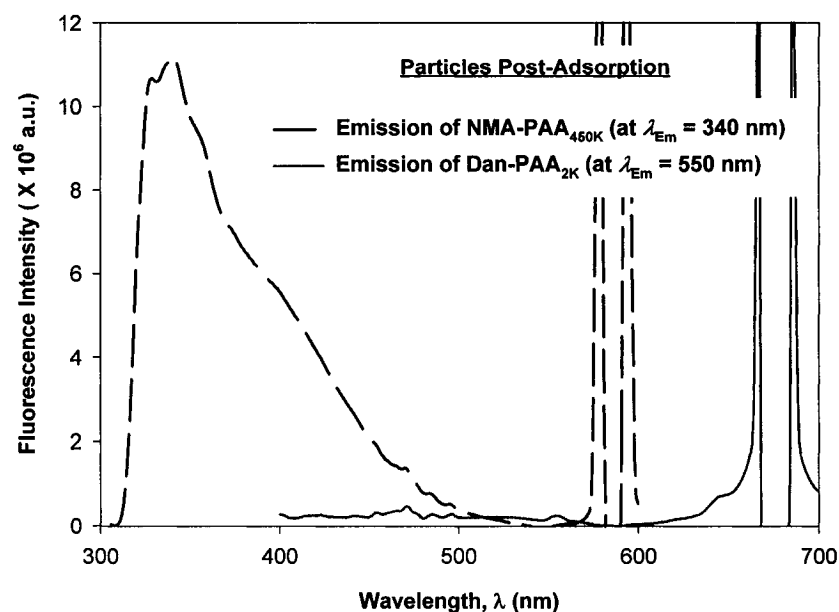
Figure 4.5 Post adsorption fluorescence emission of the PAA adsorbed on particles. A detectable fluorescence from the particles is solely from NMA-PAA$_{450K}$.
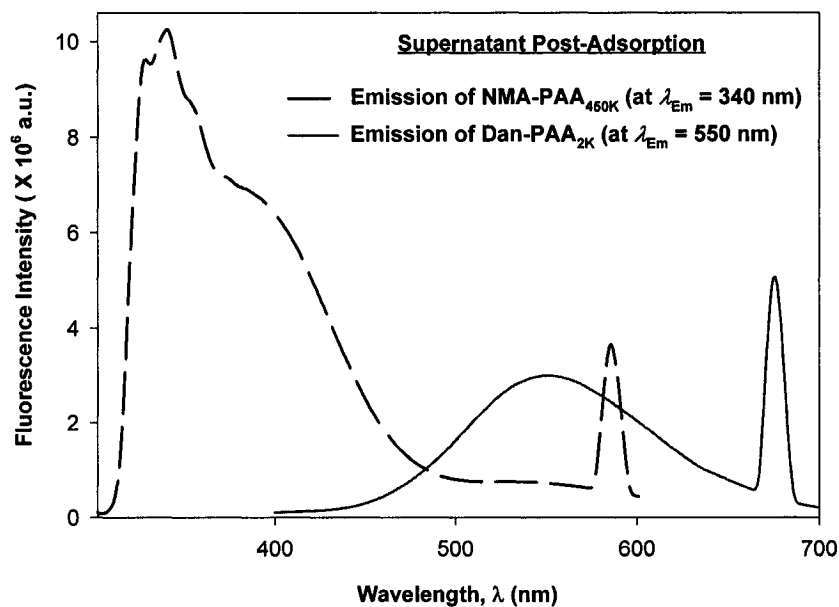
Figure 4.6 Post-adsorption fluorescence emission of PAA in the supernatant. Emission intensity ratio of NMA-PAA$_{450K}$ (λ_{Ex} = 290 nm) to Dan-PAA$_{2K}$ (λ_{Ex} = 335 nm) is reduced to 3:1.

onto the particles and the PAA remaining in the supernatant suggest the preferred adsorption of the higher molecular weight component PAA onto the PAH-coated colloidal particles after 24 hr. Also, we do not expect the effects of PAA polydispersity to significantly mislead our results since: a) the two extreme chain lengths differ by two orders of magnitude, and b) preliminary DLS characterization of the 2 K and 450 K chains showed negligible overlap in the distribution of their hydrodynamic radius.

4.4.3 General Processes in Adsorption

To understand why there is preferential adsorption of longer chains of PAA onto PAH-coated particles, it is worthwhile to examine the general steps involved in the process of polymer adsorption. The adsorption mechanism begins by the transport of bulk polymer to the surface-adsorbing site. Kinetically, this diffusion-limited step would favor the arrival of shorter chains to the surface. Transport is then followed by polymer attachment to the surface, and lastly rearrangements, which can occur in the adsorbing layer. The two initial steps generally occur rapidly and the adsorption rate is usually transport-limited since the polymer arriving at the surface adsorbs immediately.[24] As surface coverage increases, adsorption becomes hindered. At this stage, further adsorption is highly dependant on attachment to the remaining free sites.[25] At very high surface coverage and approaching maximum coverage, transport plays a minimal role and the specific attachment process becomes increasingly important.[25] Rearrangement processes are also generally much slower and thus some polymer adsorption can be considered to be irreversible at relatively short time-scales.[26,27] Therefore, in the case where adsorption is examined at time-scales much larger than that required to achieve

full surface coverage, kinetic contributions are less likely to influence the preferential adsorption of polymers and over much longer time-scales. In this plateau region of an adsorption isotherm adsorption is less dependant on transport.[25]

4.4.4 Polyelectrolyte Adsorption

In polyelectrolyte adsorption additional interactions need to be considered which have important thermodynamic implications. The theory of neutral polymer adsorption can be extended to polyelectrolyte adsorption by incorporating Debye-Hückel theory.[14] Polyelectrolytes adsorb onto oppositely charged surfaces when the energy of adsorption exceeds the net entropy resulting from the culmination of entropic losses (associated with the reduction in the number of configurations available to the polyelectrolyte), and entropic gains (associated with the release of counterions). Whether or not adsorption will occur depends on if there is sufficient energy given to the system to overcome the entropy loss i.e. if the temperature is below a critical value to reduce the free energy and to drive towards adsorption.

Enthalpic contributions include the interaction type and strength between the polyion and the surface (i.e., electrostatic attraction with each link of the order k_BT) as well as the interaction between charged segments (i.e., electrostatic repulsion), which oppose adsorption.[25,28] In the adsorption of charged polymers the surface charge is compensated when the adsorbed charge balances with the surface charge such that the electrostatic attraction of the segments with the surface is balanced by the repulsion of segments in the adsorbing layer. In polyelectrolyte multilayer adsorption the surface charge is overcompensated, causing net electrostatic repulsion. In achieving charge overcompensation, weakly charged polyelectrolytes differ from strongly charged

polyelectrolytes in that more polyion molecules have to adsorb in order to overcompensate the surface charge and this is why more polyelectrolyte adsorption is generally observed. Chain stiffness and conformation also have significant effect on adsorption, particularly in the case of weak polyelectrolytes.[29] For example, adsorption of weak charged polyelectrolytes onto an oppositely charged surface in the form of "loops and tails" can be favored over a more flat, "train-like" configuration where electrostatic interactions between polyion segments and the surface are maximized.[30] The conformation of polyelectrolyte adsorption is thus highly sensitive to the electrostatic environment during adsorption, for example,. the solvent pH and ionic strength.[31] In the case of polyelectrolyte multilayer adsorption, nonelectrostatic short range forces such as hydrophobic interactions have also been observed, which enhance stability in adsorption.[32]

4.4.5 Long- versus Short-Chain Adsorption

4.4.5a Enthalpic Considerations

In considering the preferential adsorption of PAA onto PAH-coated particles, we assume uniform capping of the SiO_2 with the polycation, PAH. Thus all potential adsorption surface sites are assumed to be entirely composed of PAH repeat units, and the adsorption occurs on a chemically homogeneous surface. This is a reasonable assumption for PAH adsorbed in excess concentration and under solution conditions that render it a weakly charged polycation (i.e., adsorption solution adjusted to pH = 9, near the pK of PAH).[19,33] This implies that all electrostatic attractions between identical polycations and polyanions are energetically equivalent (i.e., of equivalent $k_B T$, since in both cases each PAA sample contains an equal number of repeat units).[34] Additionally,

the enthalpic loss derived from displacement of counterions from their associated polyelectrolytes is also similar for the short and long chain systems. Hence, if we assume that the electrostatics is one of the dominant driving forces in multilayer formation, we can simplify the thermodynamic comparison by presenting an ideal case in which the enthalpic energy is identical in the two cases, under identical solvent conditions (i.e., pH value and salt concentration).

Interestingly, the addition of a high concentration of electrolyte has been shown to influence the adsorption of polyelectrolytes of varying chain lengths. In previous adsorption studies of a strongly charged polyelectrolyte, poly(styrene sulfonate) onto a chemically homogeneous Fe_2O_3 surface, preferential adsorption was observed for shorter chains from a salt-free solution while longer chains were preferred in the presence of 0.1 M NaCl.[35,36] Adsorption studies of PAA,[37] polyacrylate,[38] and carboxymethyl cellulose[38] adsorbed onto $BaSO_4$ report similar preferential adsorption of low molecular weight components in the absence of salt. However, these adsorption isotherms reveal significant displacement of the low molecular weight with the high molecular weight in the presence of 0.5 M NaCl.[38] This adsorption behavior is rationalized using a sequential adsorption process, which suggests that first, smaller chains are adsorbed.[39] For example, short PAA chains initially adsorbed eventually generate an electrostatic barrier from charge overcompensation occurring on the positive surface. This barrier strongly affects the diffusion of chains towards the PAA covered surface. Specifically, the barrier can prevent longer chains from accessing the surface, and thus limits their displacement of pre-adsorbed shorter chains. With an increased salt concentration the barrier is lowered, permitting longer chains to reach the surface and adsorb. At this point, the adsorption preference is shifted to longer chains as experimentally observed.[39] We

therefore suggest that our observation of preferred adsorption of longer PAA chains onto PAH after a 24 h adsorption period is likely restricted to the time-window past which such displacement effects are likely to occur. Further supporting evidence for the occurrence of short-chain displacement is given by recent adsorption experiments of model cationic oligomers onto colloids,[40] and short polyions assembled onto proteins,[41] which suggest that shorter chains have more difficulty forming loops and tails under assembly conditions where the polyion is weakly ionized. As such, adsorbed short-chain polyions can be more easily displaced by longer chains from failure to make a sufficient number of ionic contacts.

4.4.5b Entropic Considerations

Although the LBL self-assembly technique is based on electrostatic attraction of positively and negatively charged polyions, the primary driving force is presumed to be entropy and not enthalpy. In the electrostatic assembly of multilayers, the condensation of oppositely charged polyions liberates low molar mass counterions. This process increases the entropy of the system, comparable to the polyelectrolyte complexes formed in solution.[42,43] Thus, although other interactions such as hydrophobic interactions, charge transfer interactions, π-π stacking forces, or H-bonding may also contribute, the successful formation of polyelectrolyte multilayers is primarily attributed to the entropy gain from ion exchange.[32,44]

In determining the effect of entropy on the preferential adsorption of short versus long chains of polyelectrolytes, three entropic contributions need to be considered. First is the net entropy associated with the liberation of the counterions. Since we provide an

identical number of repeat units for both long- and short-chain PAA, and assume coverage adsorption in both cases, the counterion release entropy should be similar for both 2 K and 450 K. Secondly, we need to compare the configurational entropy of the short- versus long-chain polyelectrolyte upon adsorption. As the polyelectrolyte chain length is increased, the entropy penalty associated with the adsorption becomes greater. This is because there are more configurational restrictions to surface-bound long chains as compared to adsorbed short chains. The loss in configurational entropy upon adsorption is therefore expected to be much larger for the 450 K PAA, which would favor short-chain adsorption. Lastly, we need to compare the configurational entropy of the free polyelectrolytes in solution. There is a far greater entropic gain from having more shorter chains in solution, which can explore a greater number of configurational states than a fewer longer chain species in solution. Similar to the liberation of counterions which drives the LBL assembly process, the entropy gain of having more free short chains in solution favors the preferential adsorption of long-chain PAA onto the PAH surface. Experimentally, the configurational entropy difference between short and long-chains of PAA in solution appears to be the governing factor leading to the preferential adsorption of 450 K PAA. Moreover, this argument is supported by reports of shorter-chain polyelectrolyte displacement in exchange for adsorption of longer-chains on Fe_2O_3 and $BaSO_4$ in the presence of salt, as previously mentioned.[39] Analysis of both the fluorescence spectrum of the PAA-adsorbed particles, and that of the remaining supernatant after the adsorption, suggest that the preferential adsorption of long- over short-chain PAA is dominated by the entropy gain of keeping short chains free in solution.

It is important to note that the discussion of entropic and enthalpic contributions to adsorption preference of longer versus shorter chains is based solely on thermodynamic arguments. As such, polyelectrolyte multilayer formation here is treated as equilibrium in nature and thus limited since kinetic factors such as the adsorption of kinetically trapped polyions, and irreversible adsorption can also influence the chain-length preference for adsorption. For example, while we assume that the enthalpic component is identical for both the longer chain and the shorter chain (given the same concentration of repeat units for both cases), the higher degree of connectivity between the repeat units for the longer chain can restrict its desorption from a surface since there is a reduced probability for simultaneous removal of all repeat units off the surface as compared to the shorter chains. Hence a more detailed study involving examination of the kinetic influences in adsorption in addition the thermodynamic considerations outlined here would help clarify the role of kinetics on the competitive adsorption of short versus long chains in polyelectrolyte multilayer deposition.

4.5   Conclusions

Given a stoichiometric quantity for coverage of polyelectrolyte, fluorescence studies of labeled 2 K versus 450 K PAA adsorbed onto PAH-coated silica colloids showed complete preferential adsorption of the long chains after a 24 h deposition period and in a 1 mM NaCl assembly bath. Furthermore, any initially adsorbed short PAA chains on the surface are likely to be displaced by long chains after some time if the adsorption solution contains added electrolyte sufficient enough to reduce the electrostatic barrier associated with the development of charge overcompensation. The preferential adsorption of long PAA chains is primarily believed to be a consequence of

the greater configurational entropy gain in having more short chains in solution as compared to long chains. This is analogous to the large entropy gain upon liberation of counterions, which is believed to drive the LBL assembly of oppositely charged polyelectrolytes.

4.6   References and Notes

(1)   Knoll, W.; Matsuzawa, M.; Offenhausser, A.; Ruhe, J. *Isr. J. Chem.* **1997**, *36*, 357.

(2)   Edmondson, S.; Osborne, V. L.; Huck, W. T. S. *Chem. Soc. Rev.* **2004**, *33*, 14.

(3)   Hu, Z. *Macromol. Symp.* **2004**, *207*, 47.

(4)   Chen, Y. L.; Israelachvili, J. N. *J. Phys. Chem.* **1992**, *96*, 7752.

(5)   Serizawa, T. In *Supramolecular Design for Biological Applications*; Yui, N., Ed.; CRC Press LLC: Boca Raton, FLA, 2002; pp 83–93.

(6)   Decher, G. *Science* **1997**, *277*, 1232.

(7)   *Multilayer Thin Films: Sequential Assembly of Nanocomposite Materials*; Decher, G., Schlenoff, J. B., Eds.; Wiley-VCH: Germany, Weinheim, 2003.

(8)   Fleer, G. J.; Scheutjens, J. M. H. M. *Adv. Colloid Interface Sci.* **1982**, *16*, 341.

(9)   Baumgartner, A.; Muthukumar, M. *J. Chem. Phys.* **1991**, *94*, 4062.

(10)   deGennes, P. G. *J. Phys. (Paris)* **1976**, *37*, 1445.

(11)   Alexander, S. *J. Phys. (Paris)* **1977**, *38*, 977.

(12)   Cohen Stuart, M. A.; Scheutjens, J. M. H. M.; Fleer, G. J. *J. Polym. Sci., Polym. Phys. Ed.* **1980**, *18*, 559.

(13)   Felter, R. E.; Ray, L.N. *J. Colloid Interface Sci.* **1970**, *32*, 349.

(14)   Châtellier, X.; Joanny, J. F. *J. Phys. II* **1996**, *6*, 1669.

(15)   Kovacevic, D.; van der Burgh, S.; de Keizer, A.; Cohen Stuart, M. A. *Langmuir* **2002**, *18*, 5607.

(16)   Jucker, B. A.; Harms, H.; Hug, S. J.; Zehnder, A. J. B. *Colloids Surf., B* **1997**, *9*, 331.

(17)   Weber, G.; Lawrence, D. J. F. *Process Biochem.* **1954**, *56*, 31.

(18) Anghel, D. F.; Alderson, V.; Winnik, F. M.; Mizusaki, M.; Morishima, Y. *Polymer* **1998**, *39*, 3035.

(19) Burke, S. E.; Barrett, C. J. *Langmuir* **2003**, *19*, 3297.

(20) Mermut, O.; Barrett, C. J. *J. Phys. Chem. B* **2003**, *107*, 2525.

(21) Bednar, B.; Li, Z.; Huang, Y.; Chung, L.; Chang, P.; Morawetz, H. *Macromolecules* **1985**, *18*, 1829.

(22) Chen, H. L.; Morawetz, H. *Eur. Polym. J.* **1983**, *19*, 923.

(23) Smith, R. N.; McCormick, M.; Barrett, C. J.; Reven, L.; Spiess, H. W. *Macromolecules* **2004**, *37*, 4830.

(24) Dijt, J. C.; Cohen Stuart, M. A.; Hofman, J. E.; Fleer, G. J. *Colloids Surf.* **1990**, *51*, 141.

(25) Hoogeveen, N. G.; Cohen Stuart, M. A.; Fleer, G. J. *J. Colloid Interface Sci.* **1996**, *182*, 133.

(26) Cafe, M. C.; Robb, I. D. *J. Colloid Interface Sci.* **1982**, *86*, 411.

(27) Meadow, J.; Williams, P. A.; Garvey, M. J.; Harrop, R. A.; Phillips, G. O. *Colloids Surf.* **1988**, *32*, 275.

(28) von Goeler, F.; Muthukumar, M. *J. Chem. Phys.* **1994**, *100*, 7796.

(29) Dzubiella, J.; Moreira, A. G.; Pincus, P. A. *Macromolecules* **2003**, *36*, 1741.

(30) Borisov, O. V.; Zhulina, E. B.; Birshtein, T. M. *J. Phys. II* **1994**, *4*, 913.

(31) Notley, S. M.; Biggs, S.; Craig, V. S. J.; Wagberg, L. *Phys. Chem. Chem. Phys.* **2004**, *6*, 2379.

(32) Kotov, N. A. *Nanostruct. Mater.* **1999**, *B12*, 789.

(33) Smith, R. N.; Reven, L.; Barrett, C. J. *Macromolecules* **2003**, *36*, 1876.

(34) Dubas, S. T.; Schlenoff, J. B. *Macromolecules* **1999**, *32*, 8153.

(35) Ramachandran, R.; Somasundaran, P. *J. Colloid Interface Sci.* **1987**, *120*, 184.

(36) Ramachandran, R.; Somasundaran, P. *Colloids Surf.* **1988**, *32*, 307.

(37) Wright, J. A.; Harrop, R.; Williams, P. A. *Colloids Surf.* **1987**, *24*, 249.

(38) Bain, D. R.; Cafe, M. C.; Robb, I. D.; Williams, P. A. *J. Colloid Interface Sci.* **1982**, *88*, 467.

(39) de Laat, A. W. M.; van den Heuvel, G. L. T. *Colloids Surf., A* **1995**, *98*, 53.

(40) Shin, Y. W.; Roberts, J. E.; Santore, M. *J. Colloid Interface Sci.* **2001**, *244*, 190.

(41)   Houska, M.; Brynda, E.; Bohatá, K. *J. Colloid Interface Sci.* **2004**, *273*, 140.

(42)   Kabanov, V. A. *Polym. Sci. U.S.S.R.* **1994**, *36*, 143.

(43)   Philipp, B.; Dautzenber, H.; Linow, K. J.; Kötz, J. Dawydoff, W. *Prog. Polym. Sci.* **1989**, *14*, 91.

(44)   Bertrand, P.; Jonas, A.; Laschewsky, A.; Legras, R. *Macromol. Rapid Commun.* **2000**, *21*, 319.

Chapter 5

Structural and Mechanical Properties of Polyelectrolyte

Multilayer Films Studied by AFM

5.1 Preface

In the previous chapter, we examined the adsorption of a polyelectrolyte onto a surface modified with an oppositely charged weak polyelectrolyte from both a thermodynamic and kinetic point of view. Having some insight into the factors important in the mechanism of adsorption, the following chapter explores how we can achieve molecular control over the structure of the polyelectrolytes deposited into multilayers by employing weakly charged polymers in adsorption. Furthermore, we propose a simple AFM-based approach for comparing the different structural and mechanical properties obtained when multilayers are assembled with polyelectrolytes of varying charge density. Importantly, we demonstrate how AFM nanoindentation experiments can give an estimation of the relative "loop length" between "ionic cross-links" in multilayer films.

5.2 Introduction

The sequential assembly of oppositely charged polyelectrolytes in an alternating layer-by-layer fashion has recently become a useful tool for the controlled fabrication of organic thin films and modification of surfaces in aqueous media.[1,2] The promise of these multicomposite organic films as viable materials in various applications such as separation membranes and drug delivery capsules relies on the ability to direct the internal

architecture of the multilayers on a molecular level.[3,4] For example, controlling structural properties such as the density or porosity of a multilayer film is critical for their use as anti-reflection optical coatings,[5] biocompatible macromolecule encapsulates,[6,7] and gas separation membranes,[8] since the architecture governs the refractive index, molecular diffusion rates, and gas permeability respectively in the film. Furthermore, the use of weak polyelectrolytes allows flexibility in the film architecture, which can be defined either during the multilayer preparation (prepn) through pH-adjustments of the polymer ionization fraction or post self-assembly via pH-mediated porosity transitions.[9]

Early on in the study of polyelectrolyte multilayer assemblies it was shown that in cases where the polyions of constant charge density are used, the ionic strength of the adsorption solutions is a significant factor in determining both the conformation of the adsorbing polyelectrolytes[10–12] and the thickness of the adsorbed layers.[13,14] More recently, it has been demonstrated that the employment of weak polyelectrolytes (i.e., those containing pH-dependent charge density in aqueous solution) is highly advantageous due to the ability to control the layer thickness by tuning the ionization fraction of the polyions about their pK.[15–17] The diverse range of solution-dependent conformational properties that polyelectrolytes can adopt when forming multilayer assemblies have prompted several investigations aimed at examining the internal architecture of the films. Previously, x-ray and neutron reflectometry experiments have been used for small-scale structural elucidation of the films (i.e., on the order of 10 nm).[2,18] For instance, neutron experiments have been used to probe concentration gradients along the layer normal, thus revealing information about the extent of stratification of the layers, the interfacial roughness and the degree of interpenetration between subsequent layers.[19,20] However, these high-energy techniques are inefficient

requiring deuteration of the sample and are unable to measure contact-point density in multilayer films. Optical methods such as second harmonic generation (SHG) have also been useful for probing interfacial properties of anisotropically oriented polyelectrolyte layers,[21,22] while optical waveguide lightmode spectroscopy (OWLS) and scanning angle reflectometry (SAR) have also been employed to obtain structural information on multilayers.[23] While many of these techniques have been successful at characterizing the interfaces and layer architecture in the films, there is still a lack of understanding concerning some of the basic structural properties of the polymer chains forming the ionic links between the layers, i.e. the loop length between "ionic cross-links". Obtaining such information, as a function of assembly conditions has proved difficult and this task is further complicated by the presence of significant interpenetration observed between adjacent layers,[2] as revealed by reflectivity studies[11] and Förster energy transfer experiments.[24]

Previous atomic force microscopy (AFM) studies of polyelectrolyte multilayers have focused primarily on visual characterization of the thin films in response to various assembly parameters such as: the number of layers built,[25] solution salt,[26] pH conditions,[27] intermittent drying between adsorption cycles[28] and the effect of post-assembly exposure to electrolyte solution.[5,9] Extensive AFM investigations into various polyelectrolyte multilayer systems in the image mode have revealed much information regarding surface properties such as: aggregation,[29] homo/heterogeneity,[30] roughness,[31] coverage,[30] and porosity.[9] However, relatively few investigations have been conducted on the mechanical properties of layered polyelectrolyte films, in particular by AFM force-distance measurements. A few notable exceptions to this have involved using an AFM in force mode to measure dynamic interactions and friction in adsorbed single

polyelectrolyte layers.[32-33a,b] Gravimetric techniques such as quartz crystal microbalance (QCM) have also been used for mechanical characterization of the film-solution interface in polyelectrolyte multilayers via acoustic impedance measurements of a multilayered resonator. In a recent report, the viscoelastic behavior of the outermost diffuse layers in polyelectrolyte multilayer films was determined using QCM measurements and the shear modulus of the film's surface was investigated as a function of ionic strength, intrinsic polyion flexibility and variable terminating polymer layer.[34] In addition, the surface force apparatus (SFA) has been a suitable tool for in-depth examinations of the interaction forces and shear properties of adsorbed polyelectrolyte layers[35] and multilayers.[36]

In this study, we obtained elasticity measurements from the indentation curves of an AFM tip into a series of PAH/P-Azo multilayer films, prepared at various pH conditions, in order to probe the mechanical nature of the polymer layer structures resulting from assembling weakly charged polyelectrolytes at various charge densities. The elastic modulus is then determined from the force-distance data by fitting the deformation in the contact region to Hertzian mechanics. A structure-mechanical property relation in the polymer films is inferred by relating the "ionic cross-link" density (frequency of connection points between oppositely charged polyions in the multilayer) to the resulting elastic response. Consequently, we propose that mechanical force-distance measurements made using an AFM may be successfully and systematically applied in order to compare relative polymer loop length between "ionic cross-links" formed during the assembly of weak polyions into multilayer films, a measurement difficult to obtain by any other technique.

5.3   Experimental Section

5.3.1   Materials

The weakly charged polycations and polyanions assembled into multilayer films were PAH (Polysciences, M_w 60K), and P-Azo (Aldrich, M_w 90K) respectively. The chemical structures of these polyelectrolytes are shown in Figure 5.1. Aqueous solutions containing 10^{-2} M per polyion repeat unit were prepared using 18 MΩ·cm resistivity Millipore Milli-Q water. The charge density of the polyelectrolytes was adjusted by altering the pH of the assembly solutions from a value of 5.0 to 10.5 using NaOH or HCl. The pH of the polymer solutions was periodically monitored and did not deviate more than ± 0.2 pH units over the course of film fabrication.
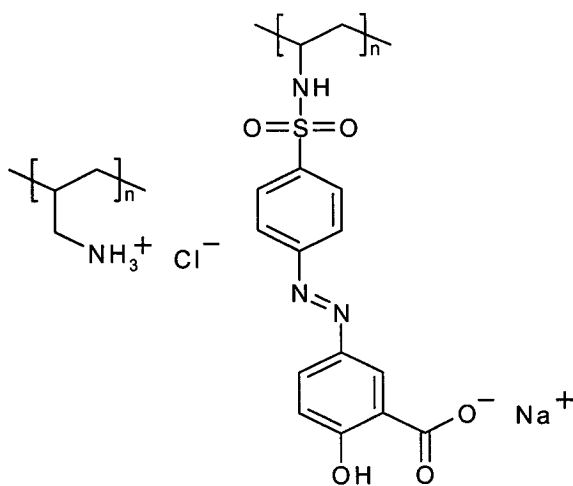
Figure 5.1   Repeat unit structures of the polycation, PAH (left), and the polyanion, P-Azo (right) used.

5.3.2 Multilayer Film Preparation

The substrates, Si (Wafernet) and glass slides (Fisherbrand), were cleaned by immersion in a bath of 25% H_2SO_4 and 75% H_2CrO_4 for 24 h. To rid the substrates of chromium and other ions, the surfaces were rinsed with a concentrated solution of HCl followed by thorough rinsing with Milli-Q water. The average contact angle of the surfaces was measured to be <10° (Optrel GBR Multiskop), ensuring that the substrates were hydrophilic prior to deposition of the initial polycationic layer. The film assembly procedure involved the alternating and repeated immersion of substrates in polycation solution, followed by the polyanion solution. Between each polyelectrolyte deposition, films were rinsed in several baths of Milli-Q water. It is known from previous time-dependent studies of various weak polyelectrolyte systems into multilayer assemblies that saturated adsorption in these systems (>80%) is readily achieved in <1 min.[37] Thus, multilayer films were constructed using a dipping time of 2 min for both polyelectrolyte solutions. Using an automatic slide stainer (Shandon), multilayer films were prepared with polyions having varying charge densities using solutions adjusted to pH values of 5.0, 7.0, 9.0, and 10.5 (matched for both polycation and polyanion) and depositing 346, 560, 116 and 76 layers respectively to make films of identical thickness (1100 ± 60 nm) on Si. A Gaertner Ellipsometer at 633 nm, (calculating both refractive index and layer thickness) was used to measure the film thickness on Si. We also confirmed that films assembled on glass slides at varying pH values were similar in optical thickness by observing the $\pi \rightarrow \pi^*$ absorbance maximum of P-Azo at λ_{max} = 365 nm using a UV-vis spectrophotometer (Varian Cary 300-Bio; scan rate 100 nm·min^{-1}).

For adhesion measurements, silicon nitride tips (Veeco, DNP probes) were modified with 75 layers of PAH/P-Azo, prepared by dipping in polycation/polyanion solutions matched at either pH = 5.0 or pH = 9.5. In all cases, the capping layer of the multilayered probe was PAH. The multilayered AFM probes and reference uncoated tips were imaged with a scanning electron microscope (SEM, JEOL 840A) at 10000x magnification.

5.3.3   Elasticity Measurements Using an AFM

Force measurements of the multilayer films were performed using an AFM in force calibration mode (Nanoscope Version 3A, Digital Instruments). The multilayer surface and the tip were brought together in a fluid cell at room temperature. We used silicon nitride probes (r = 20–60 nm) with a manufacture specified force constant, k_F, of 0.12 N/m. All elasticity measurements of the films were performed with the same AFM tip, thus no calibration for the absolute spring constant of the tip was performed. The AFM detector sensitivity was calibrated by obtaining a force curve on a bare substrate and determining the slope of the linear portion of the data after contact. Obtaining force curves of the multilayer film involved bringing the tip in close contact with the surface in aqueous media, and obtaining force measurements after allowing the system to equilibrate for 10 min, or until reproducible curves were observed. The rate of the indentation cycle was kept constant at 0.2 Hz. For elasticity measurements, 4 replicate measurements of the deflection as a function of the piezo z-position were acquired with the unmodified AFM tip indented at random coordinates on the film surface.

5.3.4 Data Analysis of Force Curves

Similar to previously described methods, we analyzed our AFM data by first characterizing the 3 main regions in the deflection curve, which depict the interaction of the tip with the substrate (both on the approach and the retraction).[38,39] In the non-contact region, the tip and surface do not interact with one another, except in the case of long-range forces, and thus no change in the cantilever deflection, d, is detected with respect to z-position of the piezo, z. After contacting the surface, deflection of the probe begins to increase and this characterizes the non-linear contact region. Provided that the film is sufficiently soft, the tip will indent the sample to a distance, δ resulting in a smaller deflection with $d = z-\delta$. At some point in the indentation, the cantilever deflection becomes linear with respect to z, upon which $d = z$, indicating that "infinite stiffness" in the sample has been reached. While a more rigorous approach using SFA can yield an absolute value for the true separation between the tip and the sample, the contact or zero point, z_0, in AFM is ascertained graphically as the initial point where the non-contact region of the curve begins to deviate from linearity. In practice, the z_0 is obtained as the intersection coordinate between the extrapolated linear pre-contact region (part a in the deflection curve, inset of Figure 5.2) with the extrapolated "infinitely stiff" portion of the contact region (part b).[40] All force measurements were obtained in 10 mM NaCl (i.e., at pH = 5.0, below the pK_a of the Si_3N_4 tip of 6.0).[40] Under these conditions, there was more efficient screening of adhesion (observed in the retraction curve when using Milli-Q water) and reduced tip-sample interactions resulting in tip instability, (i.e., near z_0 in the approach curve). Note that for ease of comparing the force data, the curves were rotated

to remove elements of long-range repulsive forces, a procedure which results in flattening the force curves.

To convert the raw deflection versus z-position data into a plot of force as a function of indentation we use Hooke's law in which the loading force, F, is related to the deflection through the cantilever force constant, k_F.[38]

$$F = k_F d = k_F(z-\delta) \qquad (5.1)$$

A final force versus separation plot is thus obtained by: a) calibrating the sensitivity, b) shifting the deflection curve to the appropriate (0,0) contact point, c) converting the z movement of the piezo to an indentation, and d) using Hooke's law to convert deflection into force.

We used Hertzian mechanics to describe the elastic deformation of the multilayer film (assumed to be a planar surface) with a spherical tip (fit to this geometry based on indentation depths into the multilayer which were less than the tip radius). Young's modulus, E, can then be calculated from the following equation.[39]

$$F = \frac{4E\sqrt{r}}{3(1-\sigma^2)}\delta^{3/2} \qquad (5.2)$$

We assume that the multilayer polymer film behaves as an elastic rubber, and thus impose a Poisson ratio of $\sigma = 0.5$. The average specified tip radius was $r \sim 40$ nm. In a linear plot of log F as a function of log δ, the elastic modulus is then extracted from the intercept value as suggested by Equation 5.3. Note that while we observed little

hysteresis between the approach and retract cycle of the nanoindentation, we analyzed the approach curves due to interference of adhesion forces exhibited during the retraction of the tip. To determine the elastic modulus of the films, the force curves in the contact region were fitted to Equation 5.3 by fixing the slope to 3/2 (with all experimental $r^2 >$ 0.92) and solved for the intercept value, b.

$$\log F = \frac{3}{2}\log \delta + \log\left(\frac{4E\sqrt{r}}{3(1-\sigma^2)}\right) \tag{5.3}$$

For the adhesion experiments, measurements of the pull-off force between a multilayered tip and multilayer films on glass slides were conducted in both Milli-Q water and 10 mM NaCl. The average adhesion values were compared for three assembly pH combinations for both the tip and the substrate (a minimum of 20 random measurements per sample over a 10 x 10 μm area).

5.4   Results and Discussion

5.4.1   Elastic Modulus of Multilayer Films

It has previously been established that the thickness of a multilayer film assembled from weakly charged PAH and P-Azo is dependent on the ionization fraction of the polyelectrolytes during assembly, in particular, that of PAH.[37] For example, when PAH/P-Azo films are prepared using a solution pH above that of the pK_a of PAH, i.e. pH ~ 8.7,[41] the per layer optical and ellipsometric thickness of the film increases significantly as compared to the film constructed with PAH when it is strongly charged at pH = 5.0 and

pH = 7.0, as indicated in Table 5.1. Using an atomic force microscope, nanoindentations of PAH/P-Azo were performed on identically thick films to determine the relative Young's modulus as a function of the polyelectrolyte charge density during assembly. For comparison, Figure 5.2 shows representative force versus indentation curves obtained
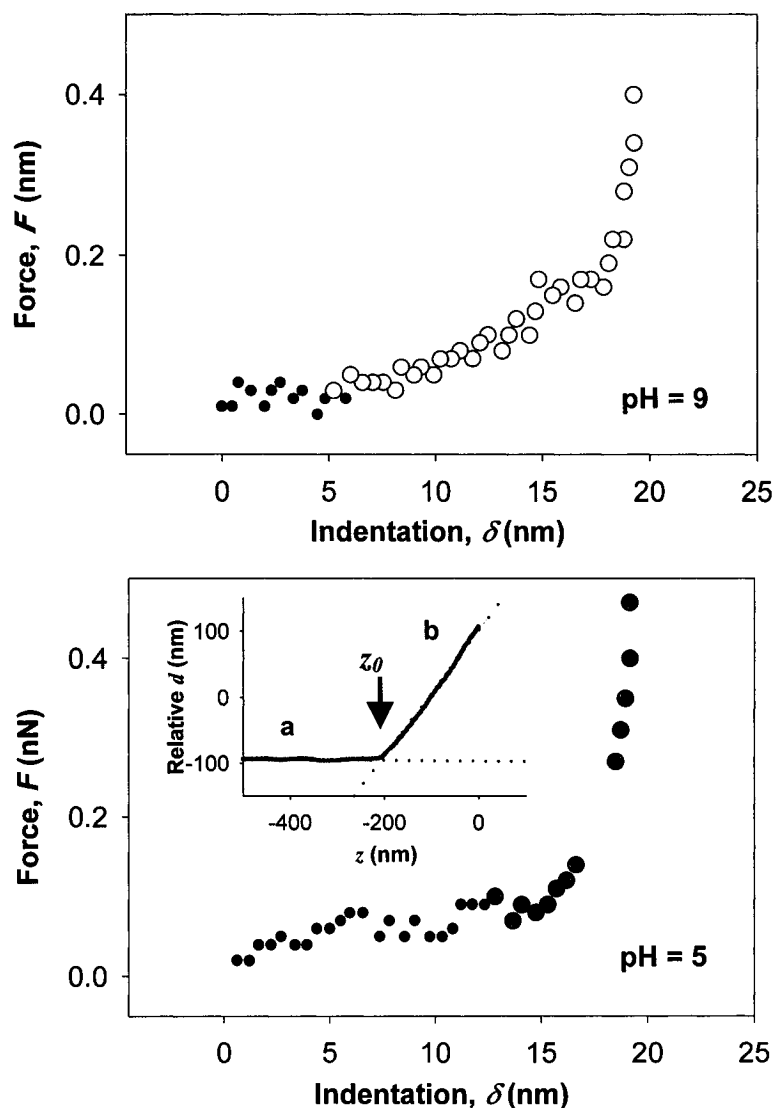
Figure 5.2 Force as a function of indentation after the tip contacts a multilayer film prepared with low charge density (pH = 9.0), and strongly charged (pH = 5.0) PAH. Empty and gray shaded circles represent the region where the indentation obeys Hertzian deformation mechanics for the respective systems. The inset illustrates a typical deflection versus z-position raw approach curve.

for films prepared above and below the pK_a of PAH. Indentation of the films was typically <50 nm, thus restricting the fit of Hertzian deformation mechanics to a spherical tip geometry.[39] Analyzing the contact region of the approach curves and applying Equation 5.3, we determined the elastic modulus of the films via the intercept value of the plot of log F vs log δ. The elasticity for films made at pH = 9.0 and pH = 5.0 was found to be 6.7 x 10^{-3}, and 1.2 x 10^{-4} nN/nm^2 respectively, as displayed in Figure 5.3.
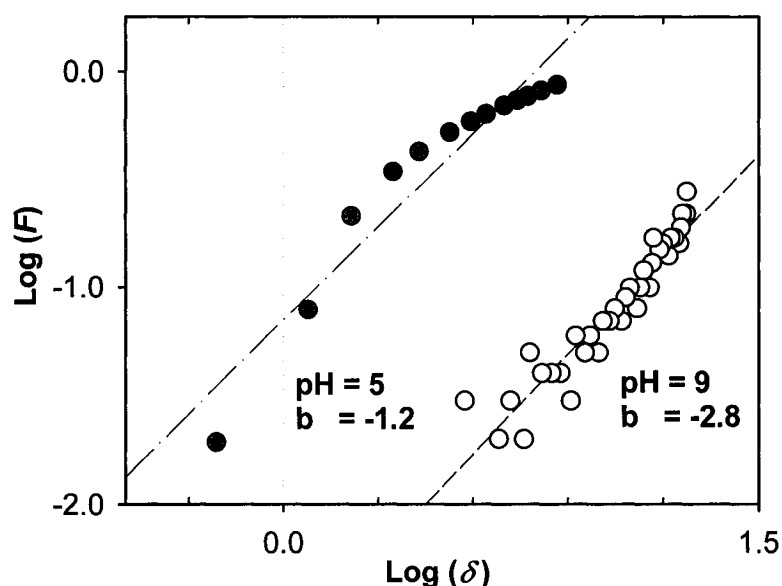
Figure 5.3   Log F vs log δ plots for the multilayer films fit to Hertzian mechanics. From Equation 5.3, the elastic modulus is determined by the intercept value, b, where Log (δ) = 0.

Similarly, we obtained force versus indentation data for films prepared at pH = 7.0 and pH = 10.5. Since the indentation depth (≤50 nm) is much smaller than the film thickness (~ 1100 nm), we assume negligible substrate effects in the determined elasticity. Figure 5.4 shows the average elastic modulus of the 4 films, determined by averaging 4 unique
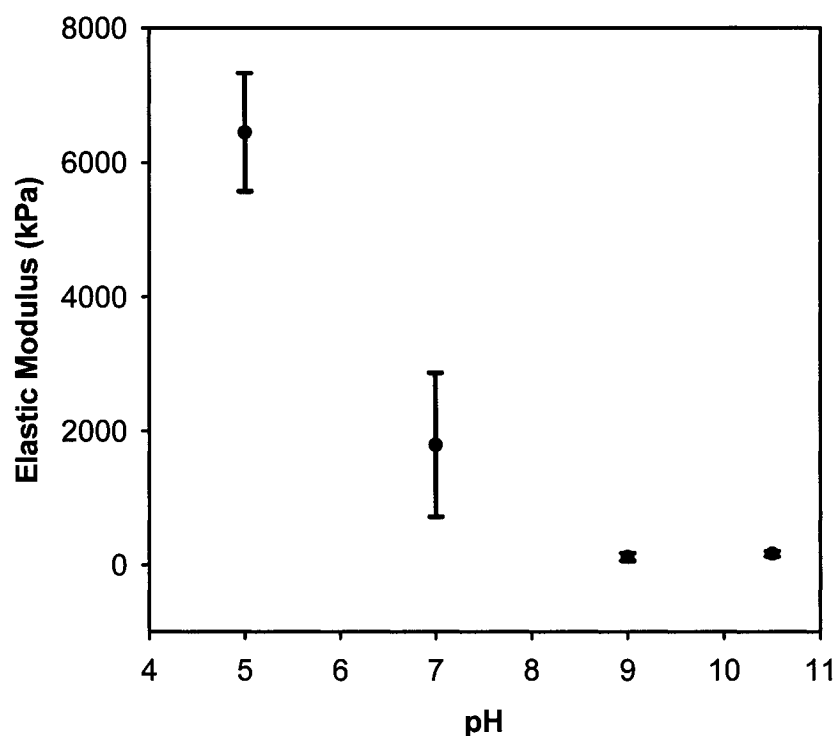
Figure 5.4   The elastic modulus of PAH/P-Azo films as a function of the assembly pH.

sets of measurements at each pH value. It was observed that both the films prepared pH = 5.0 and pH = 7.0 (i.e., employing strongly charged PAH) exhibit a Young's modulus which is on the order of 50 times greater than that of the multilayers constructed at pH = 9.0 and pH = 10.5 (i.e., assembling with weakly charged PAH).

The range of elastic modulus values for the entire series of PAH/P-Azo multilayer films analyzed was determined to be on the order of 10^2 to nearly 10^4 kPa, with modulus increasing as the assembly pH was decreased. The magnitude of our results agree with a recent QCM study of high molecular weight PSS/PDADMA films containing ≤10 layers where the "softness parameter" was found to be between 10^2–10^3 kPa for the strongly

charged system and shown to increase with the number of layers deposited.[34] In fact, the observed range in the elasticity for PAH/P-Azo multilayers of low and high ionic cross-link density is comparable to that of adsorbed mussel adhesive protein layers before, and after covalent cross-linking, respectively.[42] It appears that reducing the charge density of PAH results in multilayer films having elastic behavior, which resemble that of hydrogel-type layers.

The build-up of polyelectrolyte multilayers are known to result from the formation of a large number of weak ionic interactions (i.e., on the order of $k_B T$) established between cationic and anionic groups of the polyelectrolytes.[43] For polyelectrolytes assembled at high and low charge density the number of ionized groups and hence the percent of "ionically cross-linkable" groups between layers, are different in the two cases. This implies that the relative loop length between ionic cross-links in multilayer films may be inferred from the differences in the elastic behavior of the films, as a consequence of varying the polyelectrolyte charge density. In essence, we can use AFM force-indentation data to obtain information on the internal architecture of the film, specifically the density of the ionic cross-links connecting the layers via the positive and negative repeat units of the two polyelectrolytes. In the ideal and simplest case of vulcanized rubber (i.e., ignoring effects of "loose ends" of molecules), the relation between the degree of covalent cross-linking and the resulting network elasticity has previously been described by the following equation:[44]

$$G = 1/3E = \frac{\rho RT}{M_x} \qquad (5.4)$$

where G is the modulus of rigidity, ρ/M_x is the density of cross-links, and R, and T have their usual Boltzmann definitions. Here, we extend this equation to correlate the elastic behavior of the multilayer films to the average density of "ionic cross-links". Since G and E are directly proportional to the density of cross-links, a 50-fold increase in the observed modulus of PAH/P-Azo, resulting from decreasing the solution pH from a value of 9.0 to 5.0, corresponds to an increase in the ionic cross-link density by 50 times. Given that at solution pH = 5.0, PAH is significantly below its pK_a value, we assume that PAH is 100% charged at this pH and therefore is 100% cross-linked (every segment is paired). While QCM studies have shown evidence for the formation of a small degree of loops in even strongly charged polyelectrolyte layers adsorbed onto gold,[45] our assumption is valid for determining a relative comparison of a loop length with respect to charge density. Therefore, by normalizing the ionic cross-link density relative to the 100% cross-linked case, we have an estimate of the average relative (rel) loop length between the ionic cross-links for the various assembly pH conditions examined (Table 5.1). From the inference of the

prepn pH	h/n_L (Å)	E (kPa)	ρ/M_x (mol/m³)	% rel ρ/M_x	rel loop length
5	3.0	6500 ± 900	870	100	1
7	2.0	1800 ± 1000	240	28	4
9	9.2	120 ± 60	17	2	50
10.5	18	170 ± 40	23	3	33

Table 5.1   Calculated and Experimental Relative k for Multilayer Formation with Target Counterions.

corresponding average loop length, we find that in the case of employing weakly charged polyelectrolytes, polymer layers of 30–50 times the loop size of the strongly charged species are produced. The results in Table 5.1 also indicate that AFM nanoindentation experiments can clearly distinguish between high and low cross-link density samples of the multilayers, (i.e., attributed to use of strongly versus weakly charged polyelectrolytes respectively). However, while pH = 10.5 films are nearly twice the thickness per layer, h/n_L, of pH = 9.0 multilayers, AFM elasticity measurement are unable to clearly differentiate between varying degrees of ionic cross-links formed from a range of weakly charged polyelectrolytes (i.e., between pH = 9.0 and pH = 10.5).

5.4.2   Multilayer Adhesion and Charge Density

We also used AFM to measure the relative adhesion forces between even and odd layers in PAH/P-Azo films as a function of the ionization fraction of the polyelectrolytes. To compare the strength of interactions between identically thick multilayer films prepared at pH = 5.0 verses that at pH = 9.5, we obtained force curves between multilayers assembled on glass slides, and an AFM tip also modified with 75 PAH/P-Azo multilayers. While quantitative comparisons between various AFM probes are possible when tips are calibrated, relative adhesion measurements with the same AFM probe are preferable, since effects due to tip imperfections and variations in geometry are identically propagated with all samples examined. However, in the case of a multilayered AFM probe, even use of the same tip may introduce complications in comparing multiple adhesion measurements. Specifically, one cannot be sure that a multilayer-modified AFM probe remains constant between consecutive in situ nanoindentations into a surface also containing polyelectrolyte multilayers. To determine the severity of this problem,

115

the multilayered AFM tips were imaged by SEM to qualitatively characterize and compare the tips before and after adhesion measurements were acquired. As displayed in Figure 5.5, polymer layers are indeed adsorbed onto the tip and the structure of the adsorbed layers appears to depend on the assembly pH. In agreement with our previous
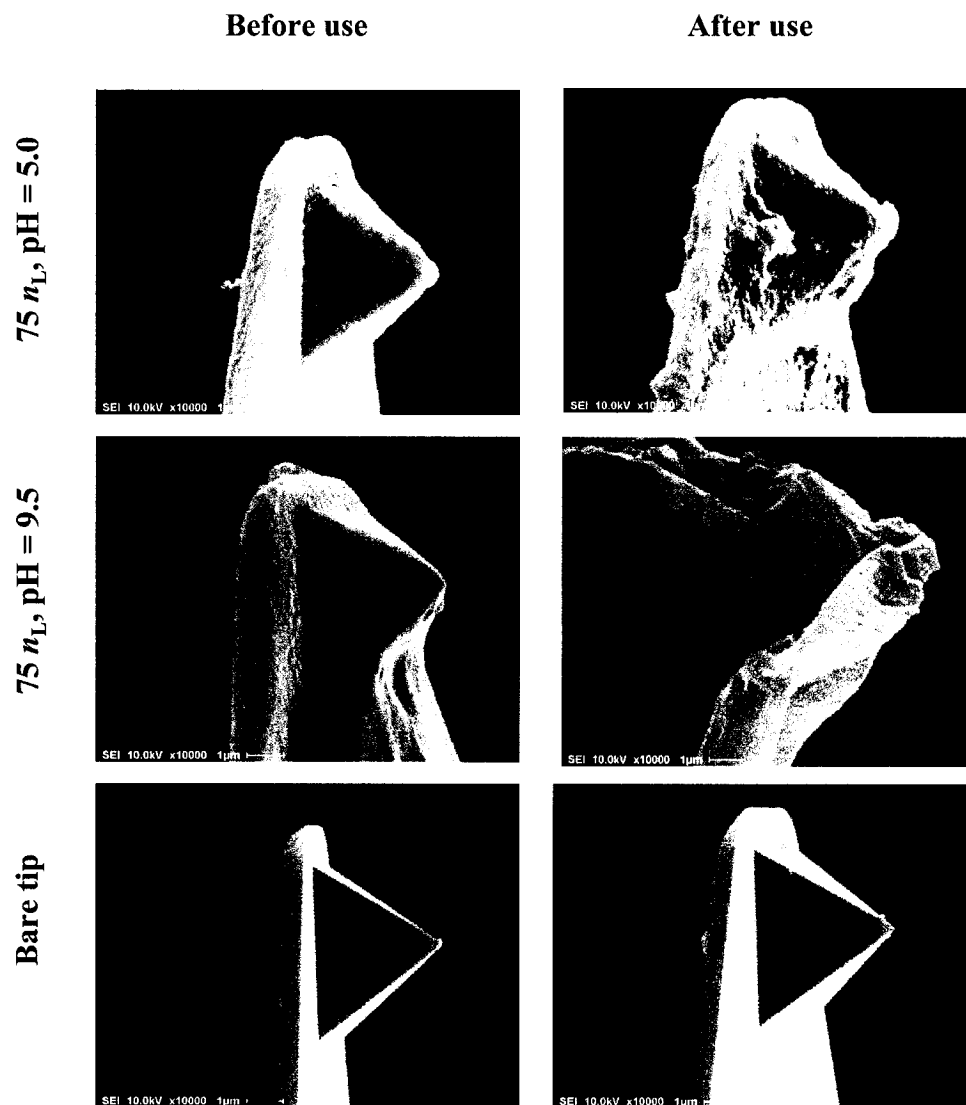
Figure 5.5 SEM micrographs (10000x magnification) of Si_3N_4 tips modified with 75 layers, n_L, of PAH/P-Azo using: **a.** assembly bath pH = 5.0, **b.** assembly bath pH = 9.5. Sample **c.** is a representative bare Si_3N_4 reference tip. The left and right columns show images of the tips prior to and post adhesion measurements, respectively.

116

studies of PAH/P-Azo on flat Si wafers, the SEM micrographs show that much thicker polymer layers are obtained in the case of multilayers prepared at pH = 9.5 compared to those at pH = 5.0. The SEM micrographs also suggest that while bare tips are not significantly altered by the adhesion measurement procedure, noticeable differences in the nature of the polymer-coated tips are observed before and after the tips are engaged in force measurements. The images presented are typical of those obtained for replicate multilayers assembled onto various other Si_3N_4 tips. We speculate that contact of the positively charged PAH surface layer on the tip with the negatively charged P-Azo surface layer on glass, in an aqueous environment, results in the exchange of multilayers.

To survey the relative adhesive forces in layers of PAH/P-Azo films, we constructed adhesion histograms for the multilayered tip and glass surface in the case of both weakly and strongly charged PAH and in the various electrolytic environments. A significant difference was observed in the adhesion of a multilayered $tip_{pH\ 5}$ and $surface_{pH\ 5}$ when measured in 10 mM NaCl (average adhesion force of 6.7 nN, displayed in Figure 6) as compared to Milli-Q water (average adhesion force of 1.4 nN, results not shown). These results suggest that the interaction forces, measured between oppositely charged polymer layers of the indenting tip and the surface, are highly dependent on the electrolyte environment. The study also shows that a markedly large variance in the distribution of adhesion forces is obtained in the former case, as indicated in Figure 6.6. Although different tips were used in the assembly of multilayers at pH = 5.0 and pH = 9.5, the adhesion between various tips prepared at pH = 9.5, and substrates multilayered at pH = 9.5, consistently resulted in lower adhesion values than any combination of tip or surface employing polyelectrolytes assembled at pH = 5.0.
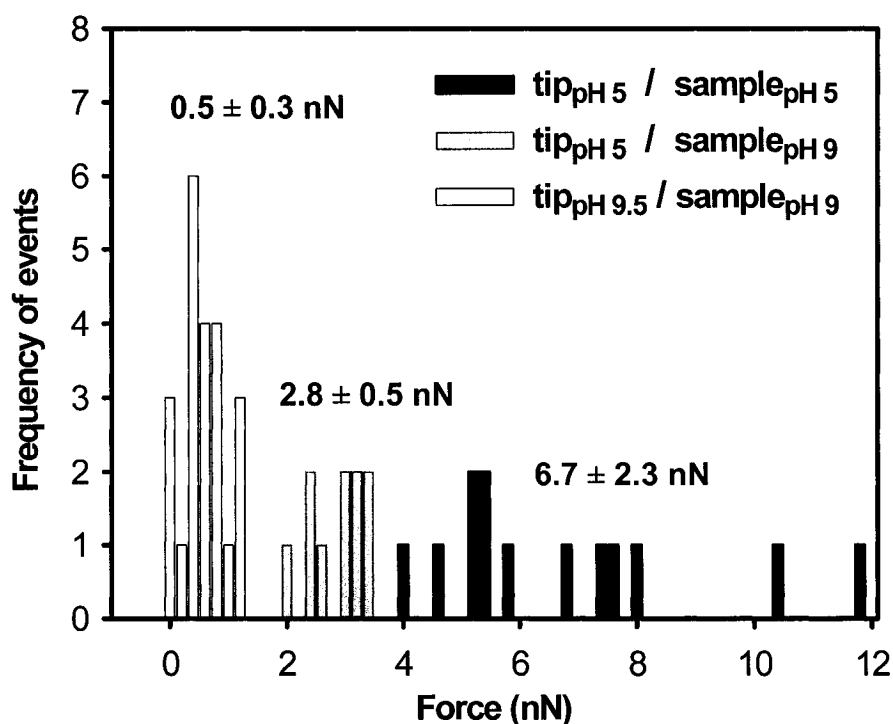
Figure 5.6   Relative adhesion between PAH/P-Azo multilayers on a tip and on a multilayered surface.

One might expect that the adhesion forces between the PAH capped tip multilayers and the P-Azo capped substrate multilayers depend on the acid-base properties of cationic and anionic functional groups. For example, the relative adhesion strength might be analogous to monolayer systems, which have previously demonstrated pK-dependent interaction between a carboxyl functionalized AFM tip and substrate.[46] In such a case, the adhesion would be dominated by the free functional units, i.e. those not involved in forming ionic cross-links. This implies that multilayer films prepared with weakly charged polyelectrolytes would exhibit larger adhesion than strongly charged systems due to a larger density of free functional groups, which are fully ionized in the

measurement solution of pH = 5.2. However, we observed the opposite trend. The weakly charged polyelectrolytes exhibited the smallest adhesion upon bringing the tip-substrate multilayers in contact. It is speculated that the reduced adhesion values observed in this case may be an effect of the different film architecture attributed to the reduced ionization fraction of PAH during multilayer assembly on the AFM probe. Elasticity measurements have demonstrated that PAH/P-Azo multilayers on an AFM tip constructed at pH = 9.5 exhibit a reduced cross-link density in precursor layers compared to samples prepared at pH = 5.0. Since the adhesion is much stronger in the case of pH = 5.0, we believe that multilayers between the tip and substrate are exchanging in situ during the adhesion measurement. Consequently, the force required to break the interactions between the layers is much greater in the case of pH = 5.0, assuming that the dominant interaction force in the multilayers is ionic. This result is consistent with the SEM data, which suggests the occurrence of mass transfer between multilayers on the tip and the substrate during subsequent force measurements (Figure 5.5).

5.5 Conclusions

The elasticity of polyelectrolyte multilayer films as a function of polymer charge density during assembly can be successfully probed with force-distance measurements using an AFM. The modulus of elasticity in turn reveals the average "loop length" between the "ionic cross-links" at the interface between the layers, thus allowing a straightforward method for comparing the internal architecture of the multilayers constructed at varying pH values. In the case of multilayers made from weakly charged PAH and P-Azo (a condition producing thick layers) we found that the relative loop length can be up to 50-fold greater than an identical system prepared using strongly

charged polyelectrolytes (resulting in much thinner layers). We also demonstrate that in situ measurements of adhesion forces between multilayered AFM probes and planar multilayered surfaces provide an estimate of the relative strength of layer-to-layer interaction as a function of the bulk ionic cross-link density of the film. While we suspect that a significant degree of mass transfer of layers occurs between the multilayered tip and surface during these AFM adhesion measurements, we consistently observed much lower adhesion forces in all cases of multilayers prepared from weakly charged polyelectrolytes. This suggests that the employment of fully ionized polyelectrolytes result in multilayers, which as a bulk appear to be more strongly interlinked due to the larger degree of association of anionic/cationic repeat units in the assembly.

5.6   References and Notes

(1)   Decher, G.; Schmitt, J. *Prog. Colloid Polym. Sci.* **1992**, *89*, 160.

(2)   Decher, G. *Science* **1997**, *277*, 1232.

(3)   Rmaile, H. H.; Schlenoff, J. B. *J. Am. Chem. Soc.* **2003**, *125*, 6602.

(4)   Qiu, X.; Leporatti, S.; Donath, E.; Möhwald, H. *Langmuir* **2001**, *17*, 5375.

(5)   Hiller, J.; Mendelsohn, J. D.; Rubner, M. F. *Nature Materials* **2002**, *1*, 59.

(6)   Schuler, C.; Caruso, F. *Biomacromolecules* **2001**, *2*, 921.

(7)   Antipov, A. A.; Sukhorukov, G. B.; Leporatti, S.; Radtchenko, I. L.; Donath, E.; Möhwald, H. *Colloid Surf., A.* **2002**, *198*, 535.

(8)   Levaesalmi, J.; McCarthy, T. J. *Macromolecules* **1997**, *30*, 1752.

(9)   Mendelsohn, J. D.; Barrett, C. J.; Chan, V. V.; Pal, A. J.; Mayes, A. M.; Rubner, M. F. *Langmuir* **2000**, *16*, 5017.

(10)   van de Steeg, H. G. M.; Cohen Stuart, M. A.; De Keizer, A.; Bijsterbosch, B. H. *Langmuir* **1992**, *8*, 2538.

(11)   Dahlgren, M. A. G.; Waltermo, A.; Blomberg, E.; Claesson, P. M.; Sjoestroem, L.; Aakesson, T.; Joensson, B. *J. Phys. Chem.* **1993**, *97*, 11769.

(12) Sukhishvili, S.; Granick, S. *J. Chem. Phys.* **1998**, *109*, 6869.

(13) Losche, M.; Schmitt, J.; Decher, G.; Bouwman, W.G.; Kjaer, K. *Macromolecules* **1998**, *31*, 8893.

(14) Dubas, S. T.; Schlenoff, J. B. *Macromolecules* **1999**, *32*, 8153.

(15) Phuvanartnuruks, V.; McCarthy, T. J. *Macromolecules* **1998**, *31*, 1906.

(16) Yoo, D.; Shiratori, S. S.; Rubner, M. F. *Macromolecules* **1998**, *31*, 4309.

(17) Shiratori, S. S.; Rubner, M. F. *Macromolecules* **2000**, *33*, 4213.

(18) Lvov, Y.; Decher, G.; Haas, H.; Möhwald, H.; Kalachev, A. *Physica B.* **1994**, *198*, 89.

(19) Kellogg, G. J.; Mayes, A. M.; Stockton, W. B.; Ferreira, M.; Rubner, M. F.; Satija, S. K. *Langmuir* **1996**, *12*, 5109.

(20) Loesche, M.; Schmitt, J.; Decher, G.; Bouwman, W. G.; Kjaer, K. *Macromolecules* **1998**, *31*, 8893.

(21) Lee, S. H.; Balasubramanian, S.; Kim, D. Y.; Viswanathan, N. K.; Bian, S.; Kumar, J.; Tripathy, S. K. *Macromolecules* **2000**, *33*, 6534.

(22) Koetse, M.; Laschewsky, A.; Jonas, A. M.; Verbiest, T. *Colloids Surf., A.* **2002**, *198-200*, 275.

(23) Picart, C.; Ladam, G.; Senger, B.; Voegel, J. C.; Schaaf, P.; Cuisinier, F. J. G.; Gergely, C. *J. Chem. Phys.* **2001**, *115*, 1086.

(24) Baur, J. W.; Rubner, M. F.; Reynolds, J. R.; Kim, S. *Langmuir* **1999**, *15*, 6460.

(25) Lavalle, P.; Gergely, C.; Cuisinier, F. J. G.; Decher, G.; Schaaf, P.; Voegel, J. C.; Picart, C. *Macromolecules* **2002**, *35*, 4458.

(26) Schoeler, B.; Kumaraswamy, G.; Caruso, F. *Macromolecules* **2002**, *35*, 889.

(27) Yamada, T. Y.; Shiratori, S. *Mol. Cryst. Liq. Cryst. Sci. Technol., Sect. A.* **2001**, *370*, 289.

(28) Lvov, Y.; Ariga, K.; Onda, M.; Ichinose, I.; Kunitake, T. *Colloids Surf., A.* **1999**, *146*, 337.

(29) Kim, D. K.; Han, S. W.; Kim, C. H.; Hong, J. D.; Kim, K. *Thin Solid Films* **1999**, *350*, 153.

(30) Picart, C.; Lavalle, P.; Hubert, P.; Cuisinier, F. J. G.; Decher, G.; Schaaf, P.; Voegel, J. C. *Langmuir* **2001**, *17*, 7414.

(31)   McAloney, R. A.; Sinyor, M.; Dudnik, V.; Goh, M. C. *Langmuir* **2001**, *17*, 6655.

(32)   Notley, S. M.; Biggs, S.; Craig, V. S. *Macromolecules* **2003**, *36*, 2903.

(33)   (a) Feiler, A.; Plunkett, M. A.; Rutland, M. W. *Langmuir* **2003**, *19*, 4173. (b) Plunkett, M. A.; Feiler, A.; Ruthland, M. W. *Langmuir* **2003**, *19*, 4180.

(34)   Lukkari, J.; Salomäki, M.; Ääritalo, T.; Loikas, K.; Laiho, T.; Kankare, J. *Langmuir* **2002**, *18*, 8496.

(35)   Lowack, K.; Helm, C. A. *Macromolecules* **1998**, *31*, 823.

(36)   Ruths, M.; Sukhishvili, S. A.; Granick, S. *J. Phys. Chem. B.* **2001**, *105*, 6202.

(37)   Mermut, O.; Barrett, C. J. *J. Phys. Chem. B.* **2003**, *107*, 2525.

(38)   Domke, J; Radmacher, M. *Langmuir* **1998**, *14*, 3320.

(39)   Akhremitchev, B. B.; Walker, G. C. *Langmuir* **1999**, *15*, 5630.

(40)   Lin, X. U.; Creuzet, F.; Arribart, H. *J. Phys. Chem.* **1993**, *97*, 7272.

(41)   Fang, M.; Kim, C. H.; Saupe, G. B.; Kim, H. N.; Waraksa, C. C.; Miwa, T.; Fujishima, A.; Mallouk, T. E. *Chem. Mater.* **1999**, *11*, 1526.

(42)   Höök, F.; Kasemo, B.; Nylander, T.; Fant, C.; Sott, K.; Elwing, H. *Anal. Chem.* **2001**, *73*, 5796.

(43)   Dubas, S, T.; Schlenoff, J. B. *Macromolecules* **1999**, *32*, 8153.

(44)   Treloar, L. R. G. The Physics of Rubber Elasticity. 2nd Ed; Oxford Clarendon Press: England, 1958; pp 187–196.

(45)   Plunkett, M. A.; Claesson, P. M.; Ernstsson, M.; Rutland, M. W. *Langmuir* **2003**, *19*, 4673.

(46)   van der Vegte, E. W.; Hadziioannou, G. *J. Phys. Chem. B.* **1997**, *101*, 9563.

Chapter 6

Stable Sensor Layers Self-Assembled onto Surfaces Using

Azobenzene-Containing Polyelectrolytes

6.1   Preface

From the previous chapters its has been demonstrated that unique adsorption behavior and tunable structural and mechanical properties arise when multilayer films are assembled from weakly charged polyelectrolytes. This type of chemical control over the kinetics and the molecular architecture is necessary in designing applications for these organic multilayer films. In the following chapter, we will show how we can readily achieve both good chemical and physical control of polyelectrolyte multilayers derived from azobenzene-containing polyelectrolytes, making them suitable for an optical sensor application. Specifically, we demonstrate that the photoisomerization of azobenzene chromophores is sensitive to the solvent pH and can therefore be used as sensor host material in polyelectrolyte multilayer films for detection of solution pH values.

6.2   Introduction

Ionically self-assembled multilayer (ISAM) films of polyelectrolytes have received much recent attention as a route to designing highly tailored surfaces,[1] for a wide range of applications. They have been employed in such areas as bio-compatiblilty,[2,3] photo-responsive materials,[4] microelectronic devices such as electroluminescent LEDs,[5-7] conducting polymer composites,[8,9] and sensitive gas sensors.[10] Sequential layer-by-layer

(LBL) physisorption of alternately charged polyelectrolytes is achieved through a method of electrostatic self-assembly first described by Decher.[11,12] With this technique, multilayer films are assembled by first immersing a negatively charged flat substrate in a positively charged polymer solution, followed by thorough rinsing of the surface in an aqueous bath to remove unadsorbed polymer. The resulting polycation coated surface is subsequently immersed in the oppositely charged polyion solution, and followed with another wash. The cycle is then repeated until a desired number of layers is achieved. This LBL coating technique is particularly attractive because of the ease and efficiency of fabrication in aqueous solution, and the versatility with respect to incorporation of secondary functionalities in the polyions assembled. The potential to create highly tailored film structures and to impose specific chemical functionalities provides an excellent opportunity for applying the ISAM technique to novel surface sensor applications. Various means exist for manipulating the material properties of ISAM films (such as layer thickness and surface chemistry) either through choice of substrate or polyion, adsorption bath conditions, or post self-assembly functionalization. The irreversible nature of the ISAM adsorption process results in films with good stability and high reproducibility. We report here our recent investigations of various strategies that can be employed for manipulating properties of organic multilayered thin films, in weak polyelectrolyte systems containing an optically responsive azobenzene chromophore. This paper seeks to present the LBL ISAM technique as a promising host platform for sensors, which is facile and inexpensive to assemble, and stable to a range of solvent environments.

One distinct advantage that ISAM films possess over other tailorable surface modification techniques, such as self-assembled monolayers (SAMs), is the potential for

the incorporation of a large number of sensor groups. In contrast to SAMs, where sensor coverage is limited to the surface area, ISAM films can be highly swollen in contact with analyte solution, and incorporate many nanometers of sensor-containing polymer layers, greatly increasing sensitivity. Furthermore, ISAM films may offer an advantage of stability to temperature, cleaning, and solvent and pH resistance. We examine in the following the applicability of the polyion layering technique to surface sensor modification through study of: (a) various methods for film thickness control with a focus on the effects of polymer charge density on film growth, (b) possible substrates amenable to LBL self-assembly, and (c) film stability/resistance to harsh solvent environments and consequences of high temperature exposure, sonication, and cleaning. As an example application of ISAM layers as sensor host materials, we will also demonstrate the applicability of these multilayers for use as hydroxide ion sensors in extreme alkaline media.

6.3   Experimental Section

6.3.1   Materials

The polyions used were commercially available poly(allyl)amine hydrochloride (PAH; Polysciences; MW 60K), poly {1-4[4-(3-carboxy-4-hydroxyphenyl-azo) benzenesulfonamido]-1,2-ethanediyl sodium salt} (P-Azo; Aldrich; MW 90K) and Poly(diallyldimethylammonium chloride) (P-DAC; Aldrich, MW 200–350K), the structures of which are presented in Figure 6.1. Azobenzene chromophore [2-[4-(diethylamino)phenylazo]benzoic acid] (ER) was obtained from Aldrich. Aqueous solutions of polyion concentration 10^{-2} M per repeat unit were prepared using Milli-Q water (18 MΩ resistivity) and the pH of both solutions were adjusted and matched (from

pH = 4 to pH = 11) with HCl and NaOH. Unless otherwise stated, multilayering was performed using pH 9 solutions. Various metallic and inorganic substrates, including Al, Au, Ag, Cu, mica, Mo, Ni, quartz, SiO_2 microscope glass slides, stainless steel, V, and 100–150 nm diameter colloidal SiO_2, were cleaned by 12 h immersion in 10^{-3} M H_2SO_4. Ellipsometry and optical absorbance measurements were conducted on Si wafer substrates (Wafernet; crystallographic orientation <100>) and Fisherbrand microscope glass slides respectively, which were similarly treated for 12 h in a bath of 75% H_2SO_4 and 25% H_2CrO_4. Subsequent washing of all substrates with neutral Milli-Q water (pH 7.5 ± 5%) was performed in preparation for electrostatic multilayer deposition.

a.   b.   c.
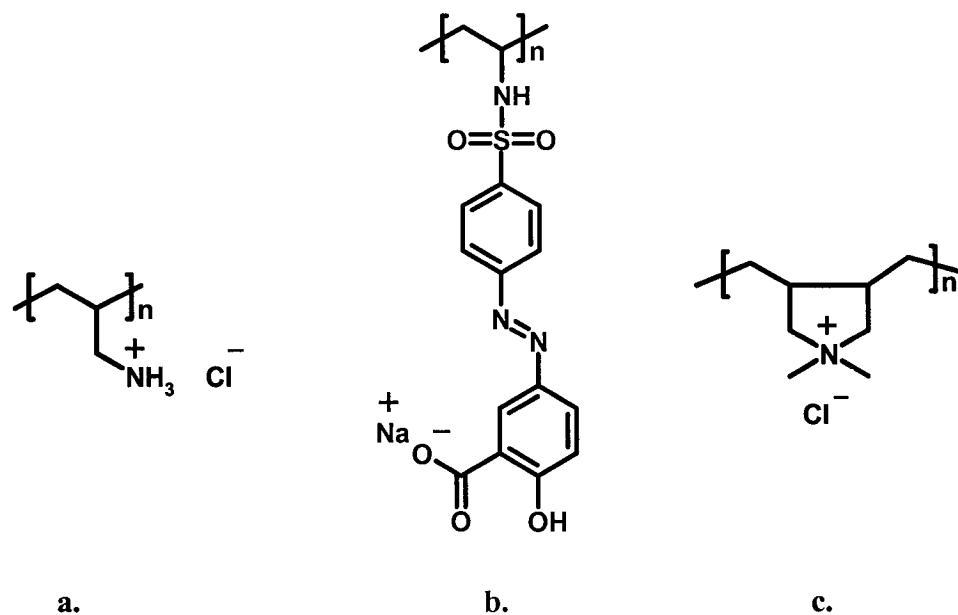
Figure 6.1   Repeat unit structures of polyelectrolytes used for multilayering: **a.** PAH (weak polycation), **b.** P-Azo (weak polyanion), and **c.** P-DAC (strong polycation).

6.3.2 Methods for Multilayer Coating

Multilayering was initiated by immersion of the cleaned substrates (with a hydroxylated surface) into the 10^{-2} M polycation solution for 12.5 min. This adsorption was then followed by washing of non-adsorbed polyion through two immersions in separate neutral Milli-Q H_2O baths for a total of 5 min. Next, a similar dipping protocol was used for adsorption of the polyanion at similar solution concentration and dipping time, with subsequent rinsing of unadsorbed polyion. This procedure was repeated until the desired number of layers was obtained. On the conclusion of the aqueous adsorption cycles, layered samples were dried in an oven at 65 °C for 2 h, and allowed to return to room temperature before measurements. Additionally, a similar multilayering scheme was applied to alternate geometries of adsorption. Three different geometries were chosen for testing the versatility of LBL multilayering: (1) high curvature surfaces, (2) confined geometries, and (3) spin-coating.

Layering on a high curvature surface was demonstrated by cyclic immersion of SiO_2 colloidal particles in alternately charged polyelectrolyte solutions. Specifically, ISAM growth on silica colloids was implemented using a procedure reported by Donath and co-workers.[13,14] Colloids (3 g) were dispersed in 500 mL of polyion solution for 30 min. This was followed by 1 h of centrifugation at 4300 rpm and removal of supernatant. Three separate washing cycles (each with 500 mL of Milli-Q H_2O), sequentially consisting of 25 min sonication, 1 h centrifugation and extraction of supernatant liquid, was then performed to remove unadsorbed polyions. Silica particles were sonicated in solution at each washing step to prevent aggregation and to exploit maximum surface area for subsequent polyelectrolyte deposition. The above procedure was then repeated for polyion deposition of the opposite charge, thereby constructing a bi-layer. The presence

of the layers was confirmed through ζ potential measurements and solid-state NMR spectroscopy.[15]

Multilayering was also attempted in a confined geometry, using 30 sequential and repetitive flow cycles of polyelectrolyte through a glass tube (<1 mm diameter and flow rate ~0.3 mL/s for 5 s). Between flow depositions of oppositely charged polyions, 3 intermittent flow-rinsing cycles were implemented (each of 5 s duration). Successful layering of dye-containing polyelectrolyte was confirmed optically.

Films of 30 spin-cast multilayers were also constructed by introducing polyion droplets (0.1 mL) on a flat Si surface or microscope side, immediately followed by rapid spinning (at 4000 rpm) using a spin coater (Precision Scientific). Similarly, three individual spin washing cycles (each of 0.5 mL H_2O) separated each subsequent layer deposition.

6.3.3 Film Thickness Measurements

The optical absorption of PAH/P-Azo multilayer films was probed by transmission studies through microscope glass slides (Varian Cary 300-Bio Spectrophotometer; scan rate of 100 nm per minute). Unless otherwise stated, reflective measurements of Si films were obtained using Gaertner Ellipsometer (with a HeNe laser at 633 nm and fitted for both layer thickness and refractive index). All ellipsometric determinations of total layer thickness are reported as the statistical mean of 13 measurements after subtraction of surface oxide layer thickness (measured average of 27 $\pm$ 3 Å).

6.4   Results and Discussion

6.4.1   Physical Control of Thickness

In order to incorporate a desired number of sensor groups in contact with a unit area of surface, it is necessary to control the total thickness of the sensor-containing polymer layers. Figure 6.2 depicts a series of typical UV-vis absorption profiles (studied on a glass slide surface) showing build-up of multilayers obtained for the PAH/P-Azo system at unaltered pH of polyelectrolyte dipping solution (measured as pH = 4.2 and pH = 8.5 for polycation and polyanion respectively). Optical measurements were taken for the $\pi \rightarrow \pi^*$ absorbance maximum centered at 365 nm for the *trans* azobenzene isomer. No appreciable variation in λ_{max} was observed throughout the layering, suggesting that the chromophore sensors are not significantly altered by the layering process. This suggests that films of a desired total thickness can be achieved by appropriate selection of the total number of layers deposited (n_L). These results concur with previous demonstrations of physical manipulation of thickness for P-DAC/P-Azo films as reported up to 100 n_L.[16] The upper limits for multilayering the same polyelectrolyte system deposited at pH 9 were similarly examined by spectroscopically tracking an off-maximum absorbance of the azobenzene moiety. Beyond an absorbance of 3 (approximately at 350 n_L), an off-maximum probe of λ = 440 nm was used to prevent detector saturation. The measured optical absorbance shown every 50 n_L up to 1000 n_L in Figure 6.3 (inset) and indicates continued linear growth behaviour in the LBL build-up for the same polyelectrolyte system. The absence of observable film desorption from the glass surface suggests stable LBL growth as tested to 1000 n_L. A corresponding optically-determined thickness of 547 nm indicates that uniformly thick films, in the micron regime, may easily be fabricated

using the ISAM method. These results suggest that choice of total layer number can be considered a simple physical approach for film fabrication to a predetermined thickness, from the angstrom to the sub-micron level.
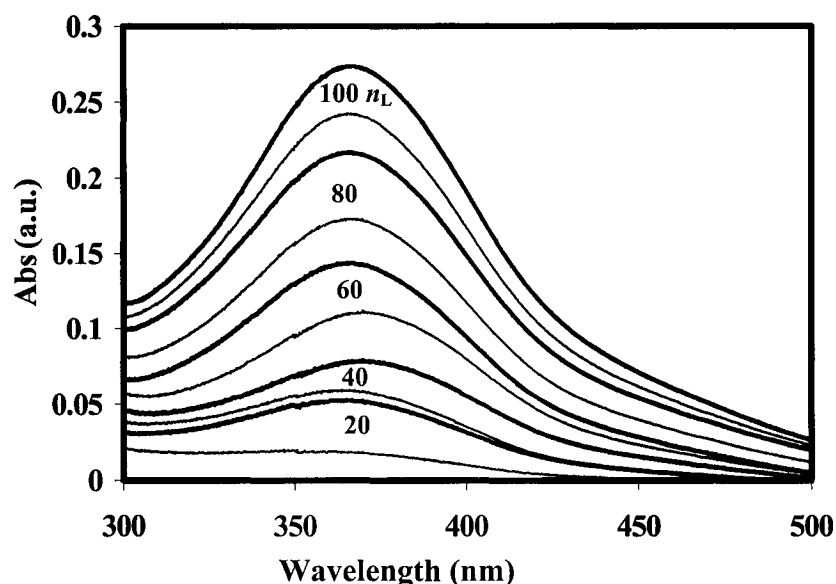
Figure 6.2 UV-vis absorbance for layer-by-layer build-up of a PAH/P-Azo multilayer film measured successively at 10 layer intervals.

6.4.2 Chemical Control of Thickness

The total layer thickness can also be controlled through varying the solution conditions of the adsorption baths. In agreement with previous investigations of ionic effects on film structure using strong polyelectrolytes,[17] the thickness of layers deposited was shown to be strongly dependant on the charge density of the ionic functionalities incorporated in the polymer chain. Specifically, recent studies have indicated that multilayer thickness and interpenetration can be altered by manipulation of polyelectrolyte ionic strength via addition of salt or adjustment of the solution pH during

the layering process.[4,18] Here, the effects of charge density with variable pH experiments were examined for the two weakly charged polyelectrolytes, PAH and P-Azo. Figure 6.3 displays a plot of absorbance as a function of n_L for the probed pH regimes of assembly dipping solutions (pH = 4 to pH = 11), which were matched for both polyelectrolytes. Comparison of the two pH extremes revealed a near 20-fold increase in optical density between a fully charged (pH = 4) verses weakly charged (pH = 11) case (the pK_a of PAH = 8.7).[19] The corresponding P-Azo thickness was determined as 1 Å/layer and 18 Å/layer for pH = 4 and pH = 11 adsorption environments respectively. This suggests significant contribution of polyelectrolyte pH in the weak/weak PAH/P-Azo system with respect to film thickness. Therefore, exploiting the polyion charge fraction can provide a
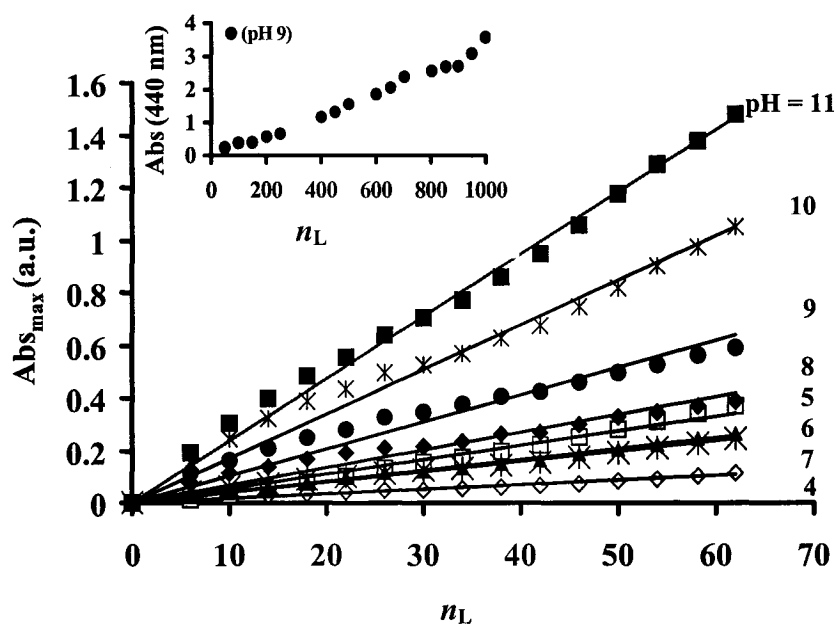
Figure 6.3 UV-vis absorbance of PAH/P-Azo multilayers assembled under various pH matched adsorption bath conditions from 0 to 62 layers, and from 50 to 1000 layers (inset).

more straightforward chemical means for obtaining control over the extent of polyion deposition through dipping bath parameters. The advantage is that a good command over ISAM film structure is achievable over a large pH range. Specifically, dipping solution conditions in LBL assembly can appropriately be set over 7 pH units, ranging from acidic to strongly basic. Sufficient polarity arising from the weakly charged polycation PAH allows for thick multilayer self-assembly at pH 9, as demonstrated experimentally by ellipsometry and UV-vis spectroscopy (Figure 6.3). Although both weak polyelectrolytes exhibit good aqueous solubility under highly alkaline conditions (pH = 12), ideal for thick film fabrication, gradual precipitation of PAH with increasing pH represents an upper limit for achieving films of a thickness greater than 20 Å/layer.

ISAMs made from weakly charged polyelectrolytes (where ionizable repeat units are not fully charged) also behave analogously to strongly charged polymers under suitable pH conditions. Evidence of this is offered by the observation of a similar film optical thickness (within 6%) for P-Azo multilayer films constructed with either strongly charged polycation P-DAC, or a weak polycation PAH, converted to the fully charged state upon altering the acidity of both the polycation and polyanion solutions to pH = 3.

6.4.3 Practical Considerations

6.4.3a Suitability of Substrates

Recent comprehensive studies of ISAMs films have mainly employed glass and Si substrates for multilayer film fabrication. This is primarily due to the ease and well-established tools that exist for reflective or absorptive spectroscopic optical measurements on these standard substrates. Both glass and Si are relatively inexpensive, are resistant to harsh cleaning protocols and extreme pH/salt conditions, and are readily available.

Additionally, it has been repeatedly demonstrated that these surfaces are highly suitable for investigations of azobenzene-containing films for application as photo-sensors and electro-optic films.[20-22] For sensor modification purposes, it is of interest to examine substrate variability with respect to the electrostatic multilayering technique by: (a) investigating the range of alternative metal oxides and native metals available, and (b) testing a range geometries available for layering.

The PAH/P-Azo deposition parameters described were implemented to build 30 layers on cleaned Al, Ag, Au, Cu, Mo, Ni, Ti, V, mica, and quartz substrates. Successful LBL physisorption was demonstrated for all tested surfaces through comparison of the multilayered thin films to the initially clean surface. The presence of adsorbed multilayers for all surfaces was optically confirmed by qualitative observation of the characteristic P-Azo absorption at $\lambda = 365$ nm. These results suggest no restrictions with respect to choice of metal oxide surface used for electrostatic self-assembly. All films exhibited stability to repeated washing cycles, and were also resistant to de-wetting when heated in an oven for >24 h at 70 °C. Similar to the results obtained for SiO_2, no indication of physical limitations on the number of layers deposited was observed for the metallic substrates, as demonstrated by multilayering 1000 n_L of PAH/P-Azo on a stainless steel surface.

6.4.3b Suitability of Various Geometries

The applicability of the ISAM method to various geometries of adsorption was also investigated for the PAH/P-Azo system. Layer-by-layer adsorption was optically demonstrated for three adsorption geometry cases tested including: (a) spin-cast

polycation/polyanion droplets on a flat glass or Si, (b) polyelectrolytes deposited on high curvature colloidal SiO_2, and (c) flow-based ISAM fabrication within a cylindrical glass tube. To determine the nature of polyion/substrate interaction, we compared optical measurements of the LBL spin-cast system of 30 n_L to the homopolymer spin coated films generated solely using PAH or P-Azo homopolymer. Both resultant films were rinsed well with water. Table 6.1 summarizes the results for UV-vis P-Azo optical density and calculated average per layer thickness obtained by ellipsometry for the two systems. Evidence of multilayer physisorption in the case of LBL polyion spinning on

Case	Surface Description	Total UV-Vis Abs$_{max}$	Ellipsometric height per layer (Å)
A	Bare glass substrate	< 0.01*	
B	Spin-cast on glass P-Azo homopolymer, [10^{-1}]	0.239	
C	Sample B and 2 min subsequent H_2O wash	< 0.01*	
D	Bare Si surface		0
E	Spin-cast on glass PAH homopolymer, [10^{-1}]		103
F	Sample E and 2 min subsequent H_2O wash		0
G	Spin-cast 30N$_L$ PAH/P-Azo, [10^{-2}]		39
H	Sample G and subsequent 25 h H_2O wash		38
	* = below detectable threshold		

Table 6.1 Optical density and per layer film thickness of PAH and P-Azo homopolymers, and PAH/P-Azo multilayers spin-cast on glass and Si surfaces.

a surface is supported by the absence of aqueous desorption observed for the 39 Å/n_L ISAM film (case G). After 24 h rinsing of the film in solvent, ellipsometry indicated a negligible difference in the layer thickness, measured as 38 Å (case H). In contrast, the spin-deposited homopolymers, PAH and P-Azo, readily and completely de-wetted from the surfaces after 2 min immersion in water, suggesting only a weak electrostatic interaction of the polyion with the surface (cases C and F). For the spin-deposited PAH, the measured de-wetting of the homopolymer was likely due to the formation of only a mono-layer, below the detection limit of the ellipsometer. Identical results were obtained for multilayering via flow of polyion through the capillary, where 30 stable layers were successfully deposited on the interior surface of a 1 mm diameter glass tube. ISAM stability within the flow cell was also confirmed by exposing the internal coating to constant aqueous washing for several minutes and film resistance to immersion in a 70 °C water bath for 2.5 h. Layering on high curvature surfaces was demonstrated by washing 100–150 nm diameter colloidal SiO_2 with alternately charged polyelectrolyte solutions, similar to previous reports on latex particles.[13,23] Results from ζ potential measurements and solid-state ^{1}H NMR spectroscopy confirm the existence of these stable deposited layers.[15] The demonstrated suitability of the ISAM technique to a variety of film casting methods such as spin-coating and flow cells, and to high curvature surfaces such as colloids, suggests that this technique can in principle be applied to sensor layering through a wide variety of processes and in 3 dimensions on the nanometer scale.

6.4.3c Film Stability

The stability of constructed PAH/P-Azo ISAMs to prolonged exposure in various solvent environments was tested. Figure 6.4 displays the measured changes in film thickness after 2.5 h heating cycles of 30 n_L films in water. A near-constant average layer thickness of 40 ± 2 Å was observed for films exposed to water baths at temperatures ranging between 25 and 90 °C, indicating resistance to any desorption up to boiling temperatures. At 100 °C, the average layer thickness was reduced to 50%, but complete de-wetting of the film was still not observed in the temperature range examined. PAH/P-Azo films were also subject to a 14 h immersion in solution environments of widely varying polarities, using a diverse range of 18 common organic solvents. The resulting
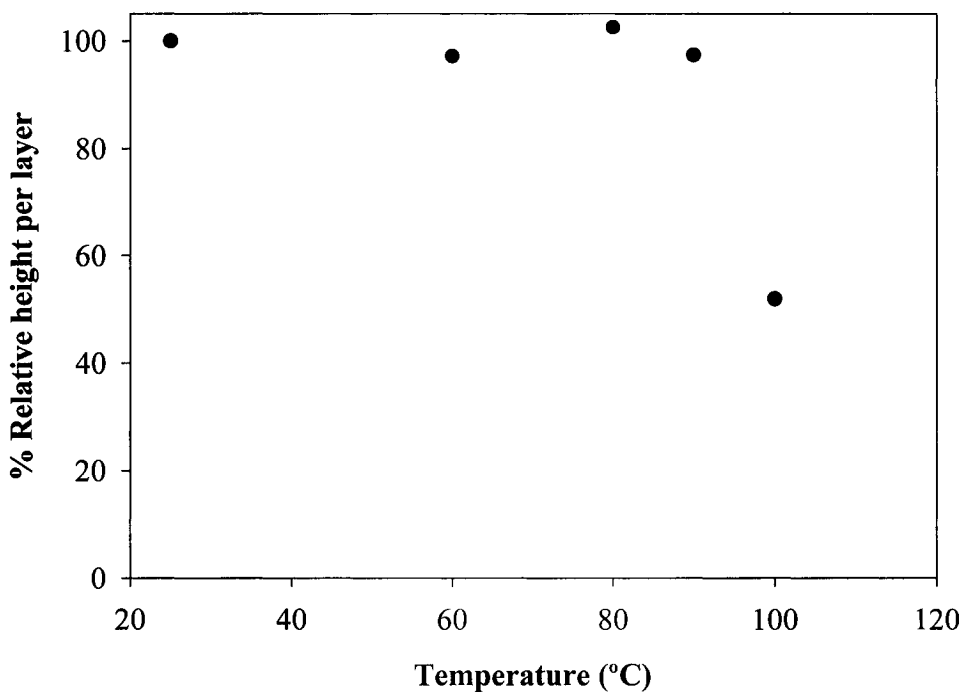
Figure 6.4   Layer thickness from ellipsometry of PAH/P-Azo films after 2 h immersion in temperature-controlled water baths.

difference in film optical density was calculated from UV-vis data after films were submerged in acetone, acetonitrile, glycerol, 1,4-dioxane, DMSO, toluene, ethylacetate, methylethyl ketone, heptane, THF, benzene, nitrobenzene, 2-propanol, ethyl alcohol, hexanes, ethyl ether, chloroform, and methylene chloride. No measurable degradation in film thickness was observed in any case. Additionally, the films were exposed to aqueous solutions of a wide range of salt concentrations, from 0.001 to 2 M, of both NaCl and NaBr. Multilayered films again remained fully intact, showing no desorption on immersion in either saturated salt solution. Desorption was only observed when the films were subject to highly acidic salt water (2 M at pH = 1).

As an important demonstration of the films ability to withstand common cleaning protocols, constructed films were also shown to withstand 1 h sonication in a high salt and extreme pH environment. Measurements of the percentage difference in UV-vis absorbance of PAH/P-Azo multilayers were made on films before and after sonication in various solutions. The films revealed good resistance to sonication with solutions of: (a) Milli-Q water, (b) 1 M NaCl, and (c) pH 12 water, yielding only a 2%, 9%, and 14% reduction in optical thickness respectively. Only after sonication in a combined solution of pH 12 and 1 M salt, did experiments show some appreciable film desorption, with an associated optical absorbance reduction of 59%. The results of film stability tests performed for varying concentrations of salt suggest that this effect may well be attributed solely to the combined and unusually harsh solvent environment, rather than the sonication process itself.

6.4.3d Example Application

While this research seeks to study the general suitability of ISAM layers as a promising sensor host material independent of individual applications, one example sensor system was investigated as proof-of-principle. ISAM films functionalized with azobenzene chromophores can make use of the readily-induced and reversible photoisomerization between the two geometric forms of *trans* and *cis*.[24,25] Under irradiation at an absorbing wavelength in the blue visible or near-UV, the more stable *trans* form is converted to the less stable *cis*, to an extent that depends on the irradiation intensity. The *cis* state then decays back to the *trans* form either photochemically, or thermally. The thermal rate constant varies widely depending on the azo chromophore, but in general varies from milliseconds to hours.[25] The absorption coefficient of the azobenzene can change dramatically on isomerization from *trans* to *cis*, which can be easily monitored by absorption spectroscopy near the λ_{max} to determine the first order rate constant. A typical *trans-cis-trans* isomerization cycle (of ER azo chromophore) is presented in Figure 6.5 (inset) where the transmission at λ_{max} is monitored over time, while a high intensity pump laser is introduced at time t = 1 s for a duration of 1 s. As the photo-generated *cis* isomer has a lower visible absorption coefficient than the *trans* isomer, the probe beam transmission signal intensity increases substantially while the pump beam is on and a photo-stationary state containing an equilibrium of both isomers is generated and maintained. With the pump beam turned off, the *cis* relaxes thermally back to the *trans* form, and the signal intensity decays exponentially. This signal decay is monoexponential, and thus a first order rate constant can be determined for the process.
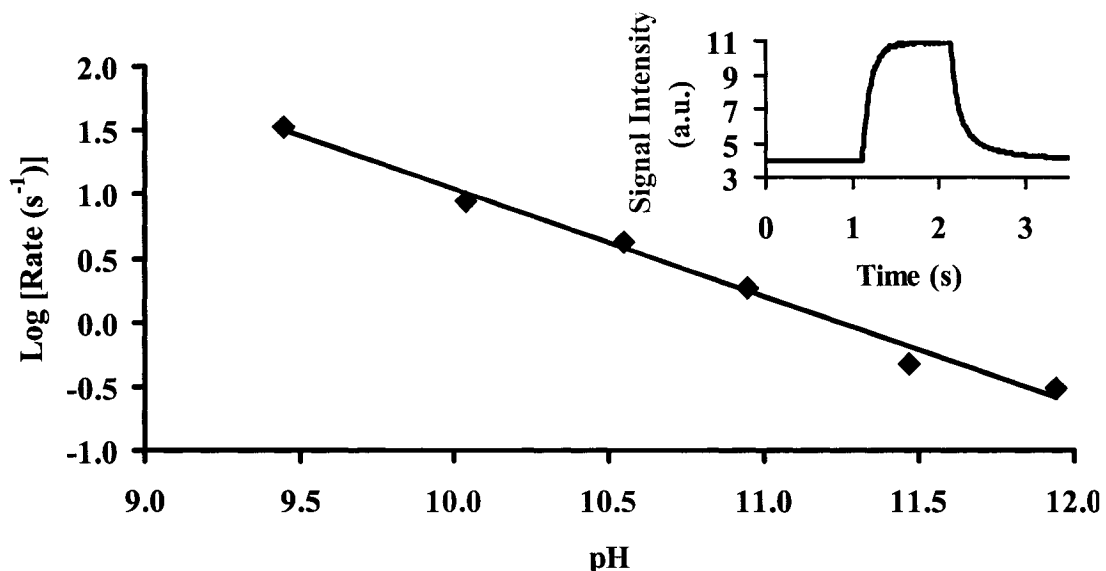
Figure 6.5   Optical transmission during photoisomerization (inset) and the resulting *trans-cis-trans* thermal isomerization rate constant as a function of pH for ER azobenzene chromophores.

This first order rate constant can depend strongly on the local solvent however, as depicted in Figure 6.5 for the isomerization taking place in aqueous solution over a range of pH values from pH = 9.5 to pH = 12.[26] The thermal isomerization rate constant varies linearly over two orders of magnitude in this range, with a time constant (1/rate constant) ranging from 30 ms at pH = 9.5 to more than 3 s at pH = 12. This therefore represents an effective and sensitive hydroxide ion sensor, which can function at high pH, of interest to many wastewater applications.[27] Although this hydroxide ion sensor relies on a spectroscopic determination of a rate constant, one could readily develop a practical sensor based on this technique using routine fibre optics, whereby the sensor layers are adsorbed either directly on a light-guiding fibre, or on top of a waveguiding layer over a support, provided appropriate refractive index contrast between material layers. With a

reflective coating at the end of this cylindrical sensor, the polymer material's absorbance could be continually monitored through reflected evanescent wave absorption with a low power probe laser, monitored at source through fibre optics. The 'pump' flash could be delivered with the same wavelength at higher power, and then the first-order return of the absorbance monitored for a few seconds to determine the rate constant, and hence the local pH. The versatility and stability of the multilayer host material, described previously in this paper, then suggests that a sensor of this type would be suitable to pH determination in highly alkaline media, and be easily cleaned with solvents and sonication without harm to the sensor material. One can envisage a wide variety of sensor groups incorporated into ISAM layers such as these (electrochemical or spectroscopic), or even multiple sensors incorporated in various layers to comprise a stable multifunctional probe, assembled easily in aqueous baths by appropriate adsorption.

6.5 Conclusions

ISAM films constructed from weak/weak polyelectrolyte systems containing chromophores can be physically and chemically controlled during self-assembly, making them promising candidates as host layers for sensor applications. PAH/P-Azo multilayer films were shown to be adsorbed under a range of layering conditions and geometries and exhibit good stability toward heat and a range of harsh solvent environments.

6.6 References and Notes

(1)   Hammond, P. *Curr. Opin. Colloid Interface Sci.* **2000**, *4*, 430.
(2)   Lvov, Y. M.; Decher, G. *Kristallografiya* **1994**, *39*, 696.

(3)   Lvov, Y. M.; Ariga, K.; Ichinose, I.; Kunitake, T. *J. Am. Chem. Soc.* **1995**, *117*, 6117.

(4)   Shiratori, S. S.; Rubner, M. F. *Macromolecules* **2000**, *33*, 4213.

(5)   Tian, J.; Wu, C. C.; Thompson, M. E.; Sturm, J. C.; Register, R. A.; Marsella, M. J.; Swager, T. S. *Adv. Mater.* **1995**, *7*, 395.

(6)   Baur, W.; Kim, S.; Balanda, P. B.; Reynolds, J. R.; Rubner, M. F. *Adv. Mater.* **1998**, *10*, 1452.

(7)   Gao, M.; Richter, B.; Kirstein, S. *Adv. Mater.* **1997**, *9*, 802.

(8)   Cheung, J. H.; Fou, A. F.; Rubner, M. F. *Thin Solid Films* **1994**, *244*, 985.

(9)   Ferreira, M.; Cheung, J. H.; Rubner, M. F. *Thin Solid Films* **1994**, *244*, 806.

(10)   Yamada, M.; Shiratori, S. S. *Sens. Actuators, B* **2000**, *B64*, 124.

(11)   Decher, G.; Hong, J. D. *Ber. Bunsen-Ges. Phys. Chem.* **1991**, *95*, 1430.

(12)   Decher, G.; Hong, J. D. *Makromol. Chem., Macromol. Symp.* **1991**, *46*, 321.

(13)   Sukhorukov, G. B.; Donath, E.; Litchtenfel, H.; Knippel, E.; Knippel, M.; Budde, A.; Möhwald, H. *Colloids Surf., A* **1998**, *137*, 253.

(14)   Caruso, F.; Trau, D.; Möhwald, H.; Renneberg, R. *Langmuir* **2000** *16*, 1485.

(15)   Rodriguez, L. N. J.; De Paul, S. M.; Barrett, C. J.; Reven, L.; Spiess, H. *Adv. Mater.* **2000**, *12*, 1934.

(16)   Dante, S.; Advincula, R.; Frank, C.; Stroeve, P. *Langmuir* **1999**, *15*, 193.

(17)   Dubas, S. T.; Schlenoff, J. B. *Macromolecules* **1999**, *32*, 8153.

(18)   Decher, G.; Schmitt, J. *Prog. Colloid Polym. Sci.* **1992**, *89*, 160.

(19)   Fang, M.; Kim, C. H.; Saupe, G. B.; Kim, H. N.; Waraksa, C. C.; Miwa, T.; Fujishima, A.; Mallouk, T. E. *Chem. Mater.* **1999**, *11*, 1526.

(20)   Fukushima, M.; Osa, T.; Ueno, A. *Chem. Lett.* **1991**, *4*, 709.

(21)   Rochon, P.; Gosselin, J.; Natansohn, A.; Xie, S. *Appl. Phys. Lett.* **1992**, *60*, 4.

(22)   He, J.; Bian, S.; Li, L.; Kumar, J.; Tripathy, S. K. *Appl. Phys. Lett.* **2000**, *76*, 3233.

(23)   Caruso, F.; Möhwald, H. *J. Am. Chem. Soc.* **1999**, *121*, 6039.

(24)   Paik, C. S.; Morawetz, H. *Macromolecules* **1972**, *5*, 171.

(25)   Barrett, C. J.; Natansohn, A. L.; Rochon, P. L. *Chem. Mater.* **1995**, *7*, 899.

(26)   Norman, L. L.; Barrett, C. J. *J. Phys. Chem. B* **2002**, *106*, 8499.

(27) Xu, H. W.; Sadik, O. A. *Analyst* **2000**, *125*, 1783.

Chapter 7

Conclusions, Contributions to Original Knowledge, and

Suggestions for Future Research

7.1 Conclusions and Contributions to Original Knowledge

Driven by an effort to find new noncovalent assembly methods for biocompatible polymer surface modification,[1] the polyelectrolyte multilayer assembly technique has proven to be a promising approach for the straightforward fabrication of functional organic surfaces in aqueous media. In contrast to other more traditional polymer coating methods,[2,3] the findings here highlight the versatile nature of this technique. Self-assembled polyelectrolyte multilayer films are amenable to a diverse range of charged polymers. The surfaces on which multilayers can be assembled are also variable with regards to the chemistry, size, geometry, and deposition set-up that can be used.

Key to exploiting polyelectrolyte multilayer films as functional surfaces is the ability to achieve good physical and chemical command over the assembly process, and thus obtain desired multilayer properties. Therefore, a fundamental understanding of significant kinetic processes, driving energetic forces involved in the layer-by-layer assembly process, and dominant adsorption variables which direct the physical properties of the film, is critical. Motivated by this goal, the studies undertaken here have focused on determining the effect of varying polyelectrolyte ionization (by manipulating the assembly pH) on the adsorption behavior and consequently, the resulting structural and mechanical film properties.

The role of ionic strength in assembly, as controlled through added electrolytes, has dominated the previous literature in the area of polyelectrolyte multilayers.[4-9] In this dissertation however, the importance of polyion charge density in multilayer formation was evaluated through mechanistic investigations and physical property determinations. Specifically, this was done by obtaining multilayer measurements of: a) the kinetic thickness and degree of counterion displacement (Chapter 3), b) the polyion chain-length adsorption preference (Chapter 4), c) the elastic modulus and layer-to-layer adhesion (Chapter 5), and d) the density of functional groups which can be incorporated (i.e., the optical loading capacity of azo-polyelectrolytes in multilayer films, Chapter 6), all as a function of the assembly solution pH.

Also of considerable impact in the area of structural determinations for polyelectrolyte multilayers has been the quantitative determination here, of the length of loops formed from electrostatic cross-linking of layers in weakly charged polyelectrolyte systems using a standard atomic force microscope (Chapter 5). Quantitative measurements of this loop length, and the effect of assembly pH on this value, have until now been lacking. Thus, this finding has been particularly valuable in response to recent multilayer reports, which predict and allude to the formation of loops resulting from reduced ionic contacts between layers of weakly charged polyelectrolytes.[10,11]

In the kinetics studies of Chapter 3, PEMs prepared from weakly charged polyion were found to exhibit anomalously rapid adsorption (on the order of seconds). At short adsorption times, PEMs prepared using either weakly charged polycations or weakly charged polyanions resulted in layers, which were 10-fold thicker than of that of films produced from strongly ionized polyelectrolytes. Moreover, if both the polycation and the polyanion are assembled at low charge fraction, films thickness values were found to

increase by as much as 30 fold in comparison to the analogous systems employing both strongly charged polyelectrolytes. By varying both time and concentration in multilayer assembly, fine control over the layer thickness was achieved, specifically, on the order of angstroms. Counterion displacement was also determined to be an influential factor affecting the degree of polyion adsorption into multilayers. For example, films assembled with strongly bound counterions, such as F^-, exhibit a reduced time-dependant adsorption by 21% as compared to those prepared with weakly bound counterions, such as I^-.

Investigations which examined short- versus long chain polyelectrolyte adsorption onto an oppositely charged polyelectrolyte surface revealed complete preference for longer chains, given a 24 h adsorption period in a solution containing 1mM NaCl. Fluorescence experiments showing this competitive adsorption behavior suggest that the configurational entropy gain from having short-chains in solution (as opposed to free long-chains) is a driving factor for the preferential assembly of long-chains. This behavior is analogous to the entropy-driven liberation of counterions, known to be necessary in the formation of multilayer assembly. Furthermore, the addition of electrolyte to the assembly solution is believed to reduce the height of the electrostatic barrier produced from charge overcompensation during layer deposition. Consequently, short-chains, which may initially be more kinetically favored towards adsorption, are likely replaced by long chains given a sufficiently long adsorption period of 24 h.

In Chapter 5, the elasticity of polyelectrolyte multilayer films, as a function of polymer charge density during assembly, was successfully probed using an AFM nanoindentation approach. In PEMs prepared with an identical thickness value, the resultant loop length in layers assembled from weakly charged polyelectrolytes was found to be up to 50-fold greater than an identical multilayer system but prepared using strongly

charged polyelectrolytes (as implied by measurements of the modulus of elasticity). Measurements of adhesion forces between multilayered AFM probes and planar multilayered surfaces in situ also provided an estimate of the relative strength of layer-to-layer interaction as a function of the bulk ionic cross-link density. Although SEM data suggest the occurrence of some mass transfer of layers during adhesion measurements, smaller adhesion forces were consistently observed in all cases where multilayers were assembled from weakly ionized polyelectrolytes. A comparison of the adhesion histograms obtained for strong versus weak PEMs suggests that strongly ionized polyelectrolytes produce multilayers which as a bulk appear to be more strongly interlinked (due to the presence of many more $k_B T$ interactions).

Lastly, in Chapter 6 it was shown that the construction of multilayers from weak/weak polyelectrolyte systems containing azo-chromophores could be physically and chemically well-controlled during self-assembly. Specifically, PAH/P-Azo multilayer films could be adsorbed under a wide range of layering conditions and geometries and exhibited good stability toward heat and a range of harsh solvent environments. These multilayers were demonstrated to be promising candidates as host layers for sensor applications based on photo-isomerization of the azo-chromophores.

All results presented here have come from investigating and comparing several model polycation/polyanion systems and as such, have led to an important general conclusion concerning the ionization of polyelectrolytes during assembly. Namely, the employment of weakly charged polyelectrolytes for multilayer assembly offers a simple but highly useful means for directing the adsorption behavior and accessing wider ranges of tunable physical properties in the resulting film.

7.2   Suggestions for Future Research

Studies of the kinetic factors which influence the rate of polyelectrolyte adsorption revealed that counterion binding strength, and hence the displacement of counterions in multilayer adsorption of polyelectrolytes, has a measurable impact on the time-dependant growth behavior of the film. It would be interesting to explore the effects of varying the series of counterions (i.e., cations of the alkali metal series) and different valencies to generalize the results observed for the halogen counterions. It would also be interesting to kinetically quantify and compare the displacement rate for a counterion series by, for example, monitoring over time the intensity of an emission signal resulting from counterion release into solution (i.e. using sensitive spectroscopic methods).

Investigation of the effects of chain length on the adsorption of a model polyanion to a model polycation indicated a sole preference for longer chains when 24 h was given for adsorption. Using solely entropic arguments, scaling arguments can be used to quantitatively model this result. Investigation of kinetic contributions to preferential adsorption could also be interesting. It is believed that diffusion-limited transport is likely to drive the shorter chains to initially adsorb, followed then by entropy-driven displacement by longer chains. The next logical experiment would therefore be a time-dependant study of preferential adsorption. With this study, one may be able to detect the expected turnover from short- to long-chain preference. Furthermore, the time-dependant preferential adsorption study could be performed over many layers, and compared under pH conditions where the polycation and polyanion are: a) both weakly charged, b) both strongly charged, and c) one weak and one strongly charged.

In Chapter 5, it was established that AFM is a powerful tool for performing nanoindenation experiments, and obtaining mechanical properties of polyelectrolyte

multilayer films. In a previous study of the mechanical properties of spin-coated azo-polymers, it was demonstrated that photoisomerization of the chromophore could lead to changes in the mechanical compliance of the film, specifically mechanical softening of the film.[12] Thus, it could be interesting to extend the AFM nanoindentation technique to explore elastic modulus changes resulting from photoisomerization of azo-containing polyelectrolytes in multilayer assemblies.

7.3   References and Notes

(1)   Ikada, Y. *Biomaterials* **1994**, *15*, 725.

(2)   Whitesides, G. M.; Ferguson, G. S.; Allara, D.; Scherson, D.; Speaker, L.; Ulman, A. *Crit. Rev. Surf. Chem.* **1993**, *3*, 49.

(3)   Ulman, A. *An Introduction to Ultrathin Organic Films: From Langmuir-Blodgett to Self-Assembly*; Academic Press: Boston, MA, 1991; pp 101–219.

(4)   Cho, J.; Char, K.; Kim, S. Y.; Hong, J. D.; Lee, S. K.; Kim, D. Y. *Thin Solid Films* **2000**, *379*, 188.

(5)   Lösche, M.; Schmitt, J.; Decher, G.; Bouwman, W. G.; Kjaer, K. *Macromolecules* **1998**, *31*, 8893.

(6)   Steitz, R.; Leiner, V.; Siebrecht, R.; von Klitzing, R. *Colloids Surf., A* **2000**, *163*, 63.

(7)   Steitz, R.; Jaeger, W.; von Klitzing, R. *Langmuir* **2001**, *17*, 4471.

(8)   McAloney, R. A.; Sinyor, M.; Dudnik, V.; Goh, C. M. *Langmuir* **2001**, *17*, 6655.

(9)   Kovacevic, D.; van der Burgh, S.; de Keizer, A.; Cohen Stuart, M. A. *Langmuir* **2002**, *18*, 5607.

(10)   Joanny, J. F.; Castelnovo, M. Polyelectrolyte Adsorption and Multilayer Formation. In *Multilayer Thin Films: Sequential Assembly of Nanocomposite Materials*; Decher, G., Schlenoff, J. B., Eds.; Wiley-VCH: Germany, Weinheim, 2003; pp 87–97.

(11)   Joanny, J. F.; Castelnovo, M.; Netz, R. *J. Phys.: Condens. Matter* **2000**, *12*, A1.

(12)   Mechau, N.; Neher, D.; Borger, V.; Menzel, H.; Urayama, K. *App. Phys. Lett.* **2002**, *81*, 4715.

Appendix

Analysis of Counterion Displacement Data and Discussion

A.1   Details of Data Treatment for the Analysis of Counterion Displacement, Chapter 3 (pp 69–73)

Comparison of the adsorption kinetics of PAH/P-Azo multilayers in the presence of F⁻, Cl⁻, Br⁻ and I⁻ was achieved by fitting the ion exchange plots of absorbance versus time (Figure 3.6) to first order kinetics.

$$A = a(1-e^{-bx})$$
(A.1)

Here, A represents the Absorbance (related to the thickness of the multilayer product), a is the final absorbance at infinite time (or final concentration of the product multilayer), b is the rate constant k, and x is time. Results of the first order fit to the different counterion series are shown below.

For I⁻
[Equation]
f=a*(1-exp(-b*x))
fit f to y
[Constraints]
b>0
[Options]
tolerance=0.000100
stepsize=100
iterations=100
R = 0.99106142   Rsqr = 0.98220274   Adj Rsqr = 0.98093150
Standard Error of Estimate = 0.0329

	Coefficient	Std. Error	t	P
a	0.6614	0.0171	38.6454	<0.0001
b	0.0332	0.0029	11.3259	<0.0001

For Br⁻
[Equation]
f=a*(1-exp(-b*x))
fit f to y

150

[Constraints]
b>0
[Options]
tolerance=0.000100
stepsize=100
iterations=100

R = 0.98740010   Rsqr = 0.97495896   Adj Rsqr = 0.97317032

Standard Error of Estimate = 0.0354

	Coefficient	Std. Error	t	P
a	0.6006	0.0177	33.9573	<0.0001
b	0.0352	0.0036	9.6334	<0.0001

For Cl⁻

[Equation]
f=a*(1-exp(-b*x))
fit f to y
[Constraints]
b>0
[Options]
tolerance=0.000100
stepsize=100
iterations=100
R = 0.98907686   Rsqr = 0.97827304   Adj Rsqr = 0.97672111
Standard Error of Estimate = 0.0303

	Coefficient	Std. Error	t	P
a	0.5590	0.0157	35.7069	<0.0001
b	0.0335	0.0032	10.4418	<0.0001

For F⁻

[Equation]
f=a*(1-exp(-b*x))
fit f to y
[Constraints]
b>0
[Options]
tolerance=0.000100
stepsize=100
iterations=100
R = 0.99133568   Rsqr = 0.98274643   Adj Rsqr = 0.98151403
Standard Error of Estimate = 0.0259

	Coefficient	Std. Error	t	P
a	0.5386	0.0137	39.1774	<0.0001
b	0.0324	0.0028	11.7067	<0.0001

A.2   Discussion of Counterion Displacement

With regards to Chapter 3, it should be clarified that the counterion displacement does not affect the rate of polyelectrolyte adsorption as much as it does the total adsorbed amount of polyelectrolyte in the multilayers (related to the final absorbance measurements in Figure 3.6), where a (in Eq. A.1) is significantly different for PEMs assembled with varying size counterions. We therefore suggest the differences in the ionic binding energies of the varying size counterions leads to varied extent of multilayer adsorption (arising from the difference in the net free energy required for displacement of a smaller counterion versus a larger one). Section 3.4.4 has thus been revised as follows to further clarify this concept.

3.4.4   Ion Displacement and Adsorption Kinetics

The role of ion exchange in the adsorption kinetics of multilayers was investigated here by comparing the relative rate of P-Azo adsorption on partially charged PAH (pH = 9) for a series of polyelectrolyte solutions containing one of NaF, NaCl, NaBr or NaI of concentration $5\times10^{-2.0}$ M. Multilayer films containing 30 layers were assembled onto glass slides using various adsorption times ranging from 1 s to 15 min for the P-Azo component while the saturated adsorption of polycation was ensured by maintaining a constant immersion time of 15 min. Reported optical measurements on multilayer films were time-corrected for prolonged polyelectrolyte adsorption resulting from significant polymer concentration at the surface of the film during rinse cycles initially, which was quantified using UV-vis.

The optical thickness measurements show that saturation is nearly achieved in approximately 60 s of adsorption time. The results from this time-dependant study of film thickness for PAH/P-Azo on glass slides is in agreement with the thickness values obtained from reflective ellipsometry measurements obtained for thickness of PAH/P-Azo (Figure 3.4), which suggests that maximum polyelectrolyte adsorption is obtained upon approaching 1 min of immersion time. No distinguishable difference in the optical absorbance resulting from P-Azo adsorption was observed up to 20 s dipping time for the films prepared with varying halogen ion salt. After 20 s, significant differences in the optical thickness revealed a reduced adsorption of the P-Azo when the multilayers were

prepared in the presence of small F⁻ counterions. Conversely, an increase of 21% in the UV-vis absorbance of multilayer films prepared from I⁻ containing solutions suggests that polymer solutions containing larger counterions exhibit greater adsorption of P-Azo than those containing an equivalent amount of F⁻ counterions.
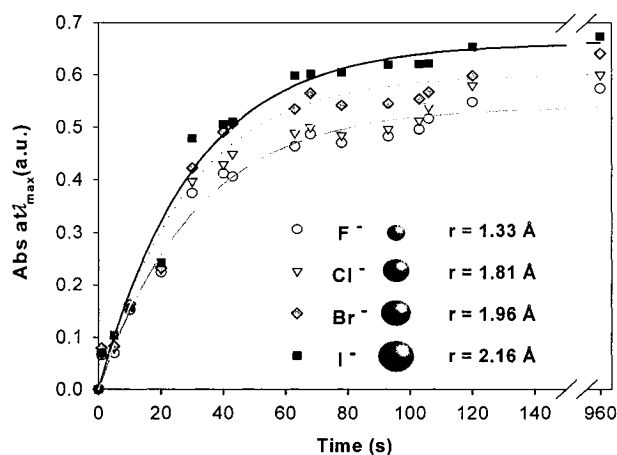

Figure 3.6   Effect of ion exchange on time-dependant adsorption of PAH/P-Azo multilayers (at a constant pH value of 9 for both polyelectrolyte solutions).

The observed variances in the extent of polyanion adsorption based on the presence of either F⁻, Cl⁻, Br⁻ or I⁻, can be rationalized using a simple electrostatic argument considering the binding energies of the tested anions with various cations (Table 3.1).   The Arrhenius equation (Equation 3.1) is used to compare the adsorption for the series of counterions at constant temperature.

$$k = A\,e^{-E_a/RT}$$
(3.1)

The time-dependant absorbance for all counterions (Figure 3.6) was found to fit well to first-order kinetics with $r^2 = 0.97$-0.98 (Appendix A.1).   As indicated in Table 3.1, the experimentally obtained rate constant, k, derived from the 1ˢᵗ order fitted curves is similar for all counterions (and hence Eq. 3.1 implies similar activation energies, Ea, for the

153

counterion series). However, the adsorbed thickness of the multilayer prepared with F⁻ was found to be 81% that of the films prepared with I⁻ counterion (as determined by the final absorbance value at time →∞ obtained from the fitted 1ˢᵗ order kinetics plot). This implies that the extent of dissociation of the counterions scales inversely with the ionic binding energy, E^*. For example, since the binding strength of the F⁻ counterion is 1.63 fold larger than the I⁻ we observe a reduced adsorption for multilayer films assembled with the smaller F⁻ counterion (by 19%).

Since P-Azo must exchange with the bound counterions existing on the PAH surface for adsorption to occur, systems with larger I⁻ ions (i.e., more loosely bound) would be expected to exchange to a greater extent (due to a greater reduction in the free energy from the dissociation process) than more tightly bound F⁻ ions, as observed.

target counterion	ionic radius (Å)	av E^* ᵃ (kcal·mol⁻¹)	E^* rel to I⁻	exptl k ᵇ	exptl rel thickness ᶜ
F⁻	1.33	137.5	1.63	0.0324	81
Cl⁻	1.81	111.9	1.32	0.0335	84
Br⁻	1.96	100.2	1.19	0.0352	91
I⁻	2.16	84.6	1	0.0332	100

ᵃ E^* determined from the average ionic binding energies of target counterion with Li⁺, Na⁺, K⁺, and Rb⁺.³⁸ ᵇ Experimental k obtained from 1ˢᵗ order kinetics fit of polyelectrolyte multilayer adsorption as a function of time (Figure 3.6 ; see Appendix A). ᶜ Experimental relative thickness at time → ∞ as indicated by the final absorbance values.

Table 3.1 Experimental Relative k and Relative Final Thickness for Multilayer Formation with Different Target Counterions

While our kinetic study of counterion displacement suggests that this process is not necessarily rate-limiting with regard to multilayer formation, it has a significant and measurable effect on the adsorbed thickness of weakly charged polyelectrolytes in multilayer films.